The suitability of biochar from non-lignocellulosic feedstocks as potential bio-based reinforcing fillers in rubber composites

By

Stephanie Greenough

Department of Bioresource Engineering

Faculty of Agricultural and Environmental Sciences

Macdonald Campus of McGill University

Sainte-Anne-de-Bellevue, Québec, Canada

March 2022

A thesis submitted to McGill University in partial fulfillment of the requirements for the degree of Master of Science.

Abstract

Bio-based alternatives to non-renewable, non-sustainable materials in composites has gained considerable attention in recent decades. Biochar, a bio-sourced material, can be synthesized from nearly any feedstock. Biochar physicochemical properties vary based on the feedstock source and the pyrolysis operating conditions. The subject of this thesis is the synthesis and characterization of biochar from non-lignocellulosic feedstocks such as chicken feather meal, municipal wastewater sludge, and canola protein. The suitability of biochar as reinforcing fillers in styrene-butadiene rubber composites was assessed based on the biochar filled rubber vulcanization behavior, morphology, tensile, and dynamic mechanical properties. Biochar from non-lignocellulosic feedstocks was evaluated as a substitute for carbon black in rubber tire applications.

As part of this thesis, chicken feather meal and municipal wastewater sludge were converted into biochar using a batch pyrolysis unit. The effects of the feedstock source and the pyrolysis temperature on the physicochemical properties of the biochar were studied. The biochars were then added to the styrene-butadiene rubber mix to produce bio-based filled rubber composites. Results showed that among other properties, the biochar had lower carbon and higher ash content, lower surface area, and larger particle sizes compared to carbon black. These unfavorable properties resulted in the inability of the biochar to reinforce the rubber. The dynamic mechanical analysis confirmed the strong filler-filler interactions, and a lower tendency for filler-rubber interactions, which was attributed to biochar physicochemical properties. Therefore, without further modification, chicken feather meal and municipal wastewater sludge were not suitable alternatives for carbon black in styrene-butadiene rubber composites.

In a second study, chicken feather meal and canola protein were evaluated as potential renewable fillers in styrene-butadiene rubber composites. It was found that steam activated biochar had improved physicochemical properties compared to the biochar in the previous study. This translated into improved tensile properties. The results of the dynamic mechanical analysis showed that canola protein pyrolyzed under nitrogen and subsequently steam cooled behaved similarly to carbon black. The slight differences were not large enough to explain the much lower reinforcement of the biochar. Further research is required to assess whether biochar surface modification can improve the compatibility with rubber.

Résumé

Au cours des dernières décennies, des alternatives biosourcés ont suscité un intérêt considérable en tant que substituts pour les matériaux non renouvelables dans les composites. Le biochar, un matériel biosourcé, peut être synthétisé à partir de quasiment tous les types de biomasse. Les propriétés physico-chimiques du biochar varient en fonction de la source de la biomasse et selon les configurations de la pyrolyse. Le sujet de cette thèse porte sur la synthèse et la caractérisation des biochars produits à partir de résidus de biomasses non-lignocellulosiques telles que la farine de plumes de poulet, les boues d'épuration municipales, et les protéines de canola. Une analyse de la vulcanisation, de la morphologie, de la traction, et de la mécanique dynamique a été réalisée afin de déterminer si le biochar peut être utilisé comme charges renforçantes dans les composites de caoutchouc styrène-butadiène. Biochar provenant de résidus de biomasses non-lignocellulosiques a été évalué comme substitut au noir de carbone dans les pneumatiques.

Dans le cadre de ce mémoire, de la farine de plumes de poulet et des boues d'épuration municipales ont été converties en biochar à l'aide d'un réacteur de pyrolyse. Les effets de la source de la biomasse et de la température de pyrolyse sur les propriétés physico-chimiques du biochar furent étudiés. Le biochar a ensuite été ajouté au composite de caoutchouc styrène-butadiène pour produire un composite de caoutchouc avec renforts biosourcés. Les résultats ont montré que, parmi d'autres propriétés, le biochar avait une teneur plus faible en carbone et plus élevée en cendres, une surface plus faible et des particules de plus grande taille que le noir de carbone. Ces propriétés défavorables ont entraîné l'incapacité du biochar à renforcer le caoutchouc. L'analyse mécanique dynamique a confirmé les fortes interactions entre les charges, et une tendance plus faible pour les interactions entre les charges et le caoutchouc, ce qui a été attribué aux propriétés physico-chimiques du biochar. Par conséquent, sans modification supplémentaire, la farine de plumes de poulet et les boues d'épuration municipales ne sont pas des alternatives appropriées au noir de carbone dans les composites de caoutchouc styrène-butadiène.

Dans une deuxième étude, la farine de plumes de poulet et les protéines de canola ont été évaluées comme charges renouvelables potentielles dans les composites de caoutchouc styrène-butadiène. Il a été constaté que le biochar activé à la vapeur avait des propriétés physico-chimiques améliorées par rapport au biochar de l'étude précédente. Cela s'est traduit par une amélioration des propriétés de traction. Les résultats de l'analyse mécanique dynamique ont montré que les protéines

de canola pyrolysées sous azote et ensuite refroidies à la vapeur se comportaient de manière similaire au noir de carbone. Les légères différences n'étaient pas assez importantes pour expliquer le renforcement beaucoup plus faible du biochar. Des recherches supplémentaires sont nécessaires pour évaluer si la modification de la surface du biochar peut améliorer la compatibilité avec le caoutchouc.

Table of Contents

List of Tables

List of Figures

Acknowledgements

I would first and foremost like to thank my supervisor, Dr. Marie-Josée Dumont, for encouraging me to pursue my graduate studies and for giving me the opportunity to be a part of the McGill-Michelin collaboration. Your support and guidance were invaluable to my success.

I would also like to thank my co-supervisor, Dr. Shiv Prasher, for his involvement in the project. I am also very grateful towards Dr. Jiby Kudakasseril Kurian for his time spent teaching me how to use the equipment and techniques required during my studies (such as the pyrolysis unit, FTIR, proximate analysis) and for his expert advice on the pyrolysis process and biochar. I would also like to thank Mr. Yvan Gariépy for his help and involvement in the project and for his guidance and feedback during the writing stages. I would like to thank Dr. Valérie Orsat for generously allowing me to use her laboratory space and equipment. I would like to thank Aleksandra Djuric for performing the BET surface area experiments and the Laboratoire d'Analyse de la Biomasse, des Bioproduits et des Bioprocédés (LAB) (Sherbrooke University) for performing the elemental analysis.

Thank you to the entire team at Michelin for performing the rubber work at Michelin Americas Research and Development Corp. in South Carolina. A special thanks to Dr. Constantine Y. Khripin and Dr. Jeremy J. Mehlem for their expert advice, time spent teaching me about rubber technology, and their editorial help during the writing of the manuscripts.

I am very grateful for the funding provided by Michelin Inc. and the Natural Science and Engineering Research Council of Canada (NSERC) through the Collaborative Research and Development Grants (CRD) without which the project would not have taken place.

Finally, I would like to thank my parents and my girlfriend for their encouragement throughout my studies. A special thanks to my dogs, Jager and Kaï, for their companionship during the research and writing process.

Contribution of Authors

The thesis is submitted in the form of a manuscript-based thesis. The candidate, Stephanie Greenough, was responsible for designing and conducting the experiments relating to the production and characterization of the biochar samples, handling the data analysis (for both the biochar and rubber composites), as well as the preparation of the individual manuscripts and the thesis. Dr. Marie-Josée Dumont, supervisor of the candidate, contributed to all aspects of the research work, including planning and directing the research, editing and reviewing the manuscripts and the thesis before submission. Dr. Shiv Prasher, co-supervisor of the candidate, and Mr. Yvan Gariépy contributed to the editing and reviewing of the thesis and individual manuscripts. Dr. Jiby Kudakasseril Kurian assisted in performing some of the experiments. Dr. Constantine Y. Khripin and Dr. Jeremy J. Mehlem, Michelin collaborators, provided expert advice and contributed to the editing and reviewing process of the manuscripts and the thesis before submission. Matthew S. Francis, Reyda Lizette Bazan Cornejo, and Shreya Thammana performed the rubber work and B. Steven Myles performed the microscopy at Michelin Inc. The details of the manuscripts that have been published or submitted for publication are provided below:

1. Greenough, S., Dumont, M.-J., & Prasher, S. (2021). The physicochemical properties of biochar and its applicability as a filler in rubber composites: a review. *Materials Today Communications*, *29*. https://doi.org/10.1016/j.mtcomm.2021.102912
2. Greenough, S., Gariépy, Y., Dumont, M.-J., Prasher, S., Francis, M.S., Myles, B.S., Khripin, C.Y., Mehlem, J.J. (2022). Investigating chicken feather meal and municipal wastewater sludge biochar as renewable fillers in styrene-butadiene rubber composites. Submitted for publication.
3. Greenough, S., Kudakasseril Kurian, J., Gariépy, Y., Dumont, M.-J., Prasher, S., Cornejo, R.L.B., Thammana, S., Myles, B.S., Khripin, C.Y., Mehlem, J.J. (2022). Chicken feather meal and canola protein as potential renewable fillers in styrene-butadiene rubber composites. Submitted for publication.

Chapter 1

Introduction

1.1 General introduction

The global consumer tire market is expected to reach over 2.75 billion units by 2024 [1,2]. With over one hundred separate components in an average tire, the sustainability of these ingredients has become of great interest to the tire industry. Environmental awareness, volatility in material prices, and shortages of petroleum-derived materials has propelled the industry to evaluate sustainable sources of ingredients that go into making a tire. Rubber is the main raw ingredient in tires and the automotive tire industry consumes over 46% of the natural rubber market annually [3]. In the tire industry, natural rubber is often used in combination with synthetic rubber polymers such as butadiene rubber and styrene butadiene rubber. Tire manufacturers have been researching the suitability of using guayule as a substitute for natural rubber and have been investigating the potential of dandelion-derived rubber [4]. Also, renewable styrene-butadiene rubber has been investigated [5]. Carbon black, a reinforcing filler, is the other primary ingredient in rubber tires. To meet sustainability objectives set by the tire manufacturers, the importance of finding sustainable fillers capable of providing similar reinforcement to carbon black is imperative. Oil, with a high content of aromatic hydrocarbons, is the feedstock used to produce carbon black [6]. The oil furnace process is the most widely used for carbon black production, which releases nearly 3 tons of CO_2 per ton of carbon black produced [7]. Although apparent that the production and use of carbon black is unsustainable, there are currently no commercially viable renewable, bio-sourced fillers. In recent years, biochar has gained considerable attention as an alternative to carbon black.

Biochar is synthesized from the pyrolysis of biomass and nearly any feedstock can be used for biochar production. Biochar physicochemical properties largely depend on the feedstock source and the pyrolysis operating conditions [8]. To date, adequate feedstock types that result in biochar with similar physicochemical properties to carbon black have not yet been identified. Rather feedstocks have been tried on a case-by-case basis. Previous studies have focused on

lignocellulosic feedstocks such as wood-based feedstocks and agricultural crops and residues [9-18].

1.2 Study objectives

Traditionally, reinforcing fillers in rubber composites are produced from petroleum-derived materials like carbon black. In recent years, bio-sourced reinforcing fillers have become of interest as alternatives to these non-renewable, non-sustainable fillers. The main objective of this study was to synthesize and characterize biochar from non-lignocellulosic feedstocks and to assess its suitability as reinforcing fillers in rubber composites. The specific objectives of this research are listed as follows:

I. To review the literature regarding current knowledge related to the physicochemical properties of biochar, to compare biochars physicochemical properties to those of carbon black, and to understand how filler properties translate into desirable mechanical properties in rubber.

II. To synthesize and characterize biochar from non-lignocellulosic feedstocks (chicken feather meal and wastewater sludge) as potential reinforcing fillers in styrene-butadiene rubber composites. To assess the effect of the feedstock type and the pyrolysis temperature on the physicochemical properties of the biochar and to compare the properties to those of carbon black. To incorporate biochar as a filler in styrene-butadiene rubber composites to assess its reinforcing mechanism, by evaluating its cure characteristics, tensile properties, dynamic mechanical properties, and morphologies.

III. To synthesize biochar from protein-based feedstocks (chicken feather meal and canola protein) and to evaluate their suitability as reinforcing fillers in styrene-butadiene rubber composites. To assess the effect of the feedstock type and the pyrolysis atmospheric conditions and activation on the physicochemical properties of the biochar and to compare the properties to those of carbon black. To incorporate the biochar as a filler in styrene-butadiene rubber composites and to evaluate its reinforcement based on the vulcanization behavior, tensile properties, dynamic mechanical properties, and morphologies.

Chapter 2

The physicochemical properties of biochar and its applicability as a filler in rubber composites: A review

Abstract

Fillers in rubber composites are nanomaterials known for their reinforcing properties in elastomer matrices. Carbon black, a non-renewable material, is currently the preferred filler in the rubber tire industry. In recent years, biochar has become of interest as a potential replacement filler for carbon black in rubber applications. The wide range and varying nature of feedstocks, and the flexibility of the pyrolysis operating conditions yield biochar with diverse and distinct physicochemical properties. The primary aim of this review is to provide an overview of the effect of the feedstock source and the process parameters on the physicochemical properties of the resulting biochar. In addition, the inherent properties of carbon black will be compared to the general properties of biochar as a mean of determining biochar's suitability as an alternative filler. Finally, biochar's mechanical performance will be compared to the reinforcing ability of carbon black.

2.1 Introduction

Globally, the demand for rubber tires is continuously increasing. Consumers associate tires with factors such as safety, security, reliability, and durability. To achieve these expectations, rubber tires are designed to fulfill a balance between quality and performance criteria, such as rigidity, flexibility, wear resistance, grip in various weather conditions, and resistance to aging [19]. The materials used in tire composites affect these factors.

Hundreds of raw materials can be used in tire composition, and are selected depending on the type of tire produced and the intended application [20]. Tires are highly engineered composite materials with 15 or more raw materials included in the rubber component alone [19]. The rubber component is the most important feature and comprises an elastomer, a reinforcing filler, vulcanizing agents, protection agents, and processing aids [19,21-23]. The elastomer is a polymer matrix material; it can either be from natural or synthetic sources. Some examples include cis-

1,4 polyisoprene (natural rubber), cis-1,4 polybutadiene, poly(isobutylene-co-isoprene) (butyl rubber), and poly(styrene-co-butadiene) 25/75 (styrene butadiene rubber, emulsion) [22]. The elastomer is a viscoelastic material which has weak intermolecular forces (low tensile strength), is highly deformable, and has a low Young's modulus [22]. Therefore, reinforcing fillers are mixed into the polymer matrix to increase the durability, elasticity, resilience, tensile strength, viscosity, hardness, and the weather resistance [22,24]. Carbon black and silica are the most commonly used fillers [19].

To create the rubber compound, elastomers require processing known as vulcanization or curing, where the long polymer chains are mixed with the reinforcing filler and the vulcanizing system, to create an elastic solid material [22]. Vulcanization is a chemical process that converts natural rubber into a crosslinked polymer [21]. Sulphur is used as the vulcanizing agent to create these crosslinks however, even at high temperatures, the reaction is slow [21]. To increase the speed at which the process occurs, a vulcanizing system is used with a crosslinking agent, and consists of primary and secondary accelerators, activators, protection agents, and processing aids. Sulphenamides like N-cyclohexyl-2-benzothiazole sulphenamide (CBS) or N-tert-butyl-2-benzothiazole sulphenamide (TBBS) are used as primary accelerators [19,21,22]. Secondary accelerators like diphenyl guanidine (DPG) are used to activate the primary accelerators [19,21,22]. Zinc oxide and stearic acid are used as activators to increase the crosslinking efficiency [21]. Additionally, softeners like oils, resins, and waxes are used as processing aids to improve the workability of the material [21]. Finally, antioxidants and antiozonants are added to the mixture as protection agents against oxygen, ozone, heat, light, and mechanical deformation of the rubber product [21]. The proportions of these components differ based on the tire and the intended application.

Various materials in the rubber compound currently rely on non-renewable, non-sustainable raw materials. Finding alternative bio-sourced materials can help reduce the environmental impact of rubber composites. Traditionally, reinforcing fillers in rubber tires are produced from petroleum-derived materials like carbon black. The majority of carbon black production is done through the oil furnace process, which is a thermal oxidative procedure that involves the partial combustion of liquid aromatic hydrocarbon oil [6]. In recent years, bio-sourced materials have become increasingly important as alternatives to these petroleum-derived reinforcing fillers. This change has been fueled by an increase in public awareness and pressure to

reduce the dependence on fossil-fuels. For example, Bridgestone has the ambitious goal that by 2050, 100% of their tires will be made from sustainable materials [25]. Similarly, Michelin's long term goal is that by 2050 100% of their tires will be produced from bio-sourced and recycled materials [5]. The use of bio-based reinforcing fillers would further help to reduce the tire industries' dependence on fossil fuels. Materials such as traditional carbon nanotubes [26] and graphene [27] have been studied as alternatives to carbon black in rubber compounds however, these materials are still non-renewable. Also, efforts have been made to replace carbon black with bio-fillers such as bamboo fiber [28], pineapple leaf fiber [29], starch [30-32], soy protein and carbohydrate [33], waste eggshell powder [34], lignin [35], and cereal straw [36]. Although some of these renewable fillers provided some desirable mechanical properties and reinforcement to the rubber composite, their physicochemical properties are fundamentally different from those of carbon black.

Recently, reinforcing rubber compounds with biochar has been the focus of several studies since it resembles carbon black and yields similar properties. Biochar synthesized from feedstocks such as corn stover [12], woody waste biomass [13], coconut shell and discarded wood pallets [14], rice bran [15], birchwood [10], coppiced wood (poplar and Paulownia) [17], rice husk [18], various lignin sources [11] and dry leaves [9], have been mixed with rubber, and their reinforcing properties have been evaluated. Also, several patents exist on the use of biochar as a renewable replacement for carbon black in composites [37-39]. Although these patents covered biochar as a replacement for carbon black in thermoplastic polymers, the information provided therein could be useful for determining biochar's suitability as a filler in other applications, such as in rubber composites.

Previous reviews have focused on the relationship between the feedstock type and the pyrolysis operating conditions on the physicochemical properties of biochar [8,40,41]. Though there are studies that have evaluated biochar as a filler in rubber compounds, no review has focused on comparing biochar and carbon black's physicochemical properties, and how this translates into desirable mechanical performance of rubber compounds. This review, therefore, focuses on current knowledge related to biochar as a potential replacement for traditional fillers in rubber applications. First, the potential feedstock types for biochar synthesis and the production method (pyrolysis) are explored. Then, the inherent physicochemical properties of carbon black are compared to the general properties of biochar. Finally, the resulting curing behavior and

mechanical properties of biochar filled and carbon black filled rubber compounds are compared to determine biochar's suitability as a reinforcing filler.

2.2 Effects of the feedstock source and its pyrolysis process on the physicochemical properties of biochar

With up to 75 parts per hundred units mass of elastomer [22], the reinforcing filler is a critical component in rubber compounds. The most common and widely used filler in the industry is carbon black, used primarily for reinforcement of the elastomer matrix. Recently, biochar, a bio-sourced material, has gained popularity as a potential replacement for carbon black. The successful application of biochar as a filler depends on whether it can be synthesized with similar physicochemical properties to carbon black and whether it can provide equivalent mechanical properties and reinforcement. With careful selection of the feedstock and by modifying the biochar production parameters (temperature, heating rate, and residence times), there is potential to "design" biochar with similar properties and characteristics to that of carbon black.

2.2.1 Effects of the feedstock source on the physicochemical properties of biochar

Biochar can be synthesized from practically any organic material and these feedstocks can be classified according to the source material [42]. The two broad groups of source materials are dedicated energy crops and low-value residues or waste materials. This review will focus on the latter group. Residues and waste materials can be further subdivided into resources from the agricultural, municipal, and forestry sectors. These sources of biomass are widely available, and their abundance makes them a viable, cost-effective resource for biochar production. These residues and wastes are either lignocellulosic or non-lignocellulosic biomass, and they produce biochar with very different physicochemical properties.

2.2.1.1 Lignocellulosic biomass

Wastes and residues derived from lignocellulosic biomass currently have limited, low-value, competing uses and therefore they are abundantly available to produce biochar. Sources of lignocellulosic biomass include agricultural and forestry residues and wastes [8,41]. Biochar has been produced from an extensive list of lignocellulosic biomass; some examples include, but are not limited to, pine wood [43,44], pitch pine [45,46], cedar wood chips [47], douglas fir [48],

poplar [48,49], spruce [49], birch wood [10], eucalyptus [45,46], oak [45], wheat straw [43,49], timothy grass [43], rice husk [18,50], rice straw [51], corn stover [52], corn stalk [53,54], corn straw [55], bagasse [46,56], banana leaves [57], corn cob [58], cacao shell [58], oat grain [59], oat straw [59], barley grain [59], and barley straw [59].

The main components of lignocellulosic biomass are lignin, cellulose, hemicellulose, extractives, and small amounts of inorganic components [40,60]. The proportion of these components differs based on the source of the lignocellulosic biomass. These components further impact properties such as the ash content of the biochar [40,61]. Kataki et al. reviewed the compositional analysis of over 200 different feedstocks and found that generally, the mean ash content was lowest for wood feedstocks and highest for agricultural stalks and straws [62]. Further, biomass with lower proportions of inorganic components yield biochar with lower ash contents. For example, generally, wood-derived biomass have lower inorganic components as compared to crop residues and consequently, wood-derived biochars tend to have lower ash contents [40,63].

2.2.1.2 Non-lignocellulosic biomass

Lignocellulosic biomass has long been used to synthesize pyrolytic biochar. In recent years, research has expanded feedstocks for biochar production to include non-lignocellulosic biomass such as sewage sludge, manure, and livestock-derived biomass (hair, bones, feathers) [41]. Some of the different feedstocks that have been studied in the literature include sewage sludge [64-66], dairy manure [67,68], poultry litter [67], feedlot manure [67], separated swine solids [67], turkey litter [67], swine manure [69], and solid food waste [70].

These renewable resources have become of interest as researchers attempt to find alternate uses for these wastes by creating value-added products. Non-lignocellulosic feedstocks are composed of proteins, lipids, saccharides, inorganics, minerals, lignin, and cellulose, among others [41]. Compared to lignocellulosic feedstocks, these sources contain more components and this can lead to more complex thermochemical reactions during the pyrolysis process [41]. Also, their complexity can lead to unfavorable biochar properties such as lower carbon content and higher ash content as compared to lignocellulosic-derived biochar [46,67]. Biochars with high ash content have been shown to have adverse effects on the reinforcing properties of rubber compounds [13].

2.2.2 Effects of the pyrolysis process on the physicochemical properties of biochar

After selecting the feedstock, the parameters for biochar production can be controlled and chosen based on the desired product distribution and properties. Pyrolysis is an oxygen-deprived thermochemical process that converts organic material into three main products: biochar, bio-oil, and syngas [71,72]. A conventional pyrolysis unit uses electrical heating to heat the outer surface of a reactor and by conductive and convective heat transfer, the feedstock within the reactor is heated and converted into solid biochar, liquid bio-oil, and combustible gases [71]. The composition of biochar can be divided into three main parts: fixed carbon, volatile matter, and inorganic matter also known as ash. The liquid bio-oil is a mixture of hydrophilic organics, water, and tars; and the combustible gases 'syngas' are generally composed of carbon dioxide, carbon monoxide, methane, and hydrogen [73]. The operating conditions of the pyrolysis unit include the highest treatment temperature (HTT), the heating rate, and the residence time. These conditions influence the yield, quality, and the potential applications of the resulting products [71,74]. The pyrolysis process is often classified according to these operating conditions and is referred to as either slow, intermediate or fast pyrolysis [73].

Fast pyrolysis is characterized by high heating rates (10–1000 °C/s), and very short vapor residence times (1–5 s) [60,71]. The high heating rate coupled with the short vapor residence time is conducive to the rapid conversion of the feedstock into condensable vapors [71,75]. By quickly removing and cooling these vapors, fast pyrolysis favors the production of bio-oil. In recent years, fast pyrolysis has attracted attention for maximizing liquid yields, with products of up to 75% wt. bio-oil [60]. In the case of biochar production, fast pyrolysis can be used to achieve high treatment temperatures in shorter periods of time. It has been shown that higher operating temperatures lead to biochar with enhanced physicochemical properties such as high carbon content, high surface area, and high adsorption [61,73,76]. In contrast, biochar yield is maximized using slow or intermediate pyrolysis, which are characterized by lower heating rates (0.1–10 °C/s) and longer residence times (seconds to days) [60,71]. One defining characteristic of slow pyrolysis is its long residence time, on the order of hours to days. This facilitates secondary thermochemical reactions to occur and results in greater biochar yields [71].

2.3 Comparison of carbon black and biochar physicochemical properties

Carbon black compatibility with the rubber matrix plays a key role in its effectiveness as a reinforcing filler in rubber composites. Some researchers believe its reinforcement can be attributed to three fundamental properties (a) high elemental carbon content; (b) low ash content; and (c) small particle size [9-11]. Other important parameters include the structure, surface chemistry, and surface area, all of which contribute to the interaction between the filler and the rubber matrix [77-79]. The inherent properties of carbon black can therefore be compared to those of biochar to help determine its applicability and performance as a replacement filler in rubber composites. In recent years, the idea of "designing" biochar with a specific application in mind has been gaining popularity. Knowing that some properties like surface chemistry [80] and particle size [10,81-83] can be modified, the feedstock as well as the pyrolysis process conditions can be chosen to yield biochar with physicochemical properties that closely resemble those of carbon black. The feedstock source (wood, agricultural wastes, animal-derived manures, etc.) and variation in the pyrolysis operating conditions (temperature, heating rate, and residence times), lead to biochars with different physicochemical properties [46,48,49,67], and can therefore be used in different engineering applications.

2.3.1 Chemical analyses

Some properties of biochar, like ash content, are heavily influenced by the feedstock source [84]. However, many other properties are obtained from the thermochemical conversion of the feedstock. An example is that the chemical composition and constituents of the feedstock are different from the synthesized biochar [49]. Performing chemical analyses of the biochar itself is important and can give insight on its characteristics, properties, and potential applications. Two common analyses performed are the ultimate/elemental analysis and proximate analysis. Comparing carbon black and biochar's basic characterizations can show similarities and differences between the chemical composition and constituents of the two materials.

Elemental analysis determines the chemical composition of the material and helps understand the structure by determining the amounts of carbon (C), hydrogen (H), nitrogen (N), sulfur (S), and oxygen (O) in the sample. Carbon black contains over 95% of carbon with small amounts of hydrogen, nitrogen, sulfur, and oxygen [6]. In contrast, as seen in Table 2.1, elemental analyses of biochar show that there is a vast variability among biochar synthesized from different

feedstocks, from different parts or sections of the same biomass, and synthesized under different pyrolysis operating conditions. From Table 2.1, wood-based feedstocks have the highest carbon content with an average of 77%wt. C, followed by agricultural residues (61%wt.), animal manures (50%wt.), and sewage sludge (15%wt.). Also, regardless of the feedstock source, an increase in pyrolytic temperatures increases the carbon content, while the hydrogen and oxygen contents decrease. This indicates that an increase in temperature leads to an increase in carbonization and aromatic structures [67,85,86]. Additionally, the higher temperatures are conducive to the removal of polar surface functional groups [67,85,86]. This also indicates that the H/C and O/C ratios of biochar tend to decrease with an increase in pyrolysis temperature. A lower H/C ratio indicates an increase in aromaticity and stability and a lower O/C ratio indicates a lower degree of polarity, and therefore exhibits more hydrophobicity [49,67].

Carbon black's high carbon content (>95%) and low inorganic content (ash) is a sought-out property for a reinforcing filler. Carbon black has a higher carbon content and lower hydrogen and oxygen contents as compared to the elemental composition of biochar (regardless of the feedstock). Therefore, carbon black has (a) a lower H/C ratio and thus has higher aromaticity; and (b) a lower O/C ratio and hence has a lower degree of polarity (is more hydrophobic and less hydrophilic) as compared to biochar. The heterogeneity of biochar from different feedstocks makes it complex to identify the optimal feedstock for application as a reinforcing filler in rubber composites, and up to now, its suitability has been researched on a case-by-case basis. Along with a high carbon content, low ash content may contribute to improved mechanical properties [10]. To determine the ash content, proximate analysis following standards by the American Society for Testing and Materials (ASTM) is performed on biochar [87].

Proximate analysis uses thermal decomposition to determine the moisture, volatile matter, ash, and fixed carbon content of biochar samples [87]. Regardless of the feedstock source, biochar volatile matter decreases and ash content increases with increasing pyrolytic temperature (Table 2.1). In general, ash content of biochar is highly dependent on the feedstock source, with wood-derived biochars having the lowest amount followed by agricultural crops and then manures. The study by Enders et al. showed that manures and waste-derived biochars (food, paper mill sludge) have the highest ash contents and wood-derived biochars have the lowest ash content [84]. The higher ash contents in manure-derived biochars may be attributed to their highly diverse composition (proteins, lipids, saccharides, inorganics, minerals, lignin, and cellulose, among

others) which makes them less homogeneous as compared to wood-based feedstocks [41]. Of several studies, the biochar with the lowest ash content (biochar from birch wood) resulted in more promising tensile properties in rubber composites as compared to higher ash biochars (coconut shell, corn stover, corn starch, switchgrass, woody waste) [12-14]. In contrast, carbon black has a very low ash content (typically <1%) and therefore contains only trace amounts of inorganics and impurities, contributing to its homogeneity as a material.

2.3.2 Chemical structure

Carbon black is a form of paracrystalline carbon [88]. As such, its structure is composed of a mixture of amorphous and crystalline forms with turbostratic stacking of quasi-graphitic layers [86,88]. The ratio of amorphous and crystalline structures differs from one carbon black grade to another. Typically, the crystalline portion increases with larger carbon black particle sizes and with an increase in the HTT [88]. For example, carbon black grade N762 has higher crystallinity than N234 due to its larger particle size and graphitized carbon black (higher heat treatment temperature). It also has a higher crystallinity than normal carbon black [88].

The morphology, and consequently the mixture of amorphous and crystalline structures of biochar, depends on both the original feedstock and the pyrolysis temperature [86,89]. Biomass undergoes both physical and chemical transformations with increasing pyrolysis temperatures, altering the molecular structure of the resulting biochar [86,89]. Keiluweit et al. researched the dynamic molecular structure of lignocellulosic-derived biochar at temperatures between 100 °C and 700 °C [86]. They proposed the five following biochar structural categories across this process temperature range: (a) unaltered feedstock material; (b) transition biochar; (c) amorphous biochar; (d) composite biochar; and (e) turbostratic biochar [86]. Their results showed that initially, the feedstock is composed of amorphous lignin, crystalline cellulose, and amorphous hemicellulose, and these structures are unaltered during the initial low temperature step of the thermochemical process. As the temperature further increases, the lignocellulosic biomass undergoes depolymerization forming volatile dissociation products, which form amorphous centers in a nearly intact cellulose crystalline matrix [86]. Further increases in temperature depolymerizes the crystalline cellulose and leaves a randomly disordered amorphous structure composed of aliphatic and aromatic carbon elements. For biochars produced from a determined feedstock, the presence of aromatic carbons in biochar generally increases as the pyrolysis temperature increases [90,91].

Upon further heating, the structure becomes a composite containing turbostratic graphitic crystallites and amorphous carbons. At or above 700 °C graphene- like sheets are formed laterally at the expense of the amorphous components, like aliphatic and aromatic units. Considering these five structural categories proposed by Keiluweit et al., the final structure of a given biochar largely depends on its HTT [86]. In general, biochar becomes more aromatic and carbonaceous with an increase in pyrolysis treatment temperatures. These changes can be observed by the surface chemistry of the biochar.

2.3.3 Surface chemistry

The surface chemistry of the filler is important for two reasons; (a) it influences the interface interactions and surface functionality between the filler and the elastomer; and (b) it determines the toxicity levels and safety levels for human health and the environment. Active points on the edges of the quasi-graphitic layers of carbon black interact with the rubber macromolecules. Other than aliphatic and aromatic groups, the surface chemistry relates to these active points and are referred to as surface functional groups. These oxygen containing functional groups can be acidic or alkaline, and can include carbonyl, carboxyl, pyrone, phenol, quinone, ketone, lactone and ether groups, among others [6]. Also, the presence of different functional groups influences the pH of the material, which has been shown to influence the scorch time during rubber vulcanization [92,93]. To identify the presence of chemical functional groups on the surface of biochar, spectroscopic procedures such as solid-state nuclear magnetic resonance spectroscopy (NMR), attenuated total reflectance Fourier transform infrared (ATR-FTIR) spectroscopy, and X-ray photoelectron spectroscopy (XPS) can be used to obtain qualitative analyses. Using these methods, the peak(s) at a wavelength number or band are assigned to a known functional group [86,91,94]. Interactions between carbon black and the elastomer matrix are in part due to the adsorption of polymeric chains onto carbon black surface oxides. Carbon black's surface contains both hydrogen and oxygen elements. Since carbon black is obtained by partially combusting liquid aromatic hydrocarbon oil, its surface contains large polycyclic aromatic rings [92]. Also, the surface oxides present on carbon black's edges often have oxygen-containing functional groups [92]. These oxygen-containing functional groups largely impact the surface properties of the carbon black and thus its suitable applications [92]. Correlations have been made between carbon black surface oxygen content and the pH whereby higher surface oxygen content results in more acidic pH values

in aqueous dispersions [92]. Looking at the spectra of carbon black, the absorption of infrared (IR) increases with the increase in wavenumber [95]. Comparatively, the spectra of biochars are highly variable and depend on the type of feedstock, pyrolysis conditions (temperature and heating rate), and the presence of inorganic constituents [94]. The high degree of variability between feedstocks leads to differences in surface functional groups however, some generalities can be made. In general, the C-H region of the spectra is mostly aliphatic for biochar's produced at low temperatures whereas this region is mostly aromatic for higher temperature biochar's [46,49,86,94]. Also, the FTIR spectra of biochar's synthesized from lignocellulosic biomass show that organic functional groups are lost as the processing temperature increases [46]. Contrarily, Domingues et al. analyzed the FTIR spectra of chicken manure and coffee husk and found that even at high temperatures, the organic functional groups remained present [46]. These non-lignocellulosic derived biochar's have higher ash contents, which may explain the presence of organic functional groups, even at high temperatures [46,84]. Biochars with high ash content have shown to hinder the formation of aromatic carbon while protecting organic functional groups [46,84].

Table 2.1 Elemental and proximate analyses of biochar from different feedstocks and pyrolysis conditions.

Feedstock	Pyrolysis conditions			Elemental analysis (% wt.)					Proximate analysis (% wt.)				References
	Temperature (°C)	Heating rate (°C/min)	Residence time	C	H	N	S	O	Moisture content	Volatile matter	Ash content	Fixed carbon	
Carbon black				96.0-99.5	0.20-1.30	0.00-0.70	0.10-1.00	0.20-0.50			<1.00		[6]
Biochar													
Pine bark	350	1.7	30 mins.	67.6	3.73		0.01	28.7		39	8.30	53.2	[46]
	450	1.7	30 mins.	75.2	2.74		0.02	24.7		29	7.90	62.8	[46]
	750	1.7	30 mins.	86.3	1.16		0.04	19.1		6.0	14.5	79.4	[46]
Pine wood	450	450	30 s.	75.5	3.70	0.20	0.10	17.0	0.4	5.6	3.50	90.5	[43]
Poplar wood	350		30 mins.	69.9							3.50	54.3	[48]
	400		10 h.	67.3	4.42	0.78					3.50		[49]
	525		10 h.	77.9	2.66	1.07					6.80		[49]
	600		30 mins.	83.1							7.17	75.0	[48]
Douglas fir	350		30 mins.	70.5							0.60	49.6	[48]
	600		30 mins.	87.8							1.13	83.2	[48]
Douglas fir bark	350		30 mins.	66.1							4.72	51.5	[48]
	600		30 mins.	78.1							8.85	73.9	[48]
Spruce wood	400		10 h.	63.5	5.48	1.02					1.90		[49]
	525		10 h.	78.3	3.04	1.17					4.70		[49]
Birch wood	550		2 h.	89.1	1.79	0.21		7.15			1.80		[10]
Oak wood	500		2 s.	85.9	1.40								[45]
Eucalyptus sawdust	350	1.7	30 mins.	70.4	3.81		0.02	24.0		37	0.90	62.2	[46]
	450	1.7	30 mins.	78.6	3.42		0.01	16.6		29	0.70	70.8	[46]
	750	1.7	30 mins.	90.9	1.52		0.04	5.60		6.5	1.10	92.4	[46]
Coffee husk	350	1.7	30 mins.	60.5	3.92		0.09	19.5		35	12.9	52.5	[46]
	450	1.7	30 mins.	61.3	3.65		0.10	19.0		26	12.9	60.9	[46]
	750	1.7	30 mins.	66.0	1.57		0.23	9.80		18	19.6	62.8	[46]
Timothy grass	450	450	30 s.	63.7	3.60	1.90	0.04	23.1	0.7	9.5	7.70	82.1	[43]

Wheat straw	400		5 h.	65.7	4.05	1.05					9.70		[49]
	450	450	30 s.	64.8	3.10	0.80	0.10	23.0	0.6	7.3	8.20	83.9	[43]
	525		5 h.	74.4	2.83	1.04					12.7		[49]
Rice husk	300	7.0	3 h.	47.7	3.19	1.10		24.7	6.8		13.6		[50]
	500	7.0	3 h.	49.1	2.09	0.99		24.8	5.0		18.0		[50]
	700	7.0	3 h.	50.6	1.29	0.65		7.67	3.4		39.2		[50]
Rice straw	300	10.	1 h.	44.7	3.06	1.62		19.3					[51]
	500	10.	1 h.	44.4	1.88	1.35		9.75					[51]
	700	10.	1 h.	44.9	1.24	1.03		5.91					[51]
Corn stover	600		45 mins.	45.1	1.86	0.44		13.0			39.6		[52]
Sugarcane bagasse	350	1.7	30 mins.	74.7	4.26		0.03	17.9		35	1.90	63.0	[46]
	450	1.7	30 mins.	81.6	3.66		0.05	11.3		24	2.10	73.9	[46]
	750	1.7	30 mins.	90.5	1.64		0.06	4.30		7.7	2.20	90.1	[46]
Sewage sludge	300		4 h.	11.8	1.37	1.73		9.27			76.7		[64]
	400		1 h.	21.9	1.85	3.10	0.85				41.3		[66]
	600		1 h.	19.9	0.71	2.04	0.87				74.0		[66]
	700		4 h.	8.10	0.08	0.65		4.11			90.7		[64]
Dairy manure	350	2.5	2 h.	55.8	4.29	2.60	0.11	18.7		54	24.2	23.2	[67]
	700	8.3	2 h.	56.7	0.94	1.51	0.15	4.13		28	39.5	34.7	[67]
Feedlot manure	350	2.5	2 h.	53.3	4.05	3.64	0.45	15.7		48	28.7	23.5	[67]
	700	8.3	2 h.	52.4	0.91	1.70	0.40	7.20		20	44.0	36.3	[67]
Poultry litter	350	2.5	2 h.	51.1	3.79	4.45	0.61	5.63		42	30.7	27.0	[67]
	700	8.3	2 h.	45.9	1.98	2.07	0.63	10.5		18	46.2	35.5	[67]
Swine solids	350	2.5	2 h.	51.5	4.91	3.54	0.80	11.1		50	32.5	17.7	[67]
	700	8.3	2 h.	44.1	0.74	2.61	0.85	4.03		13	52.9	3.80	[67]
Turkey litter	350	2.5	2 h.	49.3	3.60	4.07	0.55	15.4		42	34.8	23.1	[67]
	700	8.33	2 h.	44.8	0.91	1.94	0.41	5.8		21	49.9	29.2	[67]

2.3.3.1 pH

The pH is a simple, yet important property and is influenced by the surface functional groups of the materials [92]. Fillers typically have both acidic and alkaline functional groups present on their surface and their pH is determined by the overall presence of these surface functional groups. Therefore, a filler with an acidic pH has more acidic functional groups than basic functional groups present on its surface, and vice versa for fillers with an alkaline pH [92]. Carbon black produced through the oil furnace process typically has a pH between 4 and 9 [6]. Rositani et al. performed chemical surface analyses of carbon black by infrared transmission spectroscopy [96]. Their results showed that an increase in pH resulted in a decrease in the intensities of hydroxyl and carboxyl groups whereas carbonyl or aromatics and CH groups showed a maximum intensity at pH between 6 and 7. One of the attributes of carbon black is that it is has a low H/C ratio and therefore, is highly aromatic. Consequently, to maximize the aromatics, a filler with a neutral pH is preferred [96]. Additionally, carbon black generally has a nonpolar surface which contributes to the filler and rubber matrix compatibility [97]. Surface functionality, and thus a neutral or slightly acidic pH, contributes to the interactions between the filler-filler matrix, the filler-rubber matrix, and the crosslinking density [97]. The compatibility between these two interfaces promotes homogenous dispersion of the filler within the elastomer matrix [97]. The dispersion level and the interactions that occur between the filler and the rubber matrix have a strong influence on the mechanical properties and thus the reinforcement of the composite material [97]. Additionally, the pH of the filler is found to be a factor in the vulcanization system of the rubber composite. The period before the vulcanization of the rubber mixture begins is referred to as the scorch time. In rubber manufacturing, the scorch time is an important cure characteristic and a longer scorch time is preferred for processing safety [21]. Research shows that carbon black with an alkaline pH increases the vulcanizing reactions (reduces scorch time), whereas slightly acidic or neutral pH fillers delay these reactions (increases scorch time) [93]. To maximize the aromaticity, filler-rubber compatibility, and to increase the scorch time, a neutral or slightly acidic filler is preferred.

Generally, biochar has more alkaline pH than carbon black. However, pH values ranging between 3.1 and 12.2 have been reported in the literature [8,98,99]. Two interconnected factors influence the pH, notably the biochar ash content and the process temperature [8,98,99]. The ash content of a given biochar depends on the feedstock used, with woody feedstocks having the lowest ash content, followed by crop residues and non-lignocellulosic feedstocks [98,99]. Consequently,

biochar derived from wood-based feedstocks, in general, have the lowest pH and biochar from non-lignocellulosic feedstocks have the highest. Also, an increase in pyrolysis temperature removes acidic functional groups and forms carbonates and inorganic alkalis (ash contents) [8,99]. Therefore, an increase in the HTT of the pyrolysis process has been reported to increase the pH for a wide range of feedstocks including for pine bark and sugarcane bagasse [46], douglas fir wood, douglas fir bark, hybrid poplar [48], wheat straw, poplar wood and spruce [49], rice straw [51], sewage sludge [66], dairy manure, feedlot manure, poultry litter, swine solids, and turkey litter [67]. Based on the results from these researchers, there is a positive correlation between pyrolysis temperature, ash content, and the pH of biochar. In general, a higher ash content results in a more alkaline pH. Moreover, increasing the pyrolysis treatment temperature also increases the pH of the biochar. Most biochar samples in the literature have an alkaline pH [46,48,49,66,67]. Consequently, for better performance in a rubber mixture, the surface of biochar can be modified by acid chemical activation to yield biochar with a neutral or slightly acidic pH. Boguta et al. modified wood-based biochar using hydrochloric acid, sulfuric acid, acetic acid, and nitric acid at concentrations of 0.001 M, 0.01 M, 0.1 M, 0.5 M, and 1.0 M [80]. Their results showed that acids of increasing concentrations resulted in biochar with lower pH values. The pH of the activated biochar decreased compared to the control for all acids at all concentrations. However, the reduction at concentrations of 0.001 M and 0.01 M were minimal and resulted in a biochar that was still alkaline. At concentrations of 0.1 M, 0.5 M, and 1.0 M the activated biochar, regardless of the acid used, became acidic.

2.3.3.2 Polycyclic aromatic hydrocarbons

In recent years, biochar has received interest as an alternative filler in rubber composites but the potential negative effects of biochar should be considered. Polycyclic aromatic hydrocarbons (PAHs) are produced by the incomplete combustion of organic materials and, consequently, they are found on the surface of both carbon black and biochar [100-103]. The United States Environmental Protection Agency (USEPA) has listed 16 PAHs as priority pollutants for both human health and the environment; they include naphthalene, acenaphthylene, acenaphthene, fluorene, phenanthrene, anthracene, fluoranthene, pyrene, benzo(a)anthracene, chrysene, benzo(b)fluoranthene, benzo(k)fluoranthene, benzo(a)pyrene, dibenz(ah)anthracene, benzo(ghi)perylene, and indeno(1,2,3–c,d)pyrene [49,101,104]. The International Biochar

Initiative (IBI) and the European Biochar Certificate (EBC) are organizations that set the maximum allowable threshold limit of PAHs in biochar [49,105,106]. Previously, these two organizations had similar allowable limits of PAHs with values ranging between 6 and 20 mg/kg for the IBI, while the EBC set the PAH limit to below 4 mg/kg and 12 mg/kg for premium and basic grade biochar, respectively [105-107]. However, in 2015, the IBI updated their guidelines and the new PAH allowable limit now ranges between 6 and 300 mg/kg [106,108]. The guidelines set forth by the IBI and the EBC now have a significant difference between the maximum allowable threshold limit of PAHs in biochar and therefore, this value is not yet standardized [106].

The pyrolysis process is the key factor responsible for the occurrence of PAHs on the surface of biochar [105] and thus the PAH formation mechanisms and factors that influence their formation depend on the processing conditions. In general, the HTT during pyrolysis plays the largest role in determining the quantity of PAHs present in biochar [104-106]. However, residence time and feedstock source are also relevant factors [100]. A study by Hale et al. quantified the total PAHs present in biochar from a wide range of feedstocks such as digested dairy manure, food waste, paper mill waste, corn stover, wheat straw, and pine wood, among others; they produced 50 samples of biochar with HTTs between 250 °C and 900 °C and via slow pyrolysis, fast pyrolysis, and gasification. Their results showed that the total PAH concentrations ranged between 70 mg/kg and 45,000 mg/kg and varied based on the feedstock source, pyrolysis temperature, and residence time [100]. In the study by Hale et al., biochar produced from slow pyrolysis contained lower concentrations of PAHs as compared to those produced by fast pyrolysis [100]. Hale et al. hypothesized that during slow pyrolysis, the PAHs that are formed escape to the gaseous phase whereas during fast pyrolysis these PAHs condense onto the biochar surface [100]. Contrary to the clear trend between slow/fast pyrolysis and PAH concentration [100,105], research shows conflicting results on the relationship between HTT and PAH concentration. According to certain researchers, the concentration of PAH increases with an increase in HTT [106,109] whereas, others found that the concentration of PAHs decreased with an increase in pyrolysis temperature [100]. Moreover, in other studies, PAH concentrations reached a maximum mid-temperature range [49,104,110]. The study by Keiluweit et al. provided a qualitative and quantitative assessment of PAHs present on biochars from wood and grass feedstocks produced under different HTT [104]. Their results showed that biochars produced at temperatures of 400 °C and 500 °C had far greater concentrations of PAHs than biochars produced at lower and higher temperatures. Similar results

were shown in the study by Kloss et al. where they found higher concentrations of PAHs in biochars produced at 400 °C and 450 °C than at 525 °C [49].

These examples underline the variety of PAH concentrations that can be found in biochar and depends on the feedstock source and the pyrolysis conditions. The PAH extraction method may also play a role in the variability of PAH concentrations from one study to another [105]. In several studies [49,100,104], regardless of the feedstock source, the pyrolysis operating conditions, and the extraction method, the PAH concentrations fall within the acceptable range set forth by the IBI guidelines. To the contrary, some biochar's PAH concentrations exceeded the maximum allowable threshold limit established by the EBC. Based on the literature, producing biochar by slow pyrolysis and at higher temperatures may yield biochar with lower concentrations of PAHs.

2.3.4 Particle size distribution and surface area

The size and structure of filler particles are fundamental properties that impart reinforcement to the elastomer [10,79]. The diameter of carbon black primary (elementary) particles are between 10 and 90 nm and carbon black is therefore considered a nanomaterial [111]. These nanoparticles do not exist as separate particles, rather they form three-dimensional aggregates, held together by van de Waals forces, creating aggregate sizes between 100 and 300 nm [111]. The sequence of carbon black structural development, from primary (elementary) particles to aggregates, is shown in Fig. 2.1. The extent to which aggregates form designates its structure and depends on the manufacturing process and the carbon black grade [79,111]. The ASTM grades carbon black based on their primary particle size and their aggregate structure. Smaller primary particles form aggregates of higher structure and higher specific surface area, and thus impart more reinforcement to the elastomer [79,111]. The carbon black grading structure follows a four-character code (Nxyz) where N stands for normal curing behavior and the xyz stands for the reinforcing behavior based on the particle size and the aggregate structure of the filler [111-113]. Specifically, x refers to the average surface area and thus the primary particle size, and the yz value is assigned arbitrarily but it is generally agreed upon that a higher yz value is assigned to a carbon black that has a higher aggregate structure [111,113]. According to the ASTM standards on carbon black classification, the primary particle size is inversely proportional to the specific surface area. For example, primary particles between 1 and 10 nm give specific surface areas greater than 150 m^2g^{-1}, whereas particles between 201 and 500 nm have low specific surface areas up to 10 m^2g^{-1} [111,113]. The x value ranges from 0 to 9, where 0 refers to the highest average nitrogen surface area and the smallest

primary particle size [113]. For example, carbon black grade N330 has a higher average surface area and smaller primary particle size as compared to N772 and thus, grade N330 will provide more reinforcement to the elastomer. Smaller primary particles form aggregates of higher structure and higher specific surface area and thus, improve the rubber-filler interactions by creating more crosslinks between the filler and the polymer chains [79,111]. To improve the physical adsorption of the filler surface and the polymer chains, smaller primary particles (up to 100 nm in size), higher aggregate structure, and higher specific surface area are preferred properties of the filler material [79].

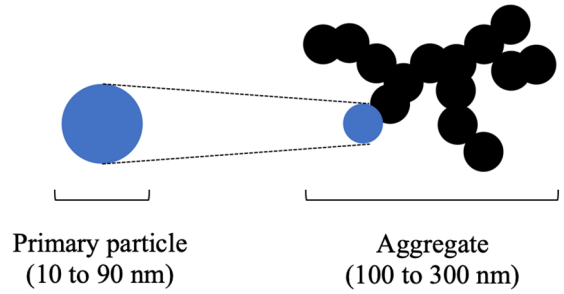

Figure 2.1 Carbon black structure development (from primary particle to aggregate structure).

The industry is looking for a material with similar characteristics to that of carbon black. In the literature, carbon black's morphology, specifically its nanoparticle size, high structure aggregates, and high specific surface area are important properties. Unlike carbon black, biochar can be synthesized from a wide range of feedstocks and pyrolysis parameters and therefore, yield biochars with different properties [114,115]. This variability doesn't allow for simple classification and biochars particle size distribution, aggregate structures, and surface areas are specific to a given feedstock and operating conditions. Accordingly, researchers have attempted to relate the physical properties of biochar to the feedstock material and pyrolysis temperature [49,52,67,76,86,116,117]. Some examples of surface areas from different feedstocks at various pyrolysis temperatures can be found in Table 2.2.

In many applications such as in soil systems smaller biochar particles are often more desirable as they have higher specific surface areas, and this allows for greater physical contact between the particles and the surrounding medium [118]. Specific to rubber composites, smaller

filler particles allow for greater interaction between the particles and the elastomer matrix, increasing the crosslinking density [79]. As seen in Table 2.2, regardless of the feedstock source, an increase in the pyrolysis temperature increases the surface area. Conversely, some researchers found that the surface area increases up to a point where structural breakdown occurs, leading to a decrease in surface area [86,115,119]. In general, the maximum surface area observed occurs between 450 °C and 750 °C, and the peak value differs based on the feedstock source [115]. A study by Kim et al. found that pitch pine biochar surface area increased from 4.8 m^2g^{-1} to 175.4 m^2g^{-1} as the HTT increased from 400 °C to 500 °C [116]. These findings are consistent with observations by Keiluweit et al. where an increase in temperature increased the surface area, and a dramatic rise in surface area was observed between 400 °C and 500 °C for wood and grass feedstocks [86]. Similar trends occur for manure-based feedstocks. Cantrell et al. synthesized biochars from dairy manure, feedlot manure, poultry litter, separated swine solids, and turkey litter [67]. Their results showed a dramatic rise in surface area between 350 °C and 700 °C for all feedstocks [67]. In a similar study, Pariyar et al. researched the effect of pyrolysis temperature (350 °C, 450 °C, 550 °C, and 650 °C) on the physicochemical changes of five different feedstocks (pine saw dust, rice husk, food waste, poultry litter, and paper sludge) [120]. Their results showed that the surface area ranged from as high as 443.79 m^2/g, and the surface area increased with increasing process temperatures. Also, the lignocellulosic feedstocks had higher surface areas as compared to the non-lignocellulosic types at the same temperatures. From the studies presented in Table 2.2, the biochar surface area was greatest for wood-based feedstocks, followed by agricultural wastes, and then non-lignocellulosic feedstocks. Regardless of the feedstock source, at pyrolysis temperatures below 400 °C, the biochars had surface areas comparable to lower grade carbon blacks (average surface areas less than 10 m^2g^{-1}). At temperatures between 450 °C and 750 °C, some biochars, such as pine saw dust, paper mill sludge, rice husk, dairy manure, and ponderosa pine, among others, had surface areas comparable to higher grade carbon blacks (average surface areas greater than 70 m^2g^{-1}).

Table 2.2 Some examples of biochar surface areas from different feedstocks and pyrolysis temperatures.

Feedstock	Pyrolysis temperature (°C)	Surface area $BET - N_2$ $(m^2 g^{-1})$	Reference
Ponderosa pine	300	3.00	[86]
	400	28.7	
	500	196	
	600	392	
	700	347	
Dairy manure	350	1.64	[67]
	700	187	
Poultry litter	350	3.93	[67]
	700	50.9	
Pitch pine	300	2.90	[116]
	500	175	
Wheat straw	400	4.80	[49]
	525	14.2	
Poplar wood	400	3.00	[49]
	525	55.7	
Sewage sludge digestate	250	0.80	[117]
	550	12.7	
Rice husk	350	11.6	[120]
	650	281	
Paper mill sludge	350	3.19	[120]
	450	15.0	
	550	61.5	
	650	87.2	
Pine saw dust	350	3.39	[120]
	450	180	
	550	432	
	650	444	

The surface area is inversely proportional to the primary particle size. Higher grade carbon blacks are characterized by having greater surface area and smaller primary particles. For biochar to be an effective reinforcing filler, its primary particles must be comparable to carbon black and thus should also be nanomaterials. The initial feedstock size can impact the biochar particle size distribution [114,116]. Yargicoglu et al. found that the biochar particle size distribution of different wood residues depend on the initial particle size of the feedstock, with smaller feedstock particles resulting in finer grained chars [114]. However, the most important factor that influences the

particle size is the pyrolysis temperature, whereby higher temperatures lead to smaller sized particles [9,115,116]. Kim et al. synthesized biochar from pitch pine and determined the biochar particle size distribution [116]. Their results showed that higher temperatures produce biochar with smaller particle size distributions; 20% and 30% of particles (by volume) were ~50 μm at 300 °C and 500 °C, respectively. At 300 °C, the particle size distribution had a wider range compared to that at 500 °C, where the biochar particle size distribution (as a cumulative volume) was evenly distributed among ~50 μm, 50–100 μm, and 100–500 μm [116]. Carbon black has a relatively narrow particle size distribution and is void of large particles [9]. Comparatively, biochar has larger primary particles than carbon black. Rather than being on the nanoscale, biochar particle size tends to be on the micrometer scale.

Although particle size tends to decrease with an increase in temperature, the particles are often still much larger than those of carbon black. Although the properties of biochar have been extensively studied in the literature, the particle size has not received much attention. Some studies have looked at biochar particle size reduction methods to achieve enhanced physical properties such as increased surface area. Although limited, these studies show that milling the biochar can significantly reduce the particle size as compared to the unmilled biochar. Biochars surface area and particle size distributions after size reduction are shown in Table 2.3, as a function of the feedstock material, milling method, and operating conditions. Peterson et al. synthesized biochar from birchwood and reduced the biochar size with a gyro puck mill [10]. Unlike gyro puck milling, ball milling is inexpensive, reproducible, and can be scaled-up [10,83]. Ball milling has been used to modify the physicochemical properties of biochar by increasing its surface area and reducing its particle size [52,81,83]. Peterson et al. synthesized biochar from switchgrass and corn stover, and after a ball milling operation step, they found that both biochars smallest aggregates were 200 nm in size [52]. Similarly, Naghdi et al. studied the milling effects (time, rotational speed, and ball to mass ratio) on the physicochemical properties of biochars synthesized from pine wood [81]. Their results showed that after milling, biochar with initial particle sizes of 3 mm could be reduced to an average particle size of 60 nm; and an increase in specific surface area was also observed. The variation in final particle sizes is due to the milling conditions where longer grinding times led to the agglomeration of the particles, and therefore shorter grinding times are favorable to produce nanobiochar [81]. A similar study by Lyu et al. reported an increase in surface area and the production of sub-micron particles after ball milling biochar [82]. It can be seen from these

Table 2.3 Biochars surface area and particle size distributions as a function of the feedstock material, milling method, and operating conditions.

Feedstock	Size reduction method	Milling conditions	Surface area $BET - N_2$ $(m^2 g^{-1})$	Particle size distribution	References
Birchwood	Gyro puck mill	- Smooth horizontal grinding with minimal vertical vibration		Most particles were smaller than 1000 nm, 19% were smaller than 300 nm, and the largest particle size was 10,000 nm	[10]
Pine wood	Planetary ball mill	- 2.4 mm stainless steel balls used as milling media - Mixed for 1.6h at 575 rpm, and 4.5 g/g ball to powder ratio	47	Average particle size of 60 nm	[81]
Sugarcane bagasse	Planetary ball mill	- Ball diameter of 6 mm used as milling media - Mixed for 12h at 300 rpm, rotation direction altered every 0.5h, and biochar to ball mass ratio of 1:100	360	140 nm	[82]
Bamboo	Planetary ball mill	- Ball diameter of 6 mm used as milling media - Mixed for 12h at 300 rpm, rotation direction altered every 0.5h, and biochar to ball mass ratio of 1:100	280	140 nm	[82]
Hickory wood chips	Planetary ball mill	- Ball diameter of 6 mm used as milling media - Mixed for 12h at 300 rpm, rotation direction altered every 0.5h, and biochar to ball mass ratio of 1:100	270	133 nm	[82]

results that milling does achieve smaller particle sizes by reducing the particles from the millimeter scale to the sub-micron scale. However, even after milling, biochar tends to have larger particles

than carbon black. Conversely, milling does make the particle size distribution of biochar more narrow, compared to the unmilled sample, which is a characteristic of carbon black.

2.4. Biochars performance as a filler in rubber composites

2.4.1 Curing characteristics

Raw rubber, being a viscoelastic material, requires processing to create crosslinks between the long polymer chains. This reaction is often called “curing” or “vulcanization” whereby the rubber is heated and mixed with the filler material, vulcanizing agent (sulphur), and the vulcanizing system to create crosslinks and transforms the viscoelastic rubber into a practical, elastic solid material. Rheological behavior obtained using a rubber process analyzer (RPA) gives insight on properties such as the processability, viscoelastic characteristics, curing properties, and physical properties of the cured rubber. In the rubber industry, the moving die rheometer (MDR) and the oscillating disk rheometer (ODR) are the most used equipment during curing to produce vulcanization curves [121]. The working principle of both these curemeters is that a rubber sample is placed inside a cavity with a rotor that oscillates at a constant angular displacement, and vulcanization occurs at a constant temperature [121]. As the rubber material undergoes vulcanization, and the crosslinks between the polymer chains are formed, the torque required to shear the compound increases [121]. The vulcanization process can be monitored using the curemeter, and a curve of torque (or modulus) versus time can be produced. An example of a carbon black N772 vulcanization curve can be seen in Fig. 2.2. The scorch time (t_{s2}), the optimum cure time (t_{90}), and the degree of vulcanization are the most important cure characteristics that can be seen on the vulcanization curve [121]. The induction period, also known as the scorch time, is required to avoid premature crosslinking and for rubber processing safety; the optimum cure time is characterized by the time necessary to achieve 90% of the maximum torque; and the degree of vulcanization refers to the marching, plateau, or reversion of the torque versus time graph [9,121]. In rubber processing, a scorch time is required and the vulcanizing curve that reaches an equilibrium (plateau) is preferred [121]. A curve that reaches a plateau is desirable as this characteristic is an indication that the optimal cure time has been reached. Processing beyond this point can produce undesirable properties and is time and energy intensive.

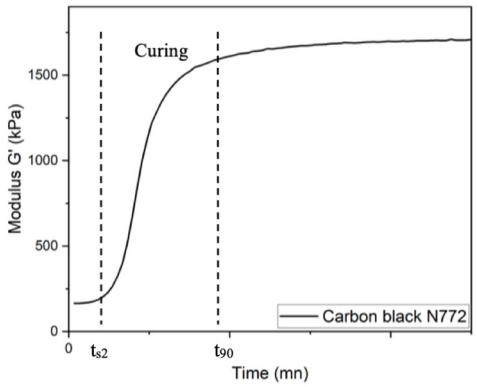

Figure 2.2 An example of a vulcanization curve.

2.4.1.1 Comparing carbon black and biochar filled rubber cure kinetics

Although there are only a few studies on the cure kinetics of biochar filled rubber, the similarities and differences between the vulcanizing behavior of rubber filled with carbon black and rubber filled with biochar can be identified. Table 2.4 presents the scorch time (t_{s2}), optimum cure time (t_{90}), minimum torque M_L, and maximum torque M_H as a function of the rubber compound and the filler loading (for both carbon black and biochar samples).

As the filler loading increases, the scorch time (t_{s2}) and the optimum cure time (t_{90}) of rubber filled with biochar and carbon black follow similar decreasing trends [9,11,112]. However, at the same filler loading, rubber filled with biochar exhibits shorter scorch and optimum cure times as compared to the carbon black filled rubber compound. This may be attributed to the surface chemistry of the biochar fillers, which may be interacting with the vulcanizing system, thus accelerating the cure time [11]. Generally, a longer scorch time is preferable to ensure processing safety and to avoid pre-mature crosslinking [9]. Therefore, the surface chemistry of biochar may be responsible for the reduced scorch times, producing an undesirable vulcanizing behavior. Contrarily, the shorter optimum cure times achieved by biochar filled rubber compared to carbon black is indicative of improved production efficiency. Another important characteristic of the vulcanization curve that was not mentioned in any of the previous studies on the cure kinetics of biochar filled rubber compounds is the presence of a plateau profile or an equilibrium.

Table 2.4 The scorch time, optimum cure time, minimum torque, and maximum torque as a function of the rubber compound and the filler loading.

Compounds	Filler loading (phr)	Scorch time t_{s2} (min)	Optimum cure time t_{90} (min)	Minimum torque M_L (Nm)	Maximum torque M_H (Nm)	Reference
CB N330 filled NR	5	2.81	5.48		0.920	[9]
	10	2.15	4.02		1.024	
	15	1.75	3.75		1.047	
CB N330 filled SBR	40	4.05	8.18	0.163	1.411	[11]
Dead leaf activated carbon filled NR	5	2.02	4.85		0.905	[9]
	10	1.51	3.11		0.944	
	15	1.08	2.47		1.090	
Lignin biochar filled SBR	10	3.58	7.98	0.089	1.022	[11]
	20	2.22	5.90	0.107	1.252	
	30	1.70	5.50	0.130	1.379	
	40	1.53	5.78	0.146	1.386	
Marble processing industry sludge biochar filled NR	60	1.76	4.86	0.043	0.352	[122]
Unfilled NR	0	3.02	6.38		0.811	[9]

A plateau profile at the end of the curve, in comparison to a marching modulus, ensures that the optimum cure time can be determined and is reached within a reasonable amount of time [123]. Also, a reversion profile is indicative that the sample has been over processed and that the crosslinks are starting to break. Some rubber mixes are characterized by having cure profiles with marching moduli [123]. For example silica filled rubber compounds often have this undesirable trait [124]. Similarly, Barana studied the effect of using softwood kraft lignin as a reinforcing filler in rubber compounds [125]. Although lignin was used directly, without undergoing any pyrolysis operations, it was shown that the vulcanizing curve never reached an equilibrium and rather, was characterized by a marching modulus [125]. A marching modulus may be caused by the filler particles flocculating during vulcanization [124]. This observed flocculation can be a result of poor compatibility between the filler and the rubber. Though the research on the cure kinetics of biochar filled rubber compounds is limited, further research would be useful in understanding biochar's degree of compatibility with rubber.

In a recent study by Lay et al., an unfilled rubber compound had a lower maximum torque as compared to a bio-based (dead leaf) activated carbon filled natural rubber, and carbon black grade N330 filled natural rubber [9]. These findings are consistent with the literature as without a

filler material, the long polymer chains of rubber are easily broken down by shear forces during mixing [9]. For both the biochar and carbon black filled rubber compounds, the maximum torque (M_H) increased with an increase in filler loading [9,11,78]. Fillers are used in rubber compounds to increase the viscosity and thus improve the stiffness of the matrix. Therefore, a larger filler loading leads to more interactions between the rubber and the filler, and increases the viscosity. The higher maximum torque achieved with an increase in filler loading is attributed to an increase in filler-rubber interactions. Carbon black's fundamental properties, notably its high surface area and small particle size, are responsible for its strong interactions with the rubber matrix. Since biochar tends to have a lower surface area and larger particle sizes, there may be fewer interactions with the rubber, which may explain why generally compounds filled with carbon black have a higher maximum torque as compared to biochar filled rubber with the same filler loading.

2.4.2 Mechanical performance

By analyzing the mechanical properties of filled rubber, the reinforcing performance of the filler within the elastomer matrix can be evaluated. In the rubber industry, standard tensile stress-strain tests are performed on unfilled and filled rubber to evaluate the influence of the filler on the mechanical performance of the rubber compound [112]. Similarly, these tensile stress-strain tests can be used to evaluate the suitability of alternative fillers, like biochar, and to compare the results to those of the industry standard filler, carbon black. The results are often displayed in the form of a stress-strain curve. When carbon black is used as a filler in rubber, there is a noticeable increase in stress with an increase in strain compared to the unfilled rubber sample [112]. This increase in tensile strength is characteristic of a reinforcing filler. Additionally, an increase in the elongation at break can be seen on the tensile stress-strain tests and is indicative of a reinforcing behavior. Robertson and Hardman proposed the following five regions of reinforcement on a typical filled rubber stress-strain curve, defined based on the slope of the stress-strain curve notably the modulus, $E=d\sigma/d\varepsilon$: (a) Payne effect; (b) minimum/transition; (c) stress upturn; (d) modulus plateau; and (e) ultimate softening [112]. In the first region, the Payne effect, a well-known feature of the stress-strain behavior of filled rubber compounds, is observed [112]. The Payne effect is characterized by a rapid reduction in the storage modulus (E') and a peak in the loss modulus (E") as the strain amplitudes are increased. In carbon black filled rubber compounds, the Payne effect can be attributed to weak physical bonds between adjacent filler aggregates [112]. A study by

Warasitthinon and Robertson found that the greatest influence to this region was the filler loading [126]. They found that rubber compounds with higher filler loadings demonstrated greater reductions in storage modulus therefore, the Payne effect was amplified [126]. The second region is a transition between the strain softening observed in Region 1 and the strain stiffening that occurs in Region 3. The third region is characterized by an increase in the storage modulus as the strain increases. This increase is a result of the filler-rubber interactions [112]. The fourth region is characterized by a plateau in the storage modulus, which indicates that the filler is well dispersed within the elastomer matrix. Upon further strain, the crosslinks between the filler and rubber chains start to break and the storage modulus decreases (Region 5). A reinforcing filler therefore increases the tensile strength and increases the elongation at break (or strain at fracture) of the rubber compound and combined, these attributes lead to an increase in material toughness.

Comparing the tensile stress-strain curves of carbon black and biochar filled rubber can give insight on the suitability of biochar as a reinforcing filler. First, the overall shape of the stress-strain curve should be analyzed. The curve should feature the five previously stated regions, proposed by Robertson and Hardman [112]. Also, the reinforcing index (RI), is used to determine the reinforcing behavior of a given filler. The value of the reinforcing index (RI) is obtained from the stress-strain curve, and is equal to the ratio of the stress at 300% strain (M300) to the stress at 100% strain (M100) (RI=M300/M100) [112]. A larger RI value is preferred and is indicative of a reinforcing behavior within the elastomer matrix [11]. For carbon black, longer mixing times lead to larger RI values [112]. The longer mixing times are conducive to the fracturing of the carbon black aggregate particles. The fractured particles are then more evenly distributed within the elastomer matrix, which improves the stress distribution. Therefore, the rubber compound can withstand more stress for a given strain and leads to a larger RI value. Although longer mixing times improve the stress-strain behavior of the carbon black filled rubber, for time efficiency and energy savings, it is preferable to find a balance between mixing times and an adequate RI value.

When determining the reinforcement of a filler, dynamic mechanical properties like the storage modulus (E' or G'), loss modulus (E" or G"), complex modulus (E* or G*), glass transition temperature (T_g), and tan δ peaks can also be evaluated to give further understanding on the compounds viscoelastic properties. The storage modulus is the ability of the material to store energy and thus, the measure of elasticity of a material. Similarly, the loss modulus is the ability of the material to dissipate energy and thus, highlights the viscous portion of the material. The

complex modulus is the sum of the storage and loss moduli. The T_g, indicates the temperature at which the material transitions from a glassy state to a viscous or rubbery state. The tan δ is defined as the ratio of the loss modulus to the storage modulus (tan δ = E''/E') and indicates the degree of energy dissipation or damping of the compound. A higher G′ at a given temperature, is indicative of stronger filler-rubber interactions which is again, attributed to carbon blacks small particle size [13,18]. Additionally, a lower tan δ peak is a result of the restrictive movement of the rubber chains caused by the strong interactions between carbon black and the rubber matrix [13,18]. The T_g, of the rubber compound can be seen on the storage modulus versus temperature graph as the temperature at which the storage modulus decreases. Similarly, on the tan δ versus temperature graph, the glass transition temperature is the temperature at which the peak of the tan δ is observed.

2.4.2.1 Mechanical performance of biochar filled polymers

Monhanty et al. have studied the use of biochar as a renewable replacement for carbon black [37-39]. Although these inventions relate to the use of biochar as a replacement filler for carbon black in thermoplastic polymers, analyzing these patents can give insights on the use of biochar as a replacement for carbon black in composite materials. This information can then be used to determine whether biochar would be suitable as a reinforcing filler in thermoset polymers such as rubber compounds. In all three patents, the selected feedstocks for biochar production included plant fibers, municipal solid waste, agricultural biomass, forest biomass, animal/bird manure, and other waste streams of agricultural products (dried distillers grains, coffee chaff, spent tea leaves, spent coffee grinds, etc.) [37]. The biochar samples were produced at temperatures ranging between 400 °C and 900 °C. In one patent, when mixing with the thermoplastic polymer, the biochar had a maximum particle size of 20 μm and a carbon content of at least 90% [37]. Although the biochar had a larger particle size and lower carbon content compared to the control carbon black sample, the mechanical properties of the biochar filled compound were equal or superior to that of carbon black [37]. Although this information is promising, the final percentage of biochar in the composite varied between 1 wt% and 6 wt% which is much lower than the filler loading required in rubber compounds. In another patent, Mohanty et al. used between 5 and 30 wt% biochar as filler in thermoplastic polymers, which is a more comparable filler loading for rubber compounds [39]. The composites had improved mechanical properties such as strength and rigidity/modulus, among others, compared to the unfilled material [39]. Similarly, they used 20–

40 wt% biochar as filler in nylon hybrid biocomposites [38]. Here, the mean particle size was smaller and ranged from 2 µm to 3.8 µm, which is closer to the particle size of carbon black. The biochar filled composites showed improved impact strength, tensile strength, and flexural strength compared to the unfilled composite [38]. Although the addition of biochar increased some mechanical properties, the results were not compared to carbon black's performance and therefore biochars suitability as a replacement for carbon black is unknown.

Recently, there has been interest in the use of biochar as a filler specifically in rubber compounds. However, the studies that evaluate the mechanical performance of biochar filled rubber are limited. Table 2.5 displays recent results of the mechanical performance of rubber compounds filled with biochar as a function of the feedstock source, pyrolysis conditions, and the biochar physicochemical properties. Small filler particles are crucial for obtaining desirable mechanical performances like high tensile strength, toughness, and storage modulus. These properties depend on strong interactions occurring between the filler and the rubber, a result of small filler particles. Biochar tends to have a wider particle size distribution and a larger average particle size compared to carbon black [9]. Therefore, the mechanical performance of biochar is expected to underperform compared to carbon black filled rubber.

2.4.2.2 Comparing the mechanical performance of carbon black and biochar filled rubber

Several researchers have studied the use of biochar as a renewable replacement for carbon black in rubber compounds [9-16,18]. These studies often compared biochars mechanical performance to that of a carbon black filled rubber control sample. The following section first compiles the results of the mechanical performance of rubber filled with carbon black. Then the performance of biochar filled rubber from different feedstocks are reviewed and the suitability as a reinforcing filler is determined by comparing the results to carbon black filled rubber.

The properties of the filler strongly influence the mechanical performance of the rubber compound. Carbon black's narrow particle size distribution and its mean particle sizes on the nano to sub-micron scale, contribute most significantly to its reinforcement in rubber [9-11,13,18]. This is highly agreed upon in the literature and is explained by smaller filler particles increasing the interactions between the filler and the rubber molecules. This leads to efficient stress transfer between the rubber and the reinforcing filler particles therefore, higher tensile strength is observed

Table 2.5 The mechanical performance of rubber compounds filled with biochar as a function of the feedstock source, pyrolysis conditions, and the biochar physicochemical properties.

Feedstock [reference]	Pyrolysis conditions	Biochar physicochemical properties				Filler loading (phr)	Mechanical performance		
		Density (g/cm^3)	%C	%Ash	Particle size (µm)		Tensile strength (MPa)	Elongation at break (%)	Toughness (MPa)
Dead leaf [9]	Prepared by pyrolysis at 1000°C at a heating rate of 10°C/min under nitrogen gas flow of 100 cm^3/min and was activated by CO_2 at 100 cm^3/min flow rate for 60 minutes when the HTT was reached	1.59	82.58		28.86	5	18	750	
						10	17	700.	
						15	16	675	
Lignin [11]	Prepared by pyrolysis at 800°C for 2h at a heating rate of 10°C/min under nitrogen gas flow of 100 ml/min		84.44		0.474	40	9.9	507	
Rice husk [18]	Pyrolysis method not specified				15.03		14	1370	
Pawlownia elongate (fast- growing hardwood tree) [16]	Pyrolysis method not specified	1.75	92.68	2.90		30	15	522	32.2
Birchwood [10]	Prepared by slow pyrolysis at 550°C for 2h	1.45	89.05	1.80	Majority smaller than 1	10	4.7	437	10.1
						20	6.6	586	20.1
						30	8.0	538	25.3
						40	8.3	447	24.6

[9,18]. Higher filler loadings have a greater number of filler-rubber interactions and therefore, tensile strength increases as the carbon black loading increases [9,10]. In the study by Lay et al., they found that stronger (or more) interactions between the rubber and carbon black particles lead to a lower elongation at break [9]. In contrast to the trend observed for the tensile strength, increasing the filler loading tends to decrease the elongation at break of the rubber compound. Adding fillers constrains the elastic behavior of the rubber by increasing the stiffness and rigidity, resulting in a decrease in elongation at break as the filler loading is increased. This was also observed in other studies [10,12]. Moreover, carbon black increases the toughness of the rubber compound [12]. A tough material is characterized by being both strong (high tensile strength) and ductile (deforms easily). In several studies, the tensile strength, elongation at break, and toughness of carbon black filled rubber varied between 1–23 MPa, 156–1225%, and 5–52 MPa, respectively [9-13,16,18].

Lay et al. studied the use of dead leaf biochar produced at 1000 °C as a potential reinforcing filler in natural rubber compounds [9]. Their results showed that compared to unfilled rubber, filling rubber with 15 phr biochar increased the tensile strength by 8% and decreased the elongation at break by 5%. This indicates that the biochar does provide some reinforcement to the rubber. However, the biochar filled rubber underperformed compared to the traditional carbon black. The tensile strength of carbon black filled rubber was higher and the elongation at break was lower compared to rubber filled with biochar [9]. The smaller particle size and thus the stronger interactions between carbon black and the rubber explains these results. When carbon black is used as the filler, the tensile strength increases and the elongation at break decreases, with filler loading. However, the reverse occurred for rubber filled with dead leaf activated carbon [9]. The inability of the biochar to homogeneously disperse within the rubber matrix may have led to particles agglomerating, leading to a decrease in tensile strength with increasing filler loading. Likewise, the increase in elongation at break with increasing filler loading is indicative of weak filler-rubber interactions. In this study, dynamic mechanical properties of the rubber compounds were not explored.

Peterson has conducted numerous studies on biochars suitability as a replacement filler for carbon black in rubber compounds [10,12,13,16]. The results from these studies have shown that carbon blacks mechanical performance outperforms that of biochar, regardless of the feedstocks used. In search of better results while attempting to replace or reduce the use of carbon black,

Peterson conducted research on different blends of fillers. The blends of fillers that were tried, as well as the most promising results are shown in Table 2.6.

Table 2.6 Different blends of fillers and results.

Fillers	Blends tried (ratio)	Results	Reference
Starch:corn stover biochar	1:3	A filler loading of 10 phr and a 3:1 blend of starch:corn stover biochar had superior reinforcement, tensile strength, and toughness when compared to a control carbon black-filled sample	[12]
	1:1		
	3:1		
Paulownia wood biochar:carbon black	75:25	A filler loading of 30 phr and a 50:50 blend of paulownia wood biochar:carbon black had equal or better elongation and toughness but had a slight decrease in tensile strength (<6%) compared to a carbon black-filled sample	[16]
	50:50		
Birchwood biochar:carbon black	25:75	A filler loading up to 30 phr and a 50:50 blend of birchwood biochar:carbon black had equal or better tensile strength, elongation, and toughness compared to a control carbon-black filled sample	[10]
	50:50		
	75:25		
Woody waste biochar:carbon black	25:75	A filler loading of 10 phr and a 50:50 blend of woody waste biochar:carbon black had equal or better tensile strength, elongation, and toughness compared to a control carbon-black filled sample	[13]
	50:50		
	75:25		

Moreover, Peterson performed dynamic mechanical analysis on the biochar filled rubber samples [10,12,13]. In all the studies, at 40 phr filler, the shear storage modulus (G′) was highest for carbon black and lowest for biochar filled rubber, at the same temperature. Also, as the ratio of biochar:carbon black blend increased, the shear storage modulus decreased. Similarly, carbon black had a lower tan δ peak compared to the biochar filled rubber, and the peak increased as the biochar:carbon black blend increased. These findings are consistent with results obtained from Lyu et al. whereby carbon black had a higher shear storage modulus and lower tan δ peak compared to biochar made from rice husk [82]. The shear storage modulus tended to increase with higher filler loadings [10,12,13]. Jiang et al. found similar results with biochar made from lignin [11]. The higher shear storage modulus and the lower tan δ peak observed with carbon black compared to biochar filled rubber is indicative that carbon black has stronger or more interactions with the rubber matrix. These results demonstrate the ability to blend different renewable materials to try and achieve a balance between favorable properties which cannot be met with the individual bio-based fillers. Although some of the blends showed equal or better results in terms of tensile

properties at higher filler loadings, the dynamic mechanical analyses showed improved results only at low filler loadings. Therefore, although the blends showed some reinforcement, the comparable results obtained only at low filler loadings suggests that further research is needed before biochar can successfully replace carbon black in rubber tires. Rubber compounds are complex materials and although these studies showed that some blends achieved desirable mechanical performance, the total effect it had on the rubber matrix was not explored.

2.4.2.3 Improving mechanical performance through particle size reduction

Since research shows that the mechanical performance of filled rubber relies on the particle size of the filler, recent studies have focused specifically on modifying the size of biochar particles to achieve improved mechanical properties [11,15,17,18,127]. Jiang et al. converted industrial waste lignin into nano-biochar as a renewable reinforcing filler of styrene-butadiene rubber (SBR) [11]. They achieved nano-scale particles (mean agglomerate particle size of 474 nm) using a planetary ball mill, a common top-down method of size reduction [11]. The biochar particle size was comparable to the commercial carbon black N330, which may be responsible for the observed reinforcement. Their results showed that at 40 phr, the mechanical performance of SBR filled with biochar was similar to that of carbon black. In another study, Li et al. evaluated the influence of rice bran carbon particle size (3.4 μm, 15.2 μm, 35.3 μm, and 57 μm) on the properties of the rubber compound [15]. They found the biochar with the smaller particle size had a more narrow particle size distribution and as the particle size increased, the particle size distribution became wider [15]. Their results showed that even the biochar with the smallest particle size (3.4 μm) did not homogeneously disperse within the rubber matrix and the dispersion became worse with larger filler particles [71]. Regardless, the rice bran carbon did provide some reinforcement to the rubber as compared to the unfilled sample. Li et al. found that the tensile strength increased as the particle sizes decreased and with higher filler loadings [15]. However, when comparing the mechanical properties to that of carbon black, the rice bran carbon underperformed. Carbon black showed stronger interactions between the filler and rubber which lead to it having a higher tensile strength (14.25 MPa) and lower elongation (664%) compared to the rice bran carbon (7.36 MPa and 776%). Therefore, although the particle size was reduced, it is equally important to increase the interactions that occur between the filler and rubber matrix which may depend on the surface activity and the particle structure of the filler material [11,15]. Although ball milling does provide

size reduction to biochar particles, they are not reduced to sizes comparable to carbon black aggregates (< 1 μm) cost-effectively [17]. A relatively new method of size reduction involves co-milling biochar with silica [17,127]. This method involves milling biochar in a planetary ball mill with standard 3 mm yttrium-stabilized zirconia (YSZ) spheres and silica as a co-milling material.

Silica has a hardness of 6–7 GPa and therefore, during milling should effectively fracture the biochar particles into smaller sizes [17]. In the rubber industry, silica is already used as a reinforcing filler. This is advantageous since it does not need to be separated from the biochar once milling is done, unlike other co-milling media like salt or sugar which must be removed before the biochar is mixed with the rubber [17]. In the study by Peterson and Joshee, the biochar was milled in a planetary ball mill with YSZ spheres and 0.5, 1, 2, and 4 wt% silica was used as the co-milling media [17]. They found that the biochar particle size was significantly reduced. Their results showed that when co-milled with 0.5–4 wt% silica, biochar at 40 phr loading could effectively replace up to 30% of carbon black in SBR with improved elongation and toughness while observing no significant loss in tensile strength [17]. In a similar study, Peterson and Kim milled biochar in a planetary ball mill with YSZ spheres and 1 wt% nano powdered silica (12 nm diameter) was used as the co-milling media [127]. Their results showed that indeed, the biochar particle size was reduced and the particle size distribution was more narrow compared to simple ball milled biochar. Also, they found that increasing the concentration of nanosilica (up to 2%) improved the tensile strength, after which the tensile strength started to decline. They explain this as low concentrations of nanosilica effectively reduced the particle size of the biochar and thus, improved tensile strength results were observed. However, at some point, the nanosilica particles started to aggregate, creating stress points in the rubber matrix which lead to a decrease in tensile strength [127]. Their results were consistent with those obtained from Peterson and Joshee, whereby biochar co-milled with silica at 40 phr loading, could replace 40% of carbon black in SBR with improved elongation and toughness, without compromising on tensile strength. Although they achieved noticeable reduction in particle size (based on SEM images), the final particle size of the biochar was not mentioned [17,127].

2.5 Conclusions

In recent years, the tire industry has been in search of a renewable material that could replace carbon black as a filler in rubber compounds. The industry is reluctant to using a material that is fundamentally different from carbon black. Biochar, a product of the pyrolysis process, is produced from renewable resources such as waste and residue materials from the agricultural, municipal, and forestry sectors. Since biochar can be produced from a wide range of lignocellulosic and non-lignocellulosic feedstocks, the extensive physicochemical properties that ensue are endless. By selecting the proper feedstock and pyrolysis operating conditions, biochar can be "designed" to share similar properties to carbon black. This characteristic has led the rubber industry to consider biochar as a renewable replacement for carbon black in rubber compounds. This would allow the rubber industry to move away from petroleum-derived fillers and bring bio-based materials to the forefront of composite materials.

Research shows that although biochar is visually similar and does share common physicochemical properties to carbon black, it still lacks fundamental properties that allow carbon black to be an effective reinforcing filler in rubber. The improved mechanical performance of carbon black filled rubber composites can be attributed to the fillers high purity. Its high elemental carbon content, low ash content, surface chemistry, and small particle size and structure, are sought out physicochemical properties of bio-based, renewable fillers. Comparatively, biochar properties vary, depending on the feedstock but typically has a lower carbon content, higher ash content, more surface functional groups, and larger particle sizes. These characteristics explain the lower mechanical performances observed in biochar filled rubber to date. At present, only blends of biochar/carbon black fillers have proven to provide equivalent tensile strength, elongation, and toughness as compared to a purely carbon black filler. However, for these blends, the dynamic mechanical properties only show improved results at low filler loadings which is not practical in the rubber tire industry. While these findings are a step in the right direction, there is an opportunity to completely replace carbon black. Its successful replacement by biochar from low-value feedstocks relies on the ability to modify its properties. Further research is needed to determine whether there are cost-effective engineering solutions that can modify biochars properties to closely resemble those of carbon black.

Connecting statement

The literature review in Chapter 2 showed that biochar physicochemical properties differ immensely based on the feedstock source. Also, the review compared the general properties of biochar and carbon black, as well as presented the physicochemical properties of fillers that play a role in its effectiveness to reinforce rubber. Biochar can be produced from a wide-range of feedstocks and to date, feedstocks for biochar production for use as reinforcing fillers in rubber composites have been tried on a case-by-case basis. Also, the focus of previous studies has been on converting lignocellulosic feedstocks into biochar. In Chapter 3, biochar from non-lignocellulosic feedstocks was synthesized and its suitability as a reinforcing filler in styrene-butadiene rubber composites was evaluated. Biochar was produced from two different feedstock sources, chicken feather meal and municipal wastewater sludge, as well as under three pyrolysis treatment temperatures. The effect of the feedstock source and the pyrolysis temperature on the physicochemical properties of the biochar was assessed. The ability of the filler to reinforce the rubber relies on the combination of both physical and chemical interactions between the filler particles and the elastomer matrix. Therefore, the properties of interest were mainly the carbon content, ash content, surface area, surface functional groups, and the particle size, because they will determine the potential of the biochar to reinforce the rubber matrix. The biochar was then added to the styrene-butadiene rubber mix and its reinforcement was evaluated.

Chapter 3

Investigating chicken feather meal and municipal wastewater sludge biochar as renewable fillers in styrene-butadiene rubber composites

Abstract

The purpose of this study was to synthesize and characterize biochar from non-lignocellulosic feedstocks for use as reinforcing fillers in styrene-butadiene rubber (SBR) composites. Chicken feather meal (CFM) and municipal wastewater sludge (MWWS) were pyrolyzed at 500, 600, and 700 °C for 1 h, at a heating rate of 50 °C·min^{-1} under a nitrogen gas flow of 400 ml·min^{-1}. The physicochemical properties of CFM and MWWS biochar were characterized based on elemental and proximate analyses, pH, and surface area. Further, structural analysis was performed using Fourier-transform infrared spectroscopy (FTIR) and the surface morphology of the biochar was assessed using a thermal field emission scanning electron microscope (FE-SEM). The cure, tensile, and dynamic mechanical properties of the rubber composites were investigated and compared to those filled with carbon black N772. The morphologies of the biochar filled rubber composites were also analyzed using FE-SEM to determine the degree of filler dispersion. The results revealed that the CFM and MWWS biochars had different physicochemical properties than carbon black. Of interest, they had lower carbon and higher ash content, higher pH, lower surface area, a greater amount of surface functional groups, and larger particle sizes. These unfavorable properties translated into reduced performances in SBR composites compared to carbon black. Although the biochars had comparable cure laws to carbon black, they exhibited a shorter scorch time and a faster cure rate. The tensile curves of the CFM and MWWS biochars showed large non-linearity, and displayed their inability to reinforce the rubber mix. These results were indicative of poor chemical and physical interactions between the biochar and the rubber. The dynamic mechanical analysis also confirmed the strong filler-filler interactions of the biochar particles. This resulted in a lower filler dispersion in rubber and a lower tendency for rubber-filler interactions, which explained the non-reinforcing mechanisms of the biochar fillers. Overall, these results showed that CFM and MWWS biochar lack physicochemical properties that are characteristic of reinforcing fillers and the lack thereof affected the mechanical performances in rubber.

3.1 Introduction

Rubber tires are composed of highly engineered composite materials with the rubber feature composed primarily of an elastomer, a filler, and a vulcanizing system. The elastomer is a viscoelastic material that has a low tensile modulus and is highly deformable [22]. To create a practical compound in the rubber tire industry, fillers are added to the elastomer matrix to increase the rigidity (among other properties) by providing reinforcement [22,24]. Currently, the most widely used filler is carbon black. The reinforcement mechanism of carbon black in styrene-butadiene rubber (SBR) composites is influenced by the compatibility between the filler and the rubber matrix. Among others, the physical and chemical interactions between carbon black and the rubber matrix plays a key role in carbon blacks' effectiveness as a reinforcing filler [9-11,78]. Carbon black has been extensively studied and thus, its reinforcing properties are well-known. However, it is produced from non-renewable, non-sustainable petroleum feedstocks.

Biochar is synthesized from the thermochemical conversion of biomass and visually resembles carbon black. Consequently, recent studies have focused on biochar as an alternative renewable filler in rubber composites [9-18]. Lay et al. studied the reinforcing performance of biochar synthesized from dead leaves [9]. Their results showed that although the biochar provided some reinforcement compared to unfilled rubber, it still underperformed compared to carbon black [9]. Similar results were obtained in other studies [10,12,13,15,16]. Also, the study by Lay et al. was performed at 5, 10, and 15 parts per hundred rubber (phr) which are considered relatively low filler loadings for use in the rubber tire industry. Jiang et al. converted waste lignin into nano-biochar for use as a reinforcing filler in SBR [11]. Their results showed that at a filler loading of 40 phr, the biochar filled rubber had similar tensile properties to the carbon black filled rubber [11]. However, the reinforcing mechanism was found to be different for both fillers, which may render the rubber tire industry reluctant to using this new material. Also, the cost of lignin is relatively high, which has pushed researchers to investigate more cost-effective feedstocks. Similarly, Peterson et al. conducted numerous studies and their results showed that at filler loadings of 30 phr, only blends of carbon black and biochar filled rubber were comparable to carbon black alone [10,12,13,16]. Currently, there is no consensus within the literature on what types of feedstocks yield biochar with favorable reinforcing properties in rubber. Rather, different feedstocks have been tried and their performances have been evaluated on a case-by-case basis.

Previous studies have focused on the conversion of conventional lignocellulosic feedstock sources into biochar, and evaluated their suitability as reinforcing fillers in rubber composites. In this study, chicken feather meal (CFM) and municipal wastewater sludge (MWWS), both non-lignocellulosic feedstocks, were investigated as substitutes for carbon black in SBR composites. These feedstocks were chosen as they are both considered waste materials from other industrial processes and are widely available. It is estimated that 4.7 million tons of chicken feathers [128] and 7.18 million tons of municipal wastewater sludge [129] are produced annually in the United States. Finding alternate, value-added uses for these waste materials would promote sustainability. Chicken feather meal is a by-product of the poultry and egg industries, and is composed of over 90% keratin [130,131]. Chicken feathers have been studied as fiber reinforcement in epoxy composites [132], unsaturated polyester resin matrices [133], poly(methyl methacrylate) matrices [134], polypropylene composites [135], copolymer styrene-butadiene [136], among others. Also, pyrolyzed chicken feathers have been used to create bio-based composite materials [128,137]. Similarly, wastewater sludge is produced as a by-product of the wastewater treatment industry. Sludge contains small amounts of lignin and cellulose, and higher amounts of hydrocarbons, amino-acids, and lipids [138]. The sludge is heterogeneous which is typical of non-lignocellulosic feedstocks [41]. Wastewater sludge biochar has been studied as a filler in poly(lactic acid) and bioplast GS2189 bio-composites [139]. Although CFM and MWWS have been used as fillers in bio-based composite applications, their potential use as reinforcing fillers in SBR composites has not been explored.

This study focuses on converting CFM and MWWS into biochar using a batch pyrolysis unit for use as reinforcing fillers in SBR composites. First, the biochar physicochemical properties were assessed by proximate and elemental analysis, pH, Brunauer-Emmett-Teller (BET) surface area, Fourier-transform infrared spectroscopy (FTIR), and thermal field emission scanning electron microscopy (FE-SEM). Then, the suitability of CFM and MWWS biochar as reinforcing fillers in SBR was assessed by analyzing the cure kinetics, morphologies, tensile properties, and dynamic mechanical performance of the rubber composites. The physicochemical properties of the bio-sourced fillers and the resulting rubber performances were compared to that of carbon black N772.

3.2 Materials and methods

3.2.1 Materials

Chicken feather meal was provided by Rothsay (Moorefield, Ontario, Canada). Dehydrated municipal wastewater sludge was provided by La Pinière wastewater treatment plant (Laval, Québec, Canada). SBR (mass percent composition: 27% styrene, 21% cis-butadiene, 35% trans-butadiene, 18% vinyl), carbon black N772, N-(1,3-dimethylbutyl)-N'-phenyl-1,4-benzenediamine (6PPD), diphenyl guanidine (DPG), zinc oxide (ZnO), stearic acid (SAD), sulfur (S), and N-cyclohexyl-2-benzothiazole sulfenamide (CBS) were provided by Michelin Inc. (Greenville, South Carolina, USA).

3.2.2 Conversion of the feedstock into biochar

The CFM and MWWS feedstocks were dried in an oven at 105 °C for 24 h. The biochar samples were produced using a lab-scale batch pyrolysis unit. The pyrolysis unit consisted of a stainless-steel tube (30 cm length and 2.5 cm diameter) which was externally heated by a semi-cylindrical ceramic heater. Compressed nitrogen gas was supplied to the pyrolysis unit to ensure an anoxic environment inside the reactor. Throughout the pyrolysis process, co-products (syngas and bio-oil) were led out through an exit pipe to two condensers. Both condensers were water cooled and connected to a round-bottom flask where the condensate was collected. Approximately 150 g of feedstock was used for each batch of pyrolysis. Pyrolysis was performed at 500, 600, and 700 °C, under a steady nitrogen flow rate of 400 $ml \cdot min^{-1}$ and a heating rate of 50 $°C \cdot min^{-1}$. The thermal process was controlled by a programmable PID controller. The pyrolysis was performed for 1 h once the highest treatment temperature (HTT) was reached. The pyrolysis unit was cooled under nitrogen gas flow, to below 200 °C to prevent immediate oxidation of the biochar. Once cooled, the biochar sample was collected from the stainless-steel tube and underwent particle size reduction. The biochar was powdered using a small kitchen blender and sieved through a No. 40 mesh (0.425 mm) sieve. The samples were then transferred to tin containers stored at room temperature until further use. Six different biochar samples were produced during this experiment, namely CFM_{500}, CFM_{600}, CFM_{700}, $MWWS_{500}$, $MWWS_{600}$, and $MWWS_{700}$ (the numbers refer to the HTT during the process).

3.2.3 Characterization of the feedstock, biochar, and carbon black samples

3.2.3.1 Proximate analysis

Proximate analysis was performed in triplicate for the CFM and MWWS feedstocks and their resulting biochar samples. For comparison, the analysis was also performed in triplicate for carbon black N772. The moisture content, volatile matter, ash content, and fixed carbon content were determined following an adaptation of the standard procedures described in ASTM D1762-84 recommended by Enders and Lehmann [140].

3.2.3.2 Elemental composition

Elemental analysis of the feedstocks, biochar samples, and carbon black N772 were conducted in triplicate at the Laboratoire des Technologies de la Biomasse (LTB) (Université de Sherbrooke, Sherbooke, Québec, Canada). The carbon content (C), hydrogen content (H), nitrogen content (N), sulfur content (S), and oxygen content (O) of the samples were obtained using an elemental analyzer 2000 Organic Elemental Analyzer (Thermo Scientific, USA) following an adaptation of ASTM D-5373-16 standard method. The detection limit of N, S, O was 0.01%, 0.2%, and 0.01%, respectively. The results are expressed in terms of mass fraction.

3.2.3.3 pH

The pH of the biochar and carbon black samples were measured in triplicate. A mixture of 1 g of sample with 10 mL of deionized water was mechanically shaken for 1 h, then the pH was measured using a pH meter with glass—calomel electrodes.

3.2.3.4 FTIR analysis

The FTIR analysis of the feedstocks, biochar samples, and carbon black N772 were conducted on a Nicolet iS5 FTIR spectrophotometer (ThermoFisher Scientific, USA). The spectra were recorded at 32 scans with a resolution of 4 cm^{-1} in the 4000-500 cm^{-1} range. The FTIR spectrum was taken in absorbance mode. The assignment of absorption peak to chemical functional group was done based on the literature.

3.2.3.5 BET surface area analysis

A TriStar 3000 surface area and pore size analyzer (Micromeritics, USA) was used to analyze the BET surface area of the biochar and carbon black N772 samples.

3.2.3.6 Morphology

The morphology of the biochar samples and carbon black N772 were investigated using a JEOL JSM-7100F thermal field emission scanning electron microscope (FE-SEM) (JEOL, Belgium). The sample was loosely sprinkled onto a conductive sticky tape. The magnification of the FE-SEM varied between 50-10,000X and the observation was carried out under an accelerating voltage of 1.00 kV.

3.2.4 Preparation of the rubber composites

The first step was to pre-grind the biochar using a BlendTec commercial kitchen blender for 3 minutes. The biochar was sieved using a No. 120 mesh (0.125 mm). Over 90% of the biochar passed through the mesh, and the residual was discarded. The biochar was then milled for 6 h at 45 Hz using a planetary ball mill (MTI Corporation, USA) where two 500 cubic centimeter stainless steel jars were each filled with 15 g of biochar, 750 g of 1 mm yttria stabilized zirconia (YSZ) ball media, and 60 g of ethanol (solvent). The contents of the mill were then placed in a vacuum oven at 70 °C overnight, and then sieved for 90 minutes to remove the media. The biochar samples were placed in a container until further use.

The compound formulations used for biochar filled and carbon black filled rubber can be seen in Table 3.1. Along with the rubber and the filler, chemicals were added during the mixing process. These included 6PPD as an antiozonant, DPG as a covering agent, ZnO as an activator, and SAD to solubilize Zn^{2+}. Sulfur and CBS were added to the rubber mixture, as curatives.

Table 3.1 The compound formulation for biochar filled and carbon black filled SBR.

Ingredients	Biochar elastomeric composition (phr)	Carbon black elastomeric composition (phr)
Elastomers		
SBR	100	100
Fillers		
Biochar	55	—
Carbon black N772	—	50
Chemicals		
6PPD	2.0	2.0
DPG	2.0	2.0
ZnO	2.0	2.0
SAD	3.2	3.2
Curatives		
S	1.5	1.5
CBS	3.0	3.0

A HAAKE PolyLab OS RheoDrive 16 (ThermoFisher Scientific, USA) was used for mixing the elastomer, the filler, and the chemicals. The Haake PolySoft OS software was used to monitor the speed of the rotors (initially set to 90 rpm) and the jacket temperature (set to 110 °C) inside the mixing chamber. The conditions for the mixing process are presented in Table 3.2.

Table 3.2 The mixing process of the elastomer, the filler, and the chemicals.

Time (minutes)	Rotor speed (rpm)	Step
0	90	Add elastomer
1	30	Add ½ biochar
2	30	Add ½ biochar
3	30 increase to 70 gradually	Add 6PPD, DPG, ZnO, SAD
4	70	Piston cleanse
5	70	Drop

After mixing, the rubber mixture was milled using a two-roll mill (C.W. Brabender, USA) at a temperature of 55 °C and a rotor speed of 9 rpm to incorporate the sulfur and CBS curatives. The target thickness of the rubber mixture was 3 mm. An Alpha Technologies 2000 rubber process analyzer (RPA) (Alpha Technologies, USA) was used to determine the shortest time required to

cure the rubber. This test was carried out at 150 °C for 60 minutes. Subsequently, the rubber compound was placed in a mold and was cured at 150 °C and 16 bar for 25 minutes using a Carver Press (Carver, Inc., USA).

3.2.5 Characterization of the rubber composites

3.2.5.1 Cure characteristics

The cure properties of the rubber compounds were analyzed using an Alpha Technologies 2000 rubber process analyzer (RPA) (Alpha Technologies, USA). During the test, mixed but non-vulcanized rubber was placed in a heated cavity (150 °C) where the upper die was stationary and the lower die oscillated.

3.2.5.2 Microscopy

The dispersion of the filler within the rubber was analyzed using a JEOL JSM-7100F thermal FE-SEM (JEOL, Belgium). The rubber sample was cut with a razor blade to expose a fresh surface. The magnification of the thermal FE-SEM varied between 200-10,000X and the observation was carried out under an accelerating voltage of 1.00 kV and 10 kV.

3.2.5.3 Tensile properties

An Instron 5966 Universal Testing Machine (Instron, USA) was used to strain dumbbell shaped rubber samples (ISO 37 type 2) at a constant rate of traverse and force, until break. Five rubber samples were tested for each biochar filled rubber composite and the most representative curve was chosen for analysis.

3.2.5.4 Dynamic mechanical properties

Dynamic mechanical properties were obtained using a Metravib dynamic mechanical analyzer (DMA) 450 Newton (Metravib, USA). The tests were performed at 10 Hz and run using a strain sweep with an imposed temperature of 23 °C, from 0 to 100% strain peak-to-peak. The DMA measured the strain ε(t) and the stress σ(t). Knowing that $G^* = \frac{\sigma_0}{\varepsilon_0}$ and that δ is the phase between

ε(t) and σ(t), the storage modulus (G′) and the loss modulus (G″) were calculated from the following equations:

$$G^* = \sqrt{G'^2 + G''^2} \quad (1)$$

$$\tan\delta = \frac{G''}{G'} \quad (2)$$

3.3 Results and discussion

3.3.1 Physicochemical properties of CFM and MWWS biochar

3.3.1.1 Biochar yield

The average yields obtained from the conversion of the feedstock to biochar are shown in Table 3.3. Generally, biochar yield decreased with increasing pyrolytic temperature due to the thermal decomposition of the components [48,141,142]. This was observed for the MWWS where yields of 52, 45, and 43 wt.% were observed for $MWWS_{500}$, $MWWS_{600}$, and $MWWS_{700}$, respectively. A decreasing trend was not observed for the CFM. Also, the biochar yields were influenced by the feedstock source [48]. At each pyrolysis temperature, MWWS resulted in far greater biochar yields compared to the CFM. For example, at 700 °C, CFM had a biochar yield of 21 wt.% whereas the yield for MWWS biochar was 43 wt.%. This was attributed to the higher ash content of MWWS, which contributed to the biochar yield [48].

3.3.1.2 FTIR

The FTIR spectra of the CFM feedstock and CFM biochar samples are shown in Figure 3.1a. The characteristic peaks of the CFM feedstock were comparable to other studies [128,143,144]. The biochars had different chemical structures than the feedstock, confirming that carbonization altered the biomass. Since CFM samples were composed of over 90% of the protein keratin, the FTIR spectra confirmed the presence of the peptide group (the structural repeat unit of proteins) by showing bands named amide A, I, II, and III [143]. CFM feedstock showed a broad peak in the range of 3600–3200 cm^{-1} which was attributed to the O–H and N–H (amide A) stretching [128,143-

146]. The distinctive absorption peaks at 2920 and 2851 cm^{-1} were attributed to C–H stretching of aliphatic compounds [143,144,146]. The peak at 1742 cm^{-1} corresponded to the C=O stretching of fatty acid esters found in animal skins [143,146]. The absorption bands at 1633, 1519, and 1455 cm^{-1} were assigned to C=O stretching (amide I), N–H bending and C–H stretching (amide II), and C–N stretching and N–H bending (amide III), respectively [128,143,145,146]. The bands at 1237 and 1172 cm^{-1} suggested the presence of thiol groups S–H [128,145]. The band centered around 1078 cm^{-1} was assigned to C–C group vibrations [136]. The peak at 873 cm^{-1} was attributed to unsaturated aromatic carbon deformations [136]. The peak at 661 cm^{-1} was attributed to C–S stretching group vibrations [136,144]. The peak at 602 cm^{-1} was associated to S–S stretching, which confirms the presence of disulfide bonds in the CFM feedstock [144,147]. The spectra of the biochar samples in the range of 3600–3000 cm^{-1} showed a decrease in peak intensity for CFM_{500} and peaks disappearing for CFM_{600} and CFM_{700}. This is consistent with other studies where pyrolyzing the feedstock resulted in the removal of functional groups [128,148]. The peaks associated with aliphatic compounds (2900 to 2800 cm^{-1}) remained in the biochar but showed a decrease in intensity as the pyrolysis temperature increased. The peaks of protein origin (amide I, amide II, and amide III) broadened after pyrolysis. This suggests that heat treatment denatured the protein which manifested as a decrease in the amide groups [149]. Conversely, the peak at 873 cm^{-1} increased after pyrolysis, suggesting the formation of unsaturated aromatic carbon deformations. The biochar samples did not show a peak around 602 cm^{-1}, suggesting pyrolysis caused disulfide bond cleavage.

The FTIR spectra of MWWS feedstock and MWWS biochar samples are shown in Figure 3.1b. The broad band between 3600 and 3000 cm^{-1} was assigned to O–H stretching [146,149] and this peak intensity decreased with increasing pyrolysis temperatures. The peaks at 2922 and 2852 cm^{-1} were assigned to C–H stretching of aliphatic compounds and corresponded to fats and lipids [149,150]. The peak at 1643 and 1582 cm^{-1} were of protein origin and were assigned to N–H bending of primary and secondary amides, respectively [146,149,150]. The sharp peak at 1029 cm^{-1} corresponded to C–O stretching of polysaccharides or polysaccharide-like substances, Si–O of silicate impurities, and clay minerals [149,150]. The IR spectra of the MWWS feedstock and the biochar samples were similar but differed slightly in the intensities of the bands. The biochar samples displayed a decrease in hydroxyl and aliphatic compounds but the peaks of protein origin

and the distinctive peak centered at 1029 cm^{-1} remained, even after high temperature pyrolysis. The high ash content observed in the MWWS biochar samples may explain these results [46].

The hydroxyl and aliphatic compounds in both the CFM and MWWS feedstocks reduced as the pyrolysis temperature increased, due to the dehydration and deoxygenation reactions [11,67,85,86]. The removal of these groups can be seen from the decrease in peak intensity of the IR spectra's in Figure 3.1a and Figure 3.1b and the elemental analysis results in Table 3.3. However, even after high temperature heat treatment, the biochars contained many surface functional groups. Their presence will influence the interface interactions that occur between the filler-filler matrix, the filler-rubber matrix, and the crosslinking density [97]. The functional groups on carbon blacks surface plays an important role in the compatibility between the filler and the rubber matrix and influences its ability to impart reinforcement [97]. The spectra in Figure 3.1a and Figure 3.1b showed that the biochars contained more functional groups compared to carbon black (Figure 3.1c). For carbon black, the peaks at 2119 cm^{-1} and 1996 cm^{-1} were attributed to C≡C stretching (alkynes) [146]. The differences observed between the functional groups present on biochar and carbon black may negatively affect the biochars ability to disperse in the polymer matrix [111].

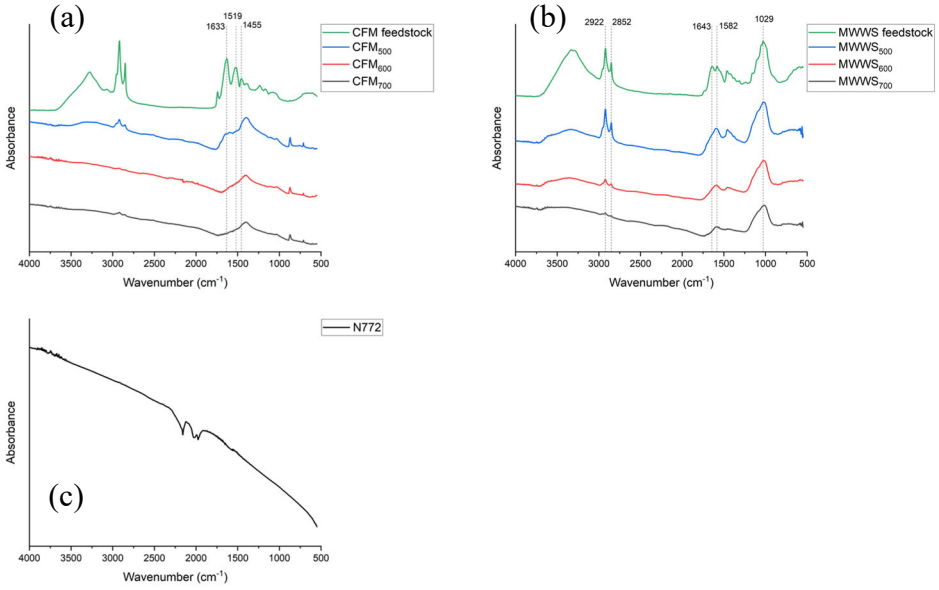

Figure 3.1 FTIR of feedstock and biochars of (a) CFM, (b) MWWS, and (c) carbon black N772.

Table 3.3 Properties of the feedstock, biochar, and carbon black samples.

Sample	Yield (wt. %)	Elemental analysis (wt.%)					Proximate analysis (wt.%)				pH	BET surface area (m^2/g)
		C	H	N	O	S	Moisture content	Volatile matter	Ash content	Fixed carbon		
CB N772	—	96.1±1.2	0.29±0.01	<LOD	0.34±0.02	1.28±0.04	0.56±0.97	2.61±0.81	0.300±0.52	97.09±0.44	7.56±0.18	28.5
CFM feedstock	—	48.0±1.2	6.94±0.24	13.3±0.4	26.3±0.2	1.41±0.06	7.17±0.01	88.1±0.47	2.689±0.45	9.225±0.03	—	—
CFM_{500}	19.91±2.12	56.3±3.2	2.68±0.09	10.4±0.90	13.0±0.80	<LOD*	5.30±0.55	22.4±1.06	12.25±0.61	65.36±1.55	8.14±0.03	0.0410
CFM_{600}	15.96±0.80	57.1±1.0	1.71±0.02	9.49±0.17	8.79±0.17	<LOD	4.32±0.02	22.6±0.34	19.59±0.24	57.78±0.57	9.58±0.11	0.277
CFM_{700}	21.58±5.52	61.9±0.4	1.75±0.11	9.48±0.46	8.03±0.74	<LOD	5.94±1.00	20.34±1.35	18.23±1.96	61.43±1.85	10.2±0.21	0.145
MWWS feedstock	—	38.0±0.4	6.03±0.07	3.13±0.03	28.1±0.6	0.40±0.01	5.88±0.43	65.81±1.80	26.63±1.46	7.560±0.43	—	—
$MWWS_{500}$	52.55±4.80	39.6±0.6	3.86±0.08	3.01±0.06	12.7±0.20	<LOD	0.92±0.93	38.09±0.54	41.79±1.08	20.13±0.66	7.04±0.53	7.50
$MWWS_{600}$	45.04±0.53	32.8±0.3	2.38±0.03	2.41±0.02	12.6±0.80	<LOD	0.00	24.68±0.69	53.79±1.20	21.53±0.90	8.21±0.04	32.9
$MWWS_{700}$	43.14±0.80	32.9±0.7	1.56±0.10	2.07±0.08	8.85±0.36	<LOD	1.64±0.57	13.33±0.50	59.00±1.49	27.66±1.00	9.22±0.03	47.2

* <LOD indicates that the amount was below the detection limit of the instrument

3.3.1.3 Elemental analysis

Table 3.3 shows the elemental analysis of the CFM and MWWS feedstocks and the biochar samples. The carbon content of the CFM biochars was higher than for the CFM feedstock. The increase in carbon content (carbonization) is typical of thermochemical processes [69,86]. For the CFM biochar, the carbon content increased while the hydrogen and oxygen contents decreased with an increase in pyrolysis temperature. This indicates that lower H/C and O/C ratios were observed at higher pyrolysis temperatures. Therefore, at 700 ºC, the CFM biochar exhibited more stability, aromaticity, and lower polarity than biochar produced at 500 ºC [49,67]. These results were consistent with observations made in other studies [128,151]. The nitrogen contents of both the CFM feedstock and biochars were found to be significantly higher than other biomasses in the literature [48,49,128]. This can be attributed to the protein nature of the feedstock. The carbon content of the MWWS biochar decreased with an increase in pyrolysis temperature. This reverse trend was also observed in other studies that pyrolyzed wastewater sludge [152,153]. Following the same trend as the CFM biochar, the hydrogen and oxygen contents decreased with increasing temperatures for the MWWS. Comparatively, the CFM biochars had higher carbon content and thus had lower H/C and O/C ratios indicative of higher aromaticity and lower polarity compared to the MWWS biochars. However, both feedstocks yielded biochars with far different elemental compositions than carbon black N772. Carbon black had a high carbon content (>96%) with only trace amounts of hydrogen, nitrogen, oxygen, and sulfur. Therefore, the biochar fillers had far greater H/C and O/C ratios compared to carbon black. This may lead to detrimental reinforcing effects as the biochar particles exhibit greater polarity. The particle network may favor filler-filler interactions rather than filler-rubber interactions, leading to a low dispersion in rubber [111].

3.3.1.4 Proximate analysis

Both the CFM and the MWWS biochar ash contents increased as the pyrolysis temperature increased from 500 ºC to 700 ºC (Table 3.3). This is consistent with findings from other studies [48,49,128]. At 700 ºC, the MWWS and CFM biochar ash contents were 59 wt.% and 18 wt.%, respectively. Accordingly, the MWWS biochars had low fixed carbon contents (20-28%) whereas the CFMs were between 57% and 66%. Also, the high ash content of MWWS suggested that these biochar samples contained a large percentage of mineral-based content in lieu of carbon. Both MWWS and CFM are non-lignocellulosic feedstocks that are heterogeneous and have highly

diverse compositions compared to lignocellulosic feedstocks [66,67]. This may explain the high ash and low fixed carbon contents of the biochars. With only trace amounts of inorganics, as expected, carbon black had a much lower ash content (<1%). Previous studies have shown that having biochar low in ash is advantageous for reinforcement [13].

3.3.1.5 pH

The pH of both the CFM and MWWS biochars increased with increasing pyrolysis temperature (Table 3.3). The biochars in this study had pH values between 7 and 10.5, agreeing with the literature where most biochars have an alkaline pH [48,49,66,67]. The pH of a filler influences certain vulcanization properties. Acidic fillers have been reported to decrease the cure rate and thus, increase the scorch time [93]. Carbon black N772 was found to have a neutral or slightly alkaline pH of around 7.5. Since the biochars in this study were found to have more alkaline pHs, they may show reduced scorch times which would influence processing safety [21].

3.3.1.6 Morphology

The BET surface area results of the CFM and MWWS biochars, can be seen in Table 3.3. Both feedstocks experienced a dramatic rise in surface area between 500 ºC and 600 ºC. This was also observed in other studies [67,86]. Regardless of the pyrolysis temperature, the CFM biochar had a very low BET surface area. The highest observed value being at 600 ºC with 0.277 m^2/g. The observed decline in surface area between 600 and 700 ºC may be due to the pores collapsing at higher processing temperatures [115]. An increase in surface area, up to a certain point, followed by a decline has also been observed in other studies [86,115,119]. Contrarily, the MWWS had a maximum surface area of 47.2 m^2/g which was found to be higher than the control carbon black (28.5 m^2/g). However, this may indicate that the MWWS biochar had undesirable micro-pores which contributed to the increase in total surface area [14].

The reinforcement stems from the degree of crosslinking and interactions between the filler and the polymer chains, and is maximized with smaller filler particles with high structure [11,14,79]. Figure 3.2a-f shows that the CFM and MWWS biochars have angular shaped aggregate particles with sizes ranging between 10 and 250 μm. In this study, no trend was found between the pyrolysis temperature and the biochar particle size. When increasing the magnification (Figure 3.2g-l), the FE-SEM images show that the aggregate particles are composed of primary particles

less than 1 μm in size. These primary particles are more representative of the particle size of the biochar filler. Once the filler is mixed with the rubber, the larger aggregate particles break apart and it is the primary particles that are dispersed in the rubber matrix. However, unlike carbon black, the biochar particles did not display any structure. Carbon black exhibits spherical shaped particles that form grape-like structures [154]. This grouping of spheres (structure) is characteristic of dendritic materials [154]. Fillers with higher structure have improved dispersion in the rubber matrix and have increased reinforcing properties [11,154]. Since the biochar particles did not exhibit any structure and were considerably large (on the micrometer scale), the ability to reinforce the rubber may be affected.

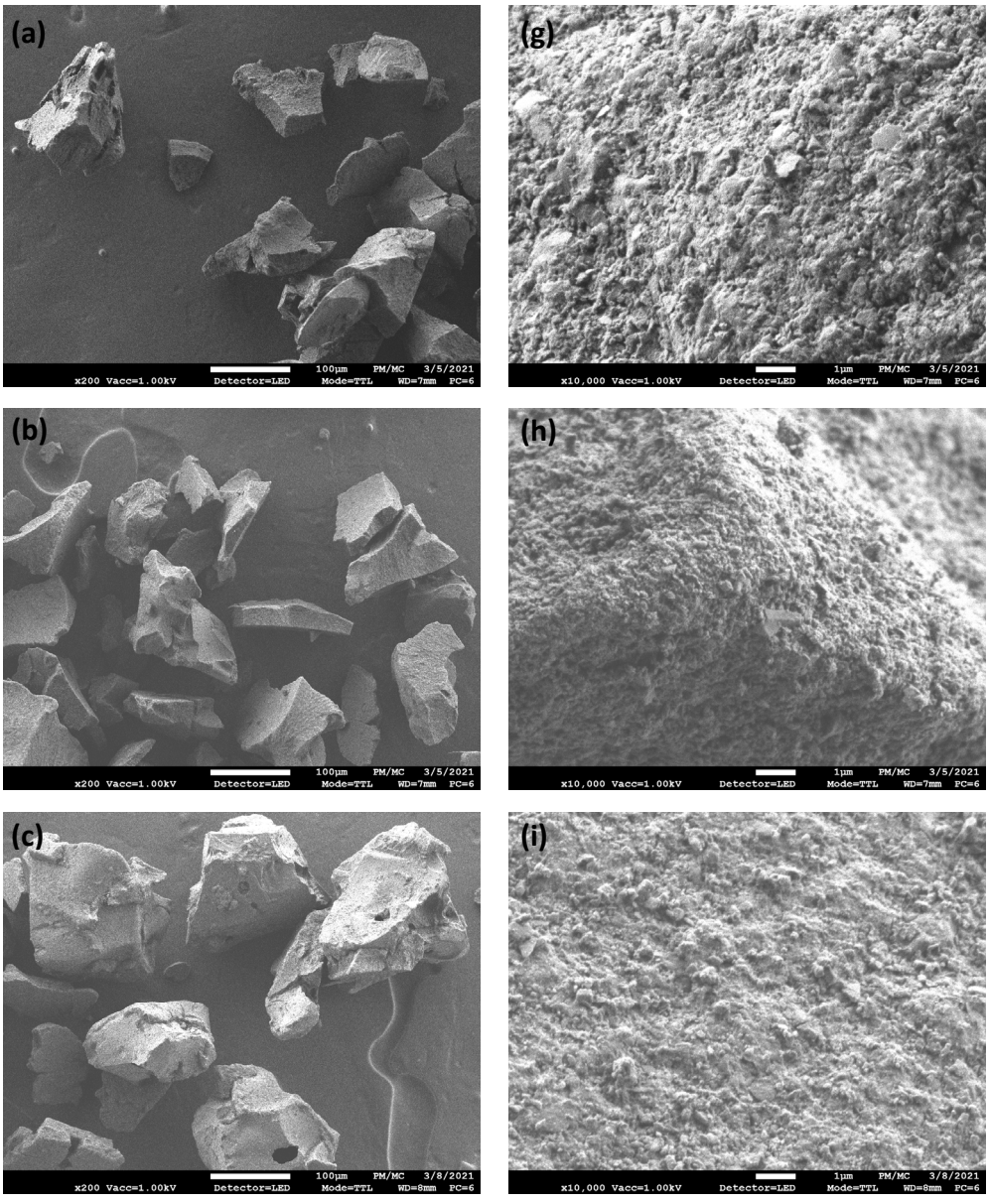

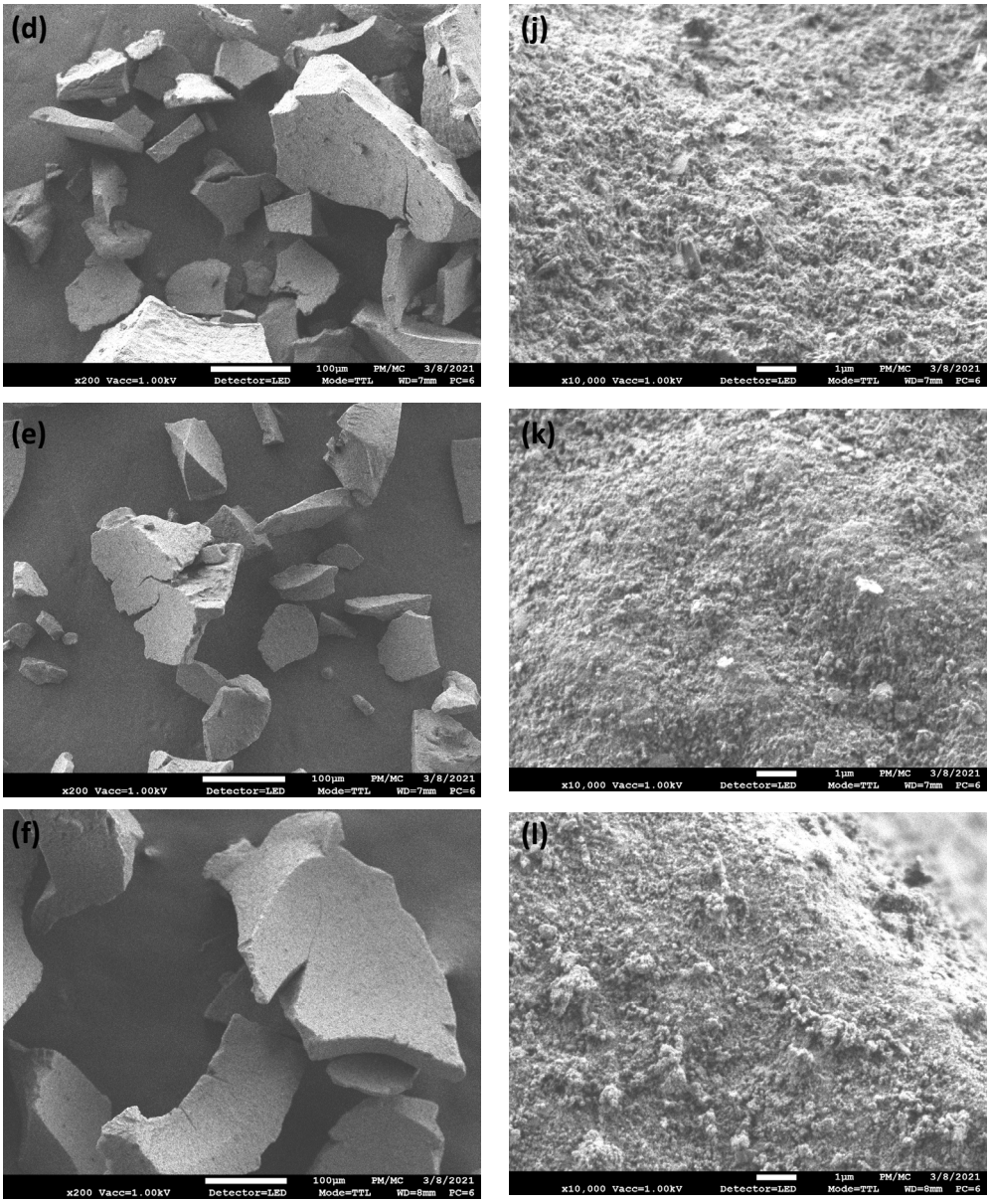

Figure 3.2 FE-SEM images of (a) CFM_{500}, (b) CFM_{600}, (c) CFM_{700}, (d) $MWWS_{500}$, (e) $MWWS_{600}$, (f) $MWWS_{700}$ at x200 magnification and FE-SEM images of (g) CFM_{500}, (h) CFM_{600}, (i) CFM_{700}, (j) $MWWS_{500}$, (k) $MWWS_{600}$, (l) $MWWS_{700}$ at x10,000 magnification.

3.3.2 Properties of the rubber composites

3.3.2.1 The cure laws

The cure laws of the different fillers are presented in Figure 3.3. No obvious improvement of the vulcanization properties was observed with increased pyrolysis temperatures. The control N772

compound showed the lowest initial modulus and longest scorch time, which allowed for better processing. A low initial modulus is indicative of the fluidity of the mix and suggests that the filler is not prematurely forming agglomerations. In general, the CFM and MWWS biochars showed reduced scorch times and change in moduli but displayed an increase in cure rate. This may be attributed to the alkaline pH or the active groups on the biochars surface interacting with the curatives. An acidic pH has been shown to increase the scorch time and decrease the cure rate [93], which was the case for carbon black. The biochars were found to have an alkaline pH and thus, the opposite was observed. The alkaline groups on the biochar surface could have interacted with the curing system, contributing to the observed acceleration of the scorch and cure rate. The cure law of the rubber filled with CFM_{500} resembled the one of the carbon black filled rubber the most, with a good scorch time and change in modulus. The optimal cure times of the samples are achieved when the moduli stabilize. The CFM_{500} and the CFM_{700} samples showed a slight reversion, which allowed to clearly show when the maximum crosslinking of the rubber was reached. Conversely, $MWWS_{600}$ and $MWWS_{700}$ had marching moduli. A marching modulus is indicative of poor dispersion of the filler within the rubber matrix and poor crosslink densities, which may be a result of poor compatibility [124]. In those cases, the modulus never stabilized therefore, the maximum crosslinking and optimal cure time were not easily defined.

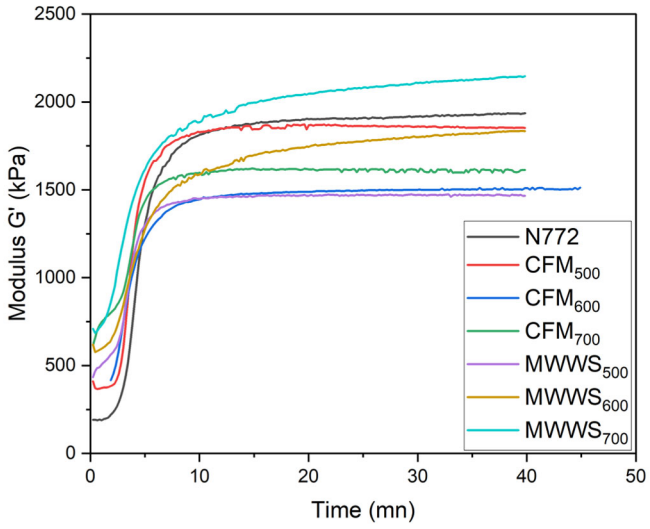

Figure 3.3 Cure laws for the biochar and carbon black samples.

3.3.2.2 Morphology

The tensile properties of biochar filled rubber are influenced by the particle size of the filler, the particle structure, and the surface chemistry [11]. These three factors influence the ability of the filler to disperse in the rubber. Figure 3.4a shows the FE-SEM image of carbon black in rubber and Figure 3.4b-f shows the biochars in rubber. In the biochar images, there are instances of undispersed particles that have flocculated. In general, the biochar mixes had fewer fine particles than carbon black. It is apparent from the images that for MWWS, increasing the pyrolysis temperature resulted in finer particles. The $MWWS_{700}$ image (Figure 3.4f) approaches carbon black in terms of fine particles and dispersion in the rubber mix.

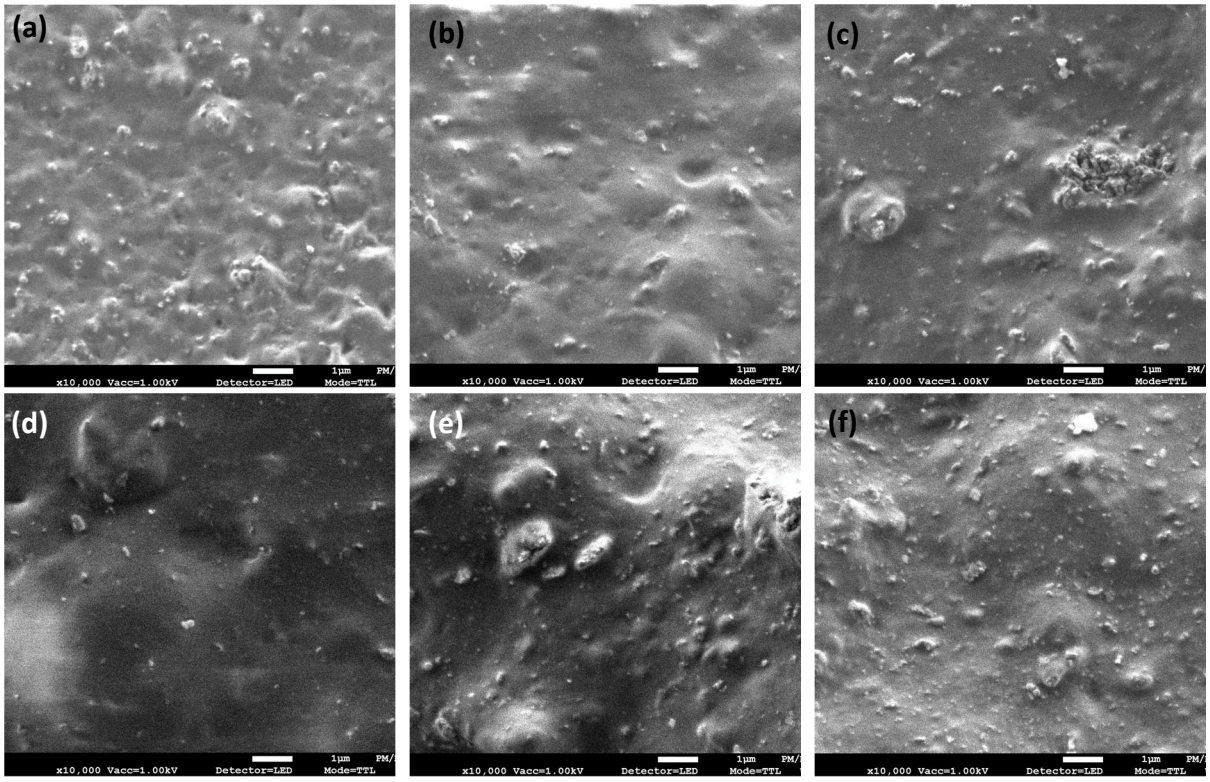

Figure 3.4 FE-SEM images of the filler in rubber of (a) N772, (b) CFM_{500}, (c) CFM_{700}, (d) $MWWS_{500}$, (e) $MWWS_{600}$, (f) $MWWS_{700}$ at x10,000 magnification.

3.3.2.3 Tensile properties

The tensile curves of the CFM and MWWS biochar filled rubber samples and the control carbon black filled rubber are shown in Figure 3.5. In this study, the biochar filled rubber samples had a filler loading of 55 phr, whereas the control carbon black filled rubber had a slightly lower filler loading of 50 phr. These ratios were selected to try to balance the rigidifying nature of the bio-

sourced and carbon black fillers, since the biochar particles did not show any structure and therefore were presumed to be less rigidifying. In this study, reinforcement was evaluated as high modulus at high strain. As seen in Figure 3.5, the carbon black sample provided far greater reinforcement as compared to the CFM and MWWS biochars. These findings may be attributed to certain biochar properties such as (I) low carbon content and high ash content, and (II) the presence of surface functional groups on the biochar, all of which may have contributed to biochars lower physical and chemical interactions with rubber. The CFM and MWWS biochars displayed high initial moduli and showed large non-linearity, indicative of low dispersion in the rubber [124,155] (confirmed from the FE-SEM images). Also, the high initial moduli of the biochar mixes suggested that the biochar particles were interacting with each other and rigidifying the mix. This was also confirmed in the FE-SEM images, where flocculated particles were observed in the biochar filled rubber mixes. However, as the sample was further strained, the filler-filler interactions were broken up, which explains the large drop in initial modulus. This is known as the Payne effect [14]. Comparatively, carbon black had much less of a drop in initial modulus, indicating that it was more compatible with the rubber. For the MWWS biochar, pyrolysis temperature seemed to impact the tensile properties of the rubber mix. $MWWS_{700}$ performed slightly better than $MWWS_{500}$ and $MWWS_{600,}$ which may be attributed to its smaller particles and better dispersion, which was confirmed in the FE-SEM images. Figure 3.5 shows that carbon black had only a slightly greater elongation at break than CFM_{500}, CFM_{600}, and $MWWS_{700}$. In general, the biochar filled rubber samples had lower elongations at break than the carbon black filled rubber. However, the biochar filled rubber mixes were performed at slightly higher filler loadings which may explain the decrease in elongations at break observed. Increasing the amount of filler within the rubber constrains the elastic behavior of the rubber, rigidifying the rubber matrix which leads to a decrease in the elongation at break [9,15]. It was also shown in other studies that carbon black consistently outperformed biochar filled rubber at high filler loadings [10,12,13].

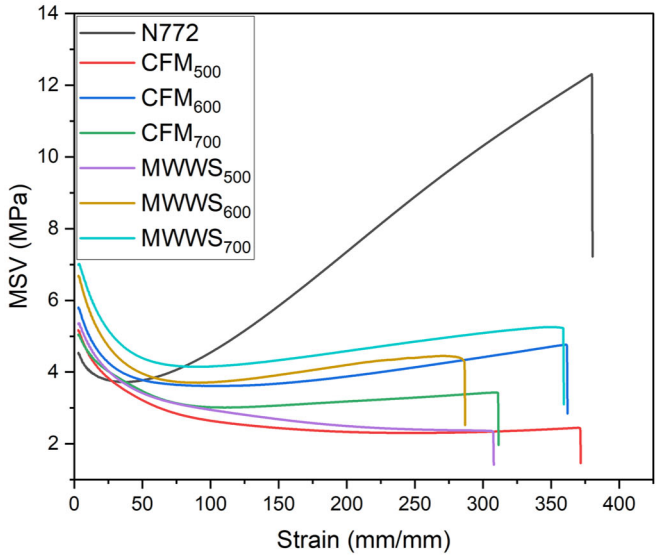

Figure 3.5 Tensile curves for the biochar and carbon black samples.

** Module secant vrai (MSV) is the true secant modulus*

3.3.2.4 Dynamic mechanical properties

The viscoelastic behavior of the rubber mixes under dynamic mechanical loading was assessed at varying strains and under constant temperature (23 ºC). A strain sweep was used to study the filler dispersion, and the filler-filler and filler-rubber interactions. Figure 3.6a, b, and c show the strain dependence of the shear storage modulus (G′), the shear loss modulus (G″), and the shear loss tangent (Tan δ) for the different biochar filled rubber composites. The results for rubber composites filled with carbon black N772 were also graphed for comparison. The G′ represents the stored energy (elastic portion), G″ can be regarded as the energy dissipated as heat (viscous portion), and tan δ is the ratio of G″/G′ and provides a measure of damping of the material [11]. As shown in Figure 3.6a, the samples displayed non-linearity, indicated by the higher low strain rigidity and the lower high strain rigidity. The upward shift in storage modulus for the biochar filled rubber composites indicated that the material was more rigid than the carbon black sample, a result of filler-filler interactions and filler loading [156]. The biochar filled rubber had slightly higher filler loadings (55 phr) than the carbon black filled rubber (50 phr). Increasing the filler

loading constrained the elastic behavior and rigidified the rubber [9]. The high polarity of the biochar favored filler-filler interactions which increased the low strain storage modulus [156,157]. Conversely, the lower polarity of carbon black improved the compatibility with the rubber, reducing the filler-filler network [156]. This may explain the lower low strain modulus of the carbon black sample. The recovery of the storage modulus was lower for the biochar samples which was indicative of poor dispersion and weaker filler-rubber interactions.

The region where the storage modulus decreased manifested as a maximum for the loss modulus and loss tangent (Figure 3.6b and 3.6c, respectively). This decrease in storage modulus and peak in loss modulus and loss tangent with increasing strain amplitude is known as the Payne effect [14,112]. The Payne effect is attributed to the breaking of bonds of the filler network with increasing strain [112,156]. As seen from the curves of the storage and loss modulus, the filler network of the biochar filled rubber samples broke down at higher strain amplitudes and over a wider-range. This can be explained by the stronger filler-filler interactions compared to carbon black [156]. These findings were also confirmed in the tan δ curves. The carbon black sample exhibited a distinct Payne effect, as seen from the bell-shaped curves in Figure 3.6b and 3.6c. Comparatively, the biochar samples did not have a distinct peak with the breakdown of the filler network. The hysteresis at low and high strains is generated by the elastomer itself, and relates to the amount of crosslinking (rather than the filler network) [156]. The biochar filled rubber samples showed high hysteresis at both low and high strain, which was indicative of poor filler-rubber interactions. The biochar may be perturbing the curing system and thus the crosslinking, which was shown from the lack of a bell-shaped curve. Although not distinct, CFM_{700} had a maximum loss modulus around 4% strain, which was comparable to carbon black N772. The CFM_{500}, $MWWS_{600}$, and $MWWS_{700}$ samples had maximums around 0.2% strain, whereas CFM_{500} and $MWWS_{500}$ had maximums around 2% strain. This may indicate that the filler-rubber interactions of carbon black N772 and CFM_{700} were stronger and could only dissociate at higher strains [158]. The absence of a peak and the upward shift in loss modulus and loss tangent of the biochar filled rubber samples was indicative of low filler-rubber interactions and crosslinking of the elastomer chains [14,156,159]. The poor dispersion of the biochar in rubber, an indication of filler-rubber interactions, was also observed in the FE-SEM images.

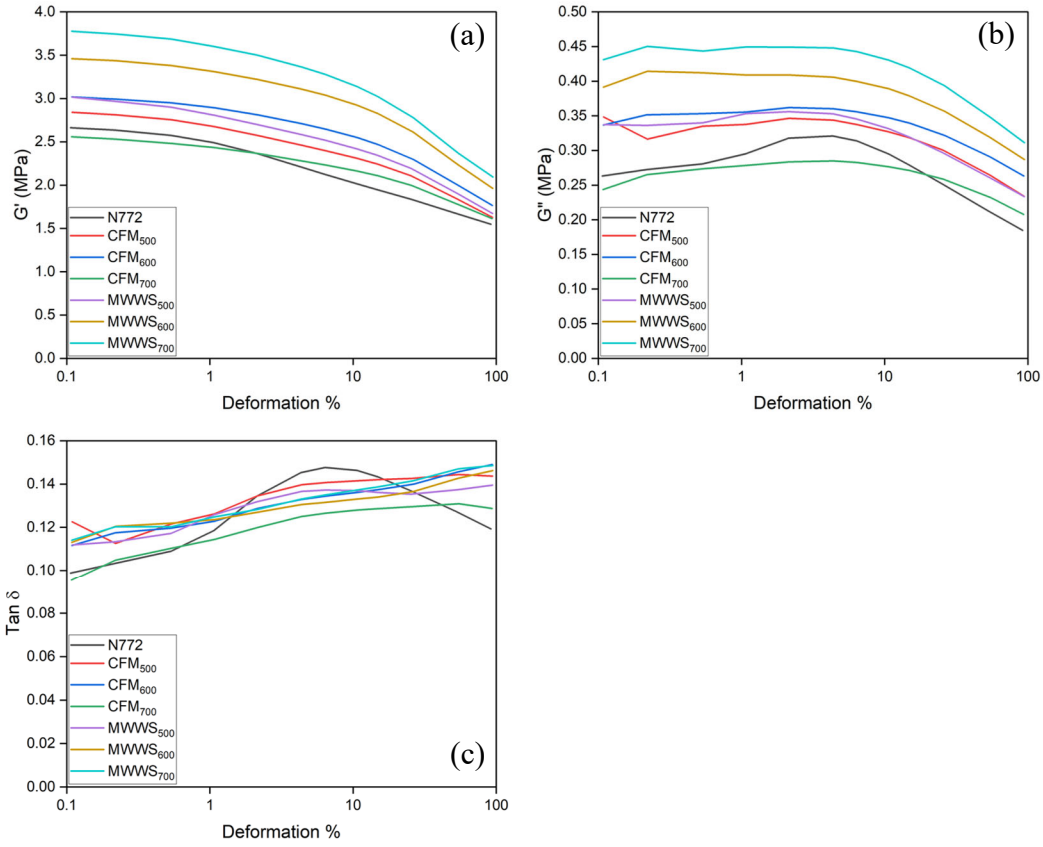

Figure 3.6 (a) Storage modulus G', (b) loss modulus G", and (c) loss tangent tan δ for CFM and MWWS biochar filled SBR composites as a function of deformation %.

3.4 Conclusion

The primary focus of this study was to assess the suitability of biochar, produced from chicken feather meal and municipal wastewater sludge, as renewable reinforcing fillers in styrene-butadiene rubber composites. For both feedstocks, regardless of the pyrolysis temperature, the biochars had lower carbon content and higher hydrogen and oxygen contents, compared to carbon black. The CFM biochars also contained high amounts of nitrogen (>9%). The biochar therefore had higher H/C and O/C ratios, indicative of lower stability, aromaticity, and higher polarity. Proximate analysis revealed that the ash contents of CFM_{700} and $MWWS_{700}$ were 18% and 59%, compared to less than 1% for carbon black. The FE-SEM images showed that the biochars had

angular shaped aggregate particles with no structure. These results showed that the CFM and MWWS biochars lack fundamental physicochemical properties that are responsible for improved mechanical performances in rubber. Carbon black demonstrated improved mechanical performances which can be attributed to these physicochemical properties such as high elemental carbon content, low ash content, surface chemistry, and small particle size and structure. The filler-filler and filler-rubber interactions are largely affected by these properties. Although the biochar samples had comparable cure laws to carbon black, they showed large non-linearity and provided no reinforcement in rubber. Dynamic mechanical analysis was used to study the filler dispersion, and the filler-filler, and filler-rubber interactions. The results showed that the particle network of biochar filled rubber favored filler-filler interactions at the expense of filler-rubber interactions. This in turn lead to a low dispersion of biochar in rubber, which was found to be detrimental to its reinforcement. These results suggest that CFM and MWWS biochar lack certain physicochemical properties, which can be attributed to the lack of homogeneity of non-lignocellulosic biomasses. Further research is needed to assess whether the properties of these biochars can be modified, using cost-effective engineering solutions, with the objective being to improve the mechanical performances and reinforcing mechanisms of biochar in SBR composites.

Connecting statement

In Chapter 3, biochar was synthesized from chicken feather meal and municipal wastewater sludge under three pyrolysis treatment temperatures. The resulting biochar physicochemical properties were compared. Municipal wastewater sludge biochar lacked physicochemical properties characteristic of reinforcing fillers, and the lack thereof negatively affected its mechanical performance in rubber. This could be attributed to the feedstocks heterogeneity. Similarly, chicken feather meal biochar did not reinforce the rubber matrix. Unlike the heterogeneity of the municipal wastewater sludge, the chicken feather meal is primarily a protein source, containing over 90% protein. In Chapter 4, chicken feather meal and canola protein were converted into biochar to evaluate whether protein-based feedstocks could be suitable as reinforcing fillers in styrene-butadiene rubber composites. Also, the feedstocks were pyrolyzed under different pyrolysis conditions to assess whether the physicochemical properties of biochar would be modified enough to improve its reinforcement in rubber. Three different atmospheric conditions were tried (nitrogen, carbon dioxide, and steam) and biochar samples were also activated with steam. The biochar was then added to the styrene-butadiene rubber mix and its reinforcement was evaluated. The effect of the protein-based feedstock, the pyrolysis atmospheric condition, and activation on the mechanical properties of the biochar filled rubber composite was studied.

Chapter 4

Chicken feather meal and canola protein biochar as potential renewable fillers in styrene-butadiene rubber composites

Abstract

In this study, chicken feather meal (CFM) and canola protein (CP) were converted into biochar and their suitability as reinforcing fillers in styrene-butadiene rubber (SBR) composites was evaluated. The protein-based feedstocks were pyrolyzed at 700 °C for 1 h, at a heating rate of 50 °C·min^{-1} under different pyrolysis atmospheric conditions (N_2, CO_2, and steam). Also, biochar was produced under N_2 and CO_2 gas flow and subsequently activated using steam. The physicochemical properties of the resulting CFM and CP biochars were characterized based on elemental and proximate analyses, surface area, and Fourier-transform infrared spectroscopy (FTIR). Results showed that activated CP, pyrolyzed under nitrogen and subsequently steam cooled (CP N_2 + SC), had enhanced physicochemical properties such as low ash content, high fixed carbon content, and reduced polar surface functional groups compared to the other studied biochars. Results also showed that CFM and CP pyrolyzed under nitrogen and subsequently steam cooled displayed higher final moduli and better filler dispersion in rubber than the other biochar samples produced in this study. Given that results showed favorable physicochemical properties and higher final moduli for CP N_2 + SC, this sample was further tested using dynamic mechanical analysis (DMA) and results showed slight differences with carbon black regarding the temperature dependence of the shear storage modulus (G′) and the loss tangent (tan δ). These differences were attributed to increased filler-filler interactions, reduced filler-rubber interactions, and a lower dispersion in rubber than carbon black. The observed differences were not large enough to explain the inability of the biochar to adequately reinforce the rubber. However, the biochar filled rubber sample had a comparable viscoelastic behavior to carbon black over the studied temperature range.

4.1 Introduction

The world's largest tire companies such as Bridgestone, Michelin, Goodyear, Continental, and Sumitomo each have objectives to promote sustainable material use in their tires [5,160-163]. Sustainability can be achieved by reducing the raw material consumption, by reusing and recycling resources, and by investigating bio-sourced raw material alternatives [5,160-163]. A combination of these strategies is required to achieve the objectives set forth by the individual tire manufacturers. The tire industry is currently investing significantly on material development to improve the durability of their tires, among other things [160]. This translates into longer product lifetimes, which contributes to the reduction in raw material consumption. These research initiatives are one of the ways the industry has been tackling the issues surrounding raw material inputs in tires. Also, efforts have been made by companies like Bridgestone and Michelin to recover and reuse carbon black from end-of-life tires, which drives the notion of sustainability [5,160]. In recent years, these tire manufacturers have been partnering with specialized companies to explore commercially viable renewable substitutes for traditional raw materials [5,161,162,164]. In the rubber compound of a tire, the elastomer is the most important component. For this reason, significant research has been conducted by tire manufacturers to find renewable sources of rubber. For example, dandelions [161,162], guayule [160], and renewable styrene-butadiene rubber (butadiene produced using ethanol from biomass and regenerated styrene from waste polystyrene) [5] have been investigated as alternatives to traditional rubber. The filler is the second most important component in the rubber compound. The most widely used filler is carbon black [19], produced from non-renewable resources. Therefore, finding alternative fillers produced from bio-sourced materials has become of great interest.

The elastomer provides the elasticity of the rubber compound but without a reinforcing filler, rubber tires would have minimal strength [165]. It is generally agreed upon that the reinforcement stems from a combination of both physical and chemical interactions between the filler particles and the elastomer matrix [9-11,77-79,97,111,165,166]. Carbon blacks' high purity, small particle size, particle structure, and surface chemistry are physicochemical properties that contribute to strong filler-filler and filler-rubber interactions. This plays a key role in its effectiveness as a reinforcing filler in rubber tires. A straightforward approach in finding a renewable substitute is to investigate materials that have similar physicochemical properties to

carbon black, with a comparable reinforcing mechanism. Accordingly, biochar has gained considerable attention as a potential alternative to carbon black.

Biochar is a product of the thermochemical conversion of biomass, and nearly any organic feedstock can be pyrolyzed for biochar production. An extensive body of research has focused on converting different feedstocks into biochar and includes both lignocellulosic (wood-based and agricultural feedstocks) and non-lignocellulosic feedstocks (sewage sludge, manures, animal hair and bones, etc.) [8,41]. Therefore, biochar is a versatile material and its physicochemical properties largely depend on the feedstock source. Furthermore, biochars properties can be altered by physical or chemical activation [9,167]. Feedstocks can simultaneously undergo thermochemical conversion (by pyrolysis) and physical activation. Of interest, steam and carbon dioxide are often used for activation as these gases partially gasify the biochar and thus increase the surface area [167]. Physically activated biochar also tends to have more active points which increase its adsorption, and thus its interactions with other molecules [9,167]. Steam activation has been shown to be more effective than carbon dioxide in terms of increasing surface area [167]. This may be a result of water molecules' smaller size, which facilitates their ability to penetrate into the pores of the biochar, as stated by Sajjadi et al. [167]. The drawbacks of long steam exposure times during pyrolysis are that it is an energy intensive process, and the ash content tends to be greater [167,168]. To circumvent these drawbacks, post pyrolysis steam activation can be used instead of steam during pyrolysis [168]. The increase in surface area might not be as pronounced as with long steam exposure times, but the increase in ash content should also be minimized.

Recent studies have converted feedstocks such as industrial waste lignin [11], dead leaves [9], birchwood [10], corn starch and corn stover [12], paulownia elongata [16], coconut shell and discarded wood pallets [14], rice bran [15], and rice husk [18] into biochar for use as fillers in rubber composites. To date, converting protein-based feedstocks into biochar to be used as a filler in rubber applications has not been explored. Rather, protein sources such as soy protein isolate or concentrate [158,169,170] and keratin from tannery effluent [171] have been studied as fillers in elastomer composites. These protein sources were added directly, without undergoing thermochemical conversions. Also, chicken feather feedstock has been converted into biochar and tried as a filler in thermoplastic polymers [128].

In this study, chicken feather meal (CFM) and canola protein (CP) isolate (with high purity levels, containing over 90% pure protein) were used to synthesize biochar and their potential as

reinforcing fillers in styrene-butadiene rubber (SBR) composites was investigated. CFM is a byproduct of the poultry industry; it is made by grinding poultry feathers. Similarly, CP is a byproduct of the canola seed oil extraction process. Using a batch pyrolysis unit biochar was produced at 700 °C, with a heating rate of 50 °C·min^{-1} and under different atmospheric conditions (N_2, CO_2, and steam) for 1 h once the highest treatment temperature (HTT) was reached. Also, biochar was synthesized under N_2 and CO_2 gas flow for 1 h once 700 °C was reached and was subsequently activated using steam until the temperature was below 200 °C. The physicochemical properties of the five biochar samples produced for each of the protein-based feedstocks were analyzed based on elemental and proximate analysis, Brunauer-Emmett-Teller (BET) surface area, and Fourier-transform infrared spectroscopy (FTIR). The biochar samples were then mixed with SBR, chemicals, and curatives and the resulting cure properties, tensile properties, morphologies, and dynamic mechanical properties were investigated. The reinforcing properties of the different biochar filled SBR samples were compared to those filled with carbon black N772.

4.2 Materials and methods

4.2.1 Materials

In this study, chicken feather meal was provided by Rothsay (Moorefield, Ontario, Canada). Canola protein isolate (90+% protein) was provided by BioExx Specialty Proteins Ltd (Toronto, Ontario, Canada). SBR (mass percent composition: 27% styrene, 21% cis-butadiene, 35% trans-butadiene, 18% vinyl), carbon black N772, N-(1,3-dimethylbutyl)-N'-phenyl-1,4-benzenediamine (6PPD), diphenyl guanidine (DPG), zinc oxide (ZnO), stearic acid (SAD), sulfur (S), and N-cyclohexyl-2-benzothiazole sulfenamide (CBS) were provided by Michelin Inc. (Greenville, South Carolina, USA).

4.2.2 Conversion of the feedstocks into biochar

The CFM and CP feedstocks were dried for 24 h in an oven at 105 °C. The biochar was synthesized in a lab-scale batch pyrolysis unit. The unit consisted of a stainless-steel tube (30 cm length and 2.5 cm diameter) that was externally heated by a semi-cylindrical ceramic heater. The tube could hold between 100 and 200 g of feedstock per batch, depending on how compact the feedstock was

inserted. Throughout the pyrolysis process, co-products (syngas and bio-oil) were led out through an exit pipe to two condensers. Both condensers were water cooled and were connected to a round-bottom flask where the condensate was collected. In this study, all the samples were pyrolyzed at 700 °C for 1 h with a heating rate of 50 °C·min^{-1}. The thermal process was controlled by a programmable PID controller. Five different pyrolysis treatments were applied to each feedstock as follows: (1) under nitrogen gas flow (no activation) (denoted by N_2); (2) under nitrogen gas flow and steam cooled (denoted by N_2 + SC); (3) steam only (denoted by steam); (4) under carbon dioxide gas flow (denoted by CO_2); and (5) under carbon dioxide gas flow and steam cooled (denoted by CO_2 + SC). Once the pyrolysis unit was cooled to below 200 °C, the biochar sample was collected from the stainless-steel tube and underwent particle size reduction. The biochar was powdered using a small kitchen blender and sieved through a No. 40 mesh (0.425 mm) sieve. The samples were then transferred to tin coated steel containers stored at room temperature until further use. Ten biochar samples were produced during this experiment and they were denoted as feedstock type followed by the pyrolysis condition/activation treatment.

4.2.3 Characterization of the feedstock and biochar samples

4.2.3.1 Proximate analysis

Proximate analysis was performed in triplicate for the CFM and CP feedstocks, the biochar samples, and the N772 carbon black. Analysis was performed following an adaptation of the standard procedures described in ASTM D1762-84 recommended by Enders and Lehmann [140].

4.2.3.2 Elemental composition

Elemental analysis of the CFM and CP feedstocks, biochar samples, and carbon black N772 were conducted in triplicate at the Laboratoire des Technologies de la Biomasse (LTB) (Université de Sherbrooke, Sherbooke, Québec, Canada). The carbon content (C), hydrogen content (H), nitrogen content (N), sulfur content (S), and oxygen content (O) of the samples were obtained using an elemental analyzer 2000 Organic Elemental Analyzer (Thermo Scientific, USA) following an adaptation of ASTM D-5373-16 standard method. The detection limit of N, S, O was 0.01%, 0.2%, and 0.01%, respectively. The results are expressed in terms of mass fraction.

4.2.3.3 FTIR analysis

The FTIR analysis of the CFM and CP feedstocks, the biochar samples, and carbon black N772 were conducted on a Nicolet iS5 FTIR spectrophotometer (ThermoFisher Scientific, USA). The FTIR spectrum was taken in absorbance mode. The spectra were recorded at 32 scans with a resolution of 4 cm^{-1} in the 4000-500 cm^{-1} range. The assignment of absorption peak to chemical functional group was done based on the literature.

4.2.3.4 BET surface area analysis

The BET surface area of the biochar and carbon black N772 samples was determined using a TriStar 3000 surface area and pore size analyzer (Micromeritics, USA).

4.2.4 Preparation of the biochar filled rubber composites

First, the biochar was ground using a BlendTec commercial kitchen blender for 3 minutes and then sieved using a No. 140 mesh (0.071 mm). Over 90% of the biochar passed through the mesh, and the residual was discarded. Two 500 cubic centimeter stainless steel jars were each filled with 15 g of pre-ground biochar, 750 g of 1 mm yttria stabilized zirconia (YSZ) ball media, and 60 g of ethanol (solvent). The biochar was then milled for 6 h at 45 Hz using a planetary ball mill (MTI Corporation, USA). The contents of the mill were then placed in a vacuum oven at 70 °C overnight, and then sieved for 90 minutes to remove the media. The biochar samples were placed in a container until further use.

The second step was the mixing procedure which incorporated the biochar with the elastomer, along with chemicals like 6PPD as antiozonants, DPG as a covering agent, ZnO as an activator, and SAD to solubilize Zn^{2+}. The compound formulations used in this study are shown in Table 4.1.

Table 4.1 The compound formulation for biochar filled and carbon black filled SBR.

Ingredients	Biochar elastomeric composition (phr)	Carbon black elastomeric composition (phr)
Elastomers		
SBR	100	100
Fillers		
Biochar	55	—
Carbon black N772	—	50
Chemicals		
6PPD	2.0	2.0
DPG	2.0	2.0
ZnO	2.0	2.0
SAD	3.2	3.2
Curatives		
S	1.5	1.5
CBS	3.0	3.0

These ingredients were mixed using a HAAKE PolyLab OS RheoDrive 16 (ThermoFisher Scientific, USA) and the Haake PolySoft OS software was used to monitor the speed of the rotors (initially set to 90 rpm) and the jacket temperature (set to 110 °C) inside the mixing chamber. The conditions for the mixing procedure are presented in Table 4.2. The mixture was then milled at 55 °C at 8.4 rpm using a two-roll mill (C.W. Brabender, USA). During milling, curatives such as sulfur and CBS were incorporated into the rubber mix. The target thickness of the rubber mixture was 3 mm. An Alpha Technologies 2000 Rubber Process Analyzer (RPA) (Alpha Technologies, USA) was used to determine the appropriate time required to cure the rubber, when at least 95% of the maximum modulus was reached. This was carried out at 150 °C for 60 minutes. Subsequently, the rubber compound was placed in a mold and was cured at 150 °C and 16 bar for the appropriate time using a Carver Press (Carver, Inc., USA).

Table 4.2 The raw ingredients mixing procedure.

Time (minutes)	Rotor speed (rpm)	Step
0	90	Add elastomer
1	30	Add ½ biochar
2	30	Add ½ biochar
3	30 increase to 70 gradually	Add 6PPD, DPG, ZnO, SAD
4	70	Piston cleanse
5	70	Drop

4.2.5 Characterization of the rubber composites

4.2.5.1 Vulcanization behavior

The cure properties of the rubber compounds were analyzed using the RPA. During the test, mixed but non-vulcanized rubber was placed in a heated cavity (150 °C) where the upper die was stationary and the lower die oscillated. The cure rate index (CRI) was calculated using equation (3), where t_{90} refers to the time at which 90% of crosslinking has occurred and t_{s2} refers to the scorch time:

$$CRI = 100/(t_{90} - t_{s2}) \quad (3)$$

4.2.5.2 Tensile properties

The tensile properties were obtained using an Instron 5966 Universal Testing Machine (Instron, USA). Dumbbell shaped rubber compounds (ISO 37 type 2) were strained at 500 mm per minute, until break. For each biochar sample, five rubber samples were strained until break. Of these, the most representative tensile curve was chosen for analysis.

4.2.5.3 Microscopy

A JEOL JSM-7100F FE-SEM (JEOL, Belgium) was used to analyze the filler particle dispersion in rubber. The rubber sample was cut with a razor blade to expose a fresh surface. The magnification of the FE-SEM varied between 200-10,000X and the observation was carried out under an accelerating voltage of 1.00 kV and 10 kV.

4.2.5.4 Dynamic mechanical properties

A Metravib 450 Newton dynamic mechanical analyzer (DMA) (Metravib, USA) was used to assess the dynamic mechanical properties of the rubber samples. The results were compared to carbon black N772. The tests were performed at 10 Hz and run using a temperature sweep with an imposed stress of 0.7 MPa from -60 °C to 120 °C.

4.3 Results and discussion

4.3.1 Physicochemical properties of the biochars

4.3.1.1 Biochar yield

The biochar yields (in wt.% dry basis) obtained from the different pyrolysis atmospheric conditions and activations are shown in Table 4.3. For both the CFM and CP feedstocks, the yield was lowest for the steam pyrolyzed biochar. This may be due to the steam partially gasifying the biochar which resulted in an increase in mass loss [167]. Since the biochar was pyrolyzed with steam for 1 h, there could have been over-activation leading to increased gasification, at the expense of the biochar yield [167]. CFM and CP N_2 + SC biochar showed a decrease in yield compared to N_2 alone. However, the biochar mass loss was not as pronounced as the steam only pyrolysis. Conversely, CFM and CP CO_2 + SC biochar had greater yields than CO_2 alone. For biochar pyrolyzed under CO_2, the Boudouard reaction ($C + CO_2 \leftrightarrow 2CO$) was involved [167,172]. At temperatures greater than 700 °C, the forward reaction occurs which promotes gasification, resulting in mass loss [167,172]. However, since the CFM and CP CO_2 and CO_2 + SC were pyrolyzed at 700 °C, the temperature may not have been high enough to favor gasification, leading to greater biochar yields compared to the biochar synthesized under steam only. When using oxidizing agents (steam or CO_2), reactions occur with the volatile organic compounds emitted during pyrolysis, which reduce the formation of biochar [167]. This explains the general higher yields observed for the CFM and CP biochar synthesized under N_2 gas flow.

4.3.1.2 Elemental analysis

The results obtained from the elemental analysis are presented in Table 4.3. Only slight variations in elemental composition were found between the different pyrolysis atmospheric conditions and activations. The biochar samples have higher carbon content and lower hydrogen, nitrogen, and oxygen contents compared to the CFM and CP feedstocks. These results are typical of carbonization and suggested a decrease in the surface functional groups [85]. The carbon content of the CFM and CP biochars were relatively similar, in the range of 60-73 wt.%, which was found to be lower than that of carbon black (96 wt.%). Similarly, the hydrogen and oxygen contents of the CFM and CP biochars were greater than carbon black. This was indicative of more organic functional groups present on the biochar surface [14,85]. Pyrolyzing the feedstocks reduced the sulfur content to below the limit of detection (LOD) of the instrument, a result of the disulfide bond cleavage that occurs due to thermal treatment [128,173,174]. The CFM and CP biochars contained significantly more nitrogen (8-12 wt.%) compared to undetectable amounts in the carbon black. The higher nitrogen content was expected since both the CFM and CP feedstocks are protein-based, and thus contain N-compounds from the amino groups in the protein [175].

The O/C and H/C atomic ratios give insight on the biochars degree of aromaticity and polarity [120,167]. In general, the biochars produced under CO_2, steam, and the steam activated biochars had lower O/C and H/C ratios, indicating greater aromaticity and decreased polarity compared to the biochar pyrolyzed under N_2. The lower polar component may result in weaker filler-filler interactions which would be beneficial for rubber reinforcement [111]. Comparatively, regardless of the pyrolysis atmospheric conditions and activation, the biochars had far greater O/C and H/C ratios compared to carbon black. Accordingly, the CFM and CP biochars may have a higher polar component and a lower tendency for dispersion in rubber compared to carbon black [111]. This may be an indication that the CFM and CP biochar have similar reinforcing mechanisms to silica, with the presence of strong filler-filler interactions leading to low dispersion in non-polar rubber [111].

4.3.1.3 Ash and fixed carbon content

Previous research has proposed that biochar with a low ash content was favorable for rubber reinforcement [13]. The biochars produced in this study all had significantly higher ash contents (>5%) than carbon black (<1%) (Table 4.3). The CFM biochar ash contents ranged between 12

and 25 wt.%, whereas the CP biochar had lower ash contents (5-15 wt.%). Accordingly, CP biochar had a greater fixed carbon content (70-81 wt.%) compared to CFM biochar (44-67 wt.%). The lower ash content and higher fixed carbon content of CP biochars suggests higher purity, and may exhibit improved reinforcing properties. Of the ten biochar samples, CP N_2 + SC had the lowest ash content (5%) and highest fixed carbon content (81%). Carbon blacks lack of impurities (97 wt.% fixed C and <1% ash) suggest its reinforcement will outperform the biochar filled rubber samples.

4.3.1.4 FTIR

The FTIR spectra of the CFM and CP feedstock and biochars are displayed in Figure 4.1a and 4.1b, respectively. Although slight variations can be seen between the CFM and CP feedstocks, the spectra show similarities, which include the following (I) a broad absorbance band between 3100 and 3700 cm^{-1} which was attributed to O–H and N–H groups (amide A); (II) the double band at 2920 cm^{-1} and 2851 cm^{-1} (CFM) and 2929 cm^{-1} and 2873 cm^{-1} (CP) which were attributed to the C–H stretching in CH_2 and CH_3 groups; (III) the peaks at 1633 cm^{-1}, 1519 cm^{-1}, and 1455 cm^{-1} (CFM) and 1643 cm^{-1}, 1537 cm^{-1}, and 1446 cm^{-1} (CP) which were associated to C=O stretching (amide I), N–H bending and C–H stretching (amide II), and C–N stretching and N–H bending (amide III), respectively [96,128,143-145,176]; (IV) the peaks at 1237 cm^{-1} and 1172 cm^{-1} (CFM) and 1240 cm^{-1} and 1159 cm^{-1} (CP) which were attributed to the presence of thiol groups S–H [128,145]; (V) the bands at 1078 cm^{-1} (CFM) and 1079 cm^{-1} (CP) which were assigned to C–C group vibrations [136]; and (VI) the peaks at 602 cm^{-1} and 613 cm^{-1} indicated S–S stretching, which confirmed the presence of disulfide bonds in both the CFM and CP feedstocks [144,147]. The CFM feedstock had a peak at 1742 cm^{-1} which was attributed to the C=O stretching of fatty acid esters, which was not present in the CP feedstock [143]. The main differences between the CFM and CP feedstocks being the intensity of the peaks, where CP showed an increase in the intensity of the absorption bands associated with the O–H and N–H groups (amide A), C=O stretching (amide I), N–H bending and C–H stretching (amide II), and C–N stretching and N–H bending (amide III) and displayed a decrease in the intensity of absorbance associated with C–H stretching in CH_2 and CH_3 groups.

Compared with the CFM feedstock, the CFM biochar samples showed no peaks in the range 3100 and 3700 cm^{-1}. This was due to the removal of surface functional groups during high

temperature pyrolysis (i.e. dehydration and deoxygenation reactions) [11,128]. This was also confirmed by the elemental analysis of the biochars, which showed increased carbon and decreased hydrogen, oxygen, and nitrogen contents. The intensities of the double bands associated with aliphatic C–H stretching (around 2920 cm^{-1} and 2851 cm^{-1}) decreased dramatically and disappeared for certain biochar samples. Also, the distinctive peaks assigned to amide I, amide II, and amide III that were observed in the CFM feedstock were absent, suggesting the denaturing of the protein structure after pyrolysis. These peaks were replaced by a broad absorption band in that region which was attributed to the formation of aromatic C=C stretching (centered at 1394 cm^{-1}) [67,96]. The formation of out-of-plane C–H groups (874 cm^{-1}) was also observed in the biochar samples [67]. There was an increase in the intensity of these absorption bands for CFM N_2 + SC and CFM CO_2 + SC. Steam being an oxidizing agent, introduced oxygen-containing functional groups onto the biochar surface which explained these increases [167]. However, this increase was not observed for steam only pyrolysis. Prolonged high temperature steam activation has been shown to decrease the presence of surface functional groups due to gasification and degradation of these groups [167]. Accordingly, some surface functional groups remained on the biochar after pyrolysis which may be due to its high ash content [46]. Comparatively, the CP samples showed reduced functional groups after carbonization. Similar results were noticeable for the CP biochars whereby pyrolysis decreased, or in some cases completely removed, the surface functional groups.

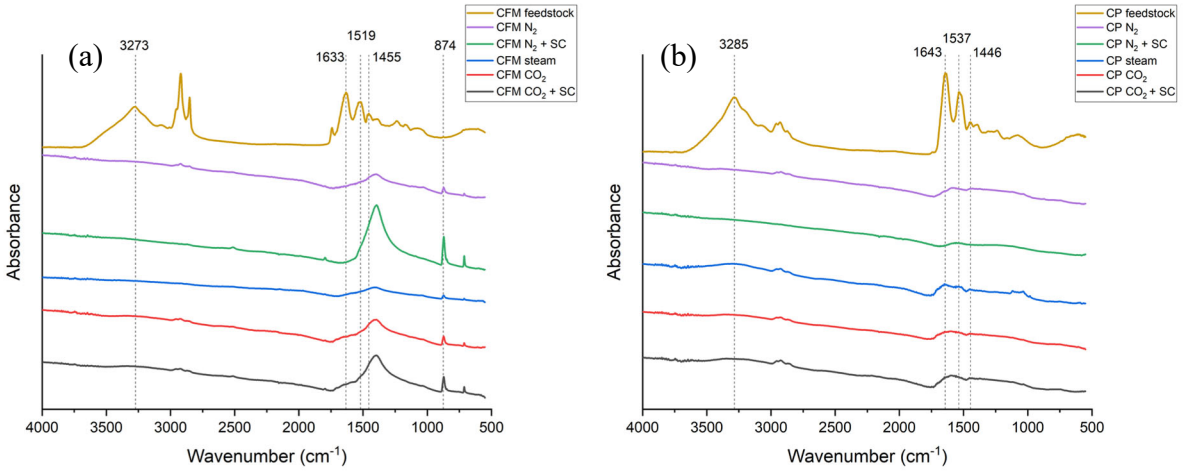

Figure 4.1 FTIR spectra of feedstock and biochars of (a) CFM and (b) CP.

Table 4.3 Basic characterization of the feedstock, biochar, and carbon black samples.

Sample	Yield (wt. %)	Elemental analysis (wt.%)					Proximate analysis (wt.%)				BET surface area (m^2/g)
		C	H	N	O	S	Moisture content	Volatile matter	Ash content	Fixed carbon	
CB N772	–	96.1±1.2	0.29±0.01	<LOD	0.34±0.02	1.28±0.04	0.56±0.97	2.61±0.81	0.300±0.52	97.09±0.44	28.5
CFM feedstock	–	48.0±1.2	6.94±0.24	13.3±0.40	26.3±0.20	1.41±0.06	7.17±0.01	88.1±0.47	2.689±0.45	9.225±0.03	–
CFM N_2	21.58±5.52	61.9±0.4	1.75±0.11	9.48±0.46	8.03±0.74	<LOD*	5.94±1.00	20.34±1.35	18.23±1.96	61.43±1.85	0.145
CFM N_2 + SC	18.87±1.64	60.4±7.5	1.35±0.08	8.94±0.49	10.6±0.50	<LOD	5.83±1.93	20.72±1.67	12.39±1.54	66.88±1.19	0.226
CFM steam	13.50±2.18	63.4±2.5	1.79±0.20	9.62±0.63	5.89±0.50	<LOD	2.56±0.56	24.01±0.65	25.00±1.96	50.99±2.16	12.0
CFM CO_2	14.79±3.14	61.8±2.3	2.35±0.25	11.0±0.20	7.16±0.54	<LOD	0.64±0.56	23.45±0.79	20.21±1.38	56.34±1.73	0.0376
CFM CO_2 + SC	17.19±0.74	66.3±2.0	1.81±0.09	10.9±0.60	6.15±0.33	<LOD	4.88±1.35	31.17±0.49	24.65±2.88	44.18±3.15	0.0760
CP feedstock	–	47.2±0.1	6.89±0.09	14.4±0.10	27.0±0.40	1.21±0.04	2.17±2.35	87.78±1.47	2.58±0.62	9.64±1.57	–
CP N_2	20.50±2.11	66.9±0.9	2.23±0.04	11.3±0.20	7.32±0.50	<LOD	5.64±1.24	17.80±0.71	10.08±0.49	72.11±1.11	0.166
CP N_2 + SC	17.16±1.69	70.1±0.2	1.64±0.04	11.7±0.10	6.44±0.28	<LOD	15.39±10.73	13.44±1.51	5.51±0.70	81.05±0.82	0.0174
CP steam	11.28±4.26	73.0±0.1	1.67±0.11	9.98±0.20	8.14±0.62	<LOD	8.23±1.15	14.04±0.23	15.08±0.84	70.88±0.62	174
CP CO_2	18.58±5.27	68.5±0.8	1.78±0.08	10.3±0.20	6.57±0.08	<LOD	6.36±1.03	14.63±0.59	10.54±0.59	74.83±1.18	0.499

CP CO_2 + SC	23.88±2.20	67.3±1.1	1.90±0.20	11.2±0.10	7.20±0.40	<LOD	5.42±0.41	17.56±1.33	11.16±1.14	71.28±0.44	0.00910

*<LOD indicates that the amount was below the detection limit of the instrument

4.3.1.5 BET surface area

Physical activation of biochar is done primarily to alter certain physicochemical properties such as the surface functional groups, the hydrophobicity, the polarity, surface area, and porosity [177]. Studies have shown that gaseous activation by steam or carbon dioxide increases the biochar surface area [167,177]. Table 4.3 shows that CFM and CP steam had increased BET surface areas compared to those produced under N_2 and CO_2 gas flow. In this study, pyrolyzing CFM under CO_2 did not appear to increase the biochar surface area, which is contrary to other studies [167]. Conversely, the surface area for CP CO_2 increased to 0.499 m^2/g, compared to 0.166 m^2/g for CP N_2. Similarly, pyrolyzing under steam increased the biochar surface area for both feedstocks. CFM steam biochar had a surface area of 12.0 m^2/g which was much greater than the other produced CFM biochars. Surprisingly, the CP steam had a surface area of 174 m^2/g. Previous studies have also shown such large increases [167]. For example, Demiral et al. activated biochar from olive bagasse with steam and the surface area increased from 0.0095 m^2/g (with no activation) to 617 m^2/g (with steam activation) [178]. CFM N_2 + SC and CFM CO_2 + SC resulted in a nearly two-fold increase in BET surface area, from 0.145 to 0.226 m^2/g and from 0.0376 to 0.0760 m^2/g, respectively. Conversely, CP N_2 + SC and CP CO_2 + SC resulted in a decrease in BET surface area compared to the N_2 and CO_2 alone. Generally, longer activation times result in greater increases in surface area [167]. This could explain the significant increase observed for the steam only pyrolysis which was not as pronounced for the steam cooled samples.

4.3.2 Properties of biochar filled rubber composites

4.3.2.1 Vulcanization behavior

Vulcanization curves of the CFM and CP biochars are illustrated in Figure 4.2a and 4.2b, respectively. Carbon black N772 was also graphed for comparison. Mixed but uncured rubber was heated to give insight on the processability and cure characteristics of the biochar filled rubber samples. The different pyrolysis atmospheric conditions and activations tested did not seem to influence the cure characteristics.

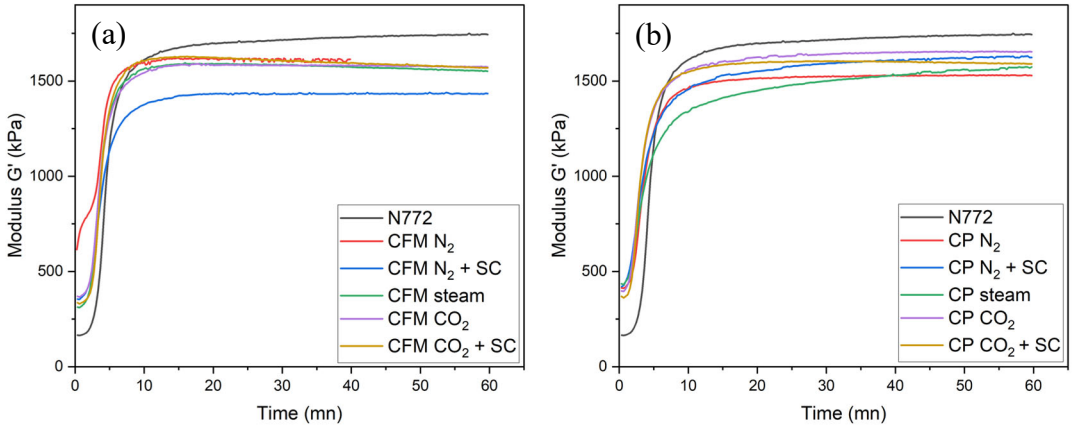

Figure 4.2 The vulcanization curves for the (a) CFM biochar and (b) CP biochar.

From this figure, the scorch time (t_{s2}), the optimum cure time (t_{90}), and the degree of vulcanization can be determined. Of these, the first region of the graph illustrated the scorch time, which determined the samples processability [9,11]. Generally, the biochar filled samples exhibited shorter scorch times compared to carbon black, which suggested that these samples were prematurely creating crosslinks [9]. The cure rate index (CRI) was calculated and gives insight on the cure rate of the sample. In general, the biochar filled rubber samples had an accelerated cure rate, which was confirmed by the higher CRI values (Table 4.4).

Table 4.4 The cure characteristics of the biochar filled rubber.

Samples	Pyrolysis conditions/activations	t_{s2} (min)	t_{90} (min)	CRI (min^{-1})
CB N772	—	4.25	8.16	25.58
CFM	N_2*	—	—	—
	N_2 + SC	3.27	6.92	27.40
	steam	3.01	6.07	32.68
	CO_2	3.09	6.25	31.65
	CO_2 + SC	3.24	5.95	36.90
CP	N_2	3.04	6.98	25.38
	N_2 + SC	2.70	9.99	13.72
	steam	3.02	14.53	8.69
	CO_2	2.54	7.41	20.53
	CO_2 + SC	2.55	6.19	27.47

*Issues encountered during testing.

These cure characteristics (lower scorch time and faster cure rate) may be attributed to the biochar properties, leading to interactions with the curing system. The FTIR spectra of the CFM and CP biochar confirmed the presence of alkaline groups on the biochar, which could be responsible for the accelerated scorch times and cure rates observed. In rubber formulations, sulfenamide type accelerators can be used to increase the rate of sulfur vulcanization [179]. In this study, CBS, a sulfenamide type accelerator, was used. It is known that high ratios of accelerator to sulfur shorten the scorch time and further accelerate the cure rate [180]. Accordingly, the amides on the biochar surface may be interacting with the curatives, increasing this ratio, which could explain the cure characteristics of CFM and CP biochar filled rubber.

The biochar samples had a lower change in modulus compared to carbon black. This is shown by the higher initial modulus and lower final modulus. The higher initial modulus could have resulted from the biochar filler particles agglomerating, reducing the fluidity of the mix. Although the biochar samples had slightly greater filler loadings, they exhibited a lower final modulus, which could be explained by poor compatibility with the rubber (low interfacial adhesion) [181]. The lower change in moduli observed suggests a lower crosslink density compared to that of carbon black [181].

4.3.2.2 Tensile properties

Figure 4.3a and 4.3b compare the tensile curves of carbon black to CFM and CP biochars, respectively. The CP biochars appear to have equivalent or higher moduli at the higher strain region than the CFM composites. However, given the large non-linearity displayed, all the biochar fillers were non-reinforcing in SBR composites. In this study, reinforcement was evaluated as high modulus at high strain. Comparatively, the carbon black provided significantly more reinforcement to the rubber composite than the biochars. The high initial moduli and the non-linearity suggests that the biochar fillers had a low dispersion in rubber. The lack of an increase in moduli and stiffness with increasing strain suggests that the biochar particles had low chemical or physical interactions with the rubber [14,124]. The high polarity of biochar (hydrophilic nature) caused poor compatibility with the hydrophobic rubber matrix [28]. This resulted in a strong polar component (filler-filler interactions) and poor adhesion to the rubber, which reduced the dispersion in rubber and thus its ability to reinforce [28]. The slightly improved results observed for the CP composites could be attributed to factors like higher carbon content and lower ash content.

Although the biochar filler loading was slightly higher (55 phr) than carbon black (50 phr), the biochar samples showed improved elongations at break. This finding was contrary to previous studies, where increasing the filler loading decreased the elongation at break [9]. Typically, increasing the filler content constrains the elastic behavior of the rubber, leading to an earlier break. Again, this may be attributed to poor interactions between the biochar and the rubber, which failed to rigidify or constrain the elastic behavior of the composite. Slight variations were observed between the different biochars. Notably, the CFM N_2 + SC and CP N_2 + SC showed higher final moduli compared to the other biochar fillers. This can be attributed to certain biochar properties such as (I) higher fixed carbon and lower ash content, which contributed to increasing the purity of the material; and (II) a reduction in polar surface functional groups, which may have decreased the polar component of these fillers and increased their dispersion in the rubber.

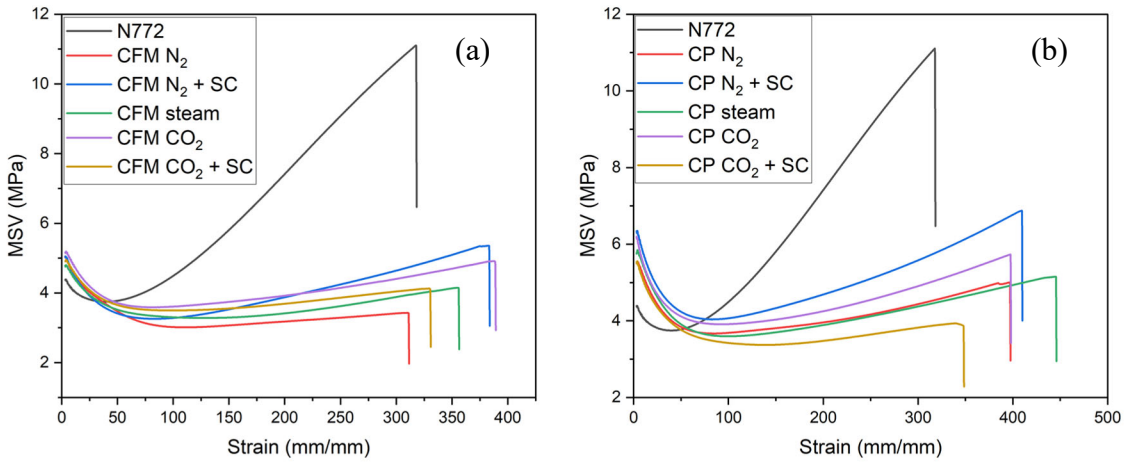

Figure 4.3 Tensile curves for the (a) CFM biochar filled rubber and (b) CP biochar filled rubber composites.

4.3.2.3 Morphology

Biochar from CFM N_2 + SC and CP N_2 + SC showed improved tensile properties compared to the other biochar samples. Considering these results coupled with their favorable physicochemical properties, their morphologies were analyzed to determine their degree of dispersion in the rubber mix. CFM N_2 and CP N_2 were also analyzed to observe whether their reduced tensile properties could be attributed to a lower dispersion in rubber. Carbon black was also included for comparison. Figure 4.4a-e shows the FE-SEM images of the carbon black and biochar filled rubber composites.

These images support the idea that the improved performance of CFM N_2 + SC stems from its improved dispersion in the rubber mix. CFM N_2 is shown in Figure 4.4b and shows undispersed particles that have flocculated. Comparatively, the FE-SEM images of CFM N_2 + SC showed a drastic improvement in the number of fine particles and their degree of dispersion in the rubber composite (Figure 4.4c). The CFM N_2 + SC filled rubber samples uniform dispersion approaches that of carbon black (Figure 4.4a). Figure 4d shows that CP N_2 had more fine particles and fewer instances of large particles, which could have contributed to its improved tensile properties compared to CFM N_2 filled rubber. Similar results were obtained for the CP biochars, where CP N_2 (Figure 4.4d) displayed fewer finely dispersed particles compared to CP N_2 + SC (Figure 4.4e). The improved dispersion observed in the activated biochars (N_2 + SC) can be attributed to the interactions between the filler and the rubber matrix. The favorable physicochemical properties of the filler (increased carbon content, reduced ash content, and reduced polar surface functional groups) played a key role in improving the interactions and thus the compatibility with the rubber matrix.

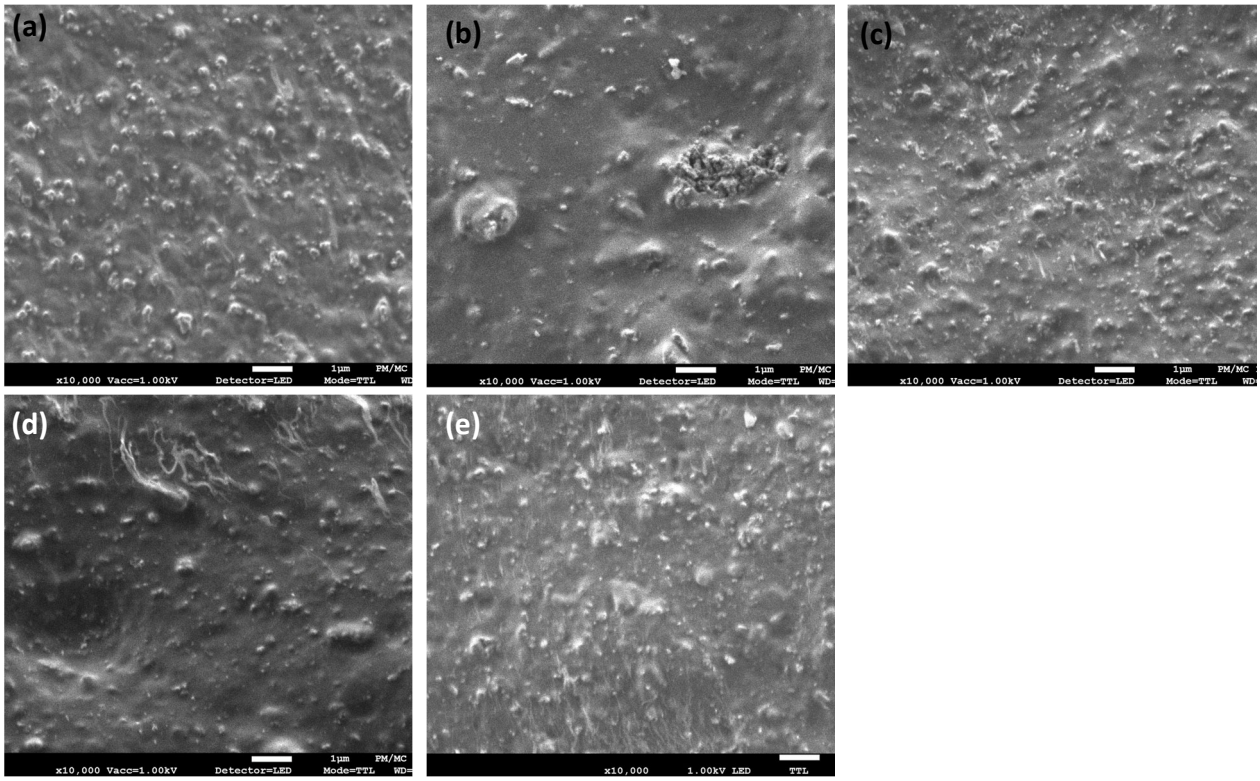

Figure 4.4 FE-SEM images of the fillers in rubber (a) N772, (b) CFM N_2, (c) CFM N_2 + SC, (d) CP N_2, and (e) CP N_2 + SC at x10,000 magnification.

4.3.2.4 Dynamic mechanical properties

The previous analyses showed that CP N_2 + SC had favorable physicochemical properties with a high carbon content, a low ash content, and a reduction in polar surface functional groups, compared to the other studied biochars. Previous studies have noted that these are fundamental properties for reinforcing fillers in rubber composites [9-11]. Despite CP N_2 + SC having properties that more closely approach traditional fillers, its tensile properties underperformed compared to carbon black filled rubber. This sample was further tested using DMA to attempt to understand the reduced reinforcing mechanism observed. In this study, the DMA was run using a temperature sweep from -60 °C to 120 °C (at an imposed stress of 0.7 MPa).

Figure 4.5a and b show the temperature dependence of the shear storage modulus (G′) and the loss tangent (tan δ), respectively. The temperature sweeps showed that CP N_2 + SC behaved similarly to carbon black N772 over the studied temperature range. The G′ of the biochar filled rubber was slightly higher than the carbon black sample at low temperatures. At these temperatures, the rubber chains were frozen and the G′ observed was mainly from the filler-filler interactions, as stated by Li et al. [18,182]. The higher G′ of the biochar sample at the glassy state platform was indicative of a strong filler network, caused by biochars physicochemical properties which favored these interactions. As the temperature increased, the G′ observed was mainly from the filler-rubber interactions [18,182]. The G′ of the carbon black sample became greater than that of biochar at the onset of the transition region, indicative of greater filler-rubber interactions. This can be attributed to low biochar-rubber compatibility, which prevented the formation of strong interactions between the filler particles and the rubber chains and therefore, the composite displayed lower stiffness. These findings were consistent with results from other studies [10,12,13,16,18]. Generally, increasing the filler loading tends to increase the material stiffness, and thus would display a greater G′ at any given temperature [11]. The biochar had a slightly higher filler loading (55 phr) compared to carbon black (50 phr) however, at low temperatures the biochar did not display a higher G′. This was however observed between -10 °C and 50 °C, before falling below carbon black again at higher temperatures. The biochar composite had a higher tan δ peak at a lower glass transition temperature (T_g) than the carbon black composite. A higher δ peak is indicative of reduced filler dispersion and less effective mobility restrictions imposed on the rubber by the filler particles [11,13,18]. The lower tan δ peak observed for the carbon black

composite suggested improved filler-rubber interactions which were effective in restricting the movement of the rubber chains. In addition, the lower T_g and the increase in tan δ at high temperature observed for the CP N_2 + SC composite may be a result of the lower vulcanization of the biochar mix. This in turn also explains the reduction of G′ at high temperature.

The DMA showed that CP N_2 + SC behaved similarly to the carbon black filled composite over the given temperature range. Slight differences were observed which were attributed to differences in the filler-filler and filler-rubber interactions and to the degree of filler dispersion within the rubber. The observed differences in dynamic mechanical properties between biochar filled and carbon black filled rubber do not adequately explain the large difference in tensile properties between the two composite materials. Compatibility between the biochar filler and the rubber could have been compromised by its polarity, being hydrophilic, whereas the rubber is hydrophobic [183]. There is potential to improve the compatibility of the biochar filler with rubber by surface modification.

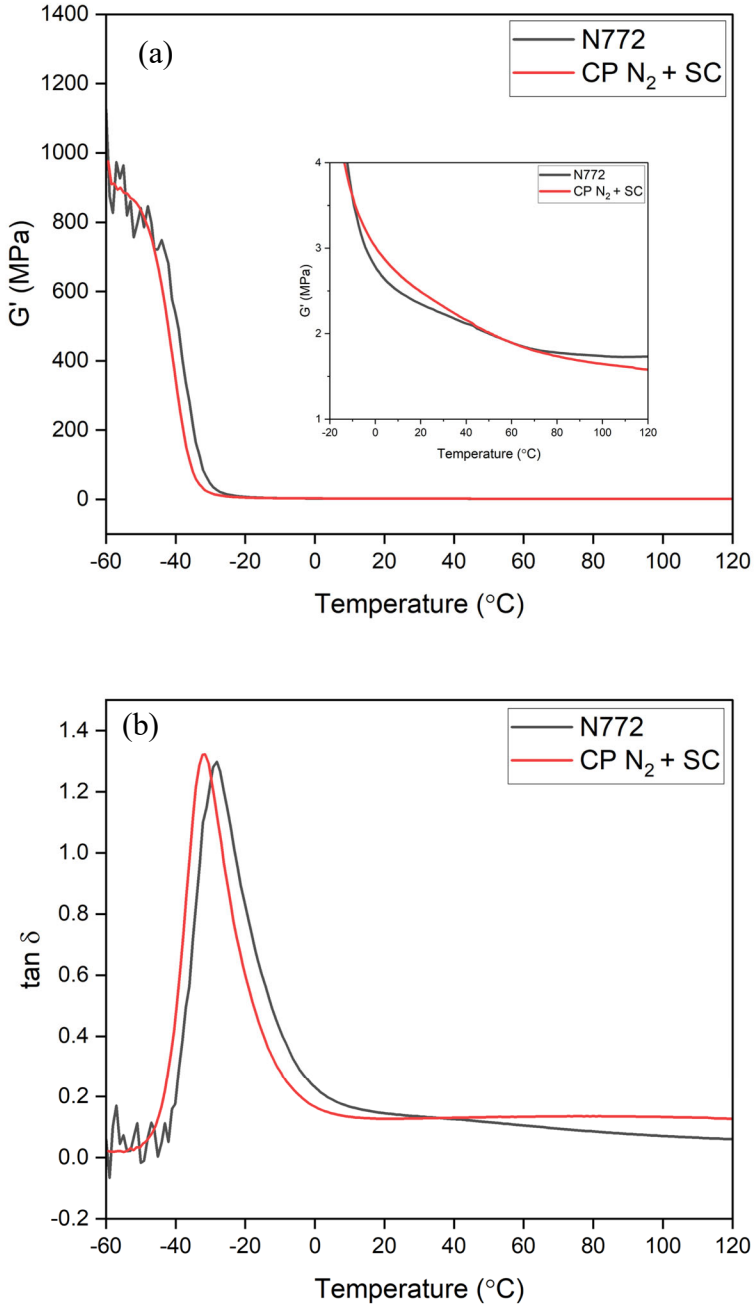

Figure 4.5 Temperature dependence of (a) the storage modulus G' and (b) the loss tangent (tan δ) of carbon black N772 and CP N_2 + SC biochar.

4.4. Conclusion

The primary focus of this study was to determine the potential of substituting non-renewable carbon black by biochar synthesized from protein-based feedstocks. Chicken feather meal and canola protein isolate were converted into biochar and their suitability as reinforcing fillers in styrene-butadiene rubber composites was assessed. Carbon black filled composites outperformed all ten biochar samples regardless of the feedstock source, pyrolysis atmospheric conditions, or physical activation in terms of physicochemical properties as well as vulcanization, tensile, morphological, and dynamic mechanical properties. Under the pyrolysis conditions used, it appears that only slight variations in physicochemical properties were observed between the different biochar samples which translated into similar properties in rubber. Of the ten synthesized biochar samples, CP N_2 + SC had physicochemical properties that were sought out for reinforcing fillers. These included low ash content (5%), high fixed carbon content (81%), and a reduction in polar surface functional groups. Accordingly, this biochar sample had improved tensile properties compared to the other synthesized biochars that were tried as fillers in rubber composites. FE-SEM images showed that CP N_2 + SC had improved dispersion in rubber, which was attributed to its physicochemical properties. Also, dynamic mechanical analysis revealed that the biochar samples viscoelastic behavior was comparable to that of carbon black. Slight differences were observed but they were not enough to explain the inability of the biochar to reinforce the rubber matrix. Future research could assess whether surface modification of the biochar could improve the compatibility between the biochar and the rubber, which would improve filler-rubber interactions and could lead to better reinforcement.

Chapter 5

General conclusion and recommendations

5.1 General conclusion

The primary objectives of this research were to synthesize biochar from non-lignocellulosic feedstocks (chicken feather meal, municipal wastewater sludge) and under different pyrolysis treatment temperatures to determine their effect on biochar physicochemical properties. The suitability of the biochar as reinforcing fillers in styrene-butadiene rubber composites was evaluated. Then, the focus was on protein-based feedstocks and whether pyrolysis atmospheric conditions and activations would modify the physicochemical properties of the biochar to improve its reinforcement in rubber applications. The conclusions relating to these objectives are listed below:

- Chicken feather meal and municipal wastewater sludge were used to synthesize biochar under three pyrolysis treatment temperatures: 500 °C, 600 °C, and 700 °C. It was found that regardless of the feedstock source and the pyrolysis temperature, the biochar lacked physicochemical properties that makes carbon black an effective reinforcing filler in rubber composites. Of interest, the biochar had lower carbon content, higher ash content, and larger particles (with no structure) compared to carbon black. The reinforcing mechanism of the filler material largely depends on the filler-filler and filler-rubber interactions, which are determined in part by the filler physicochemical properties. The physicochemical properties of the biochar favored filler-filler interactions, which led to a lower dispersion in rubber and resulted in the inability of the biochar to reinforce the rubber.
- Protein-based feedstocks (chicken feather meal and canola protein) were converted into biochar under different pyrolysis atmospheric conditions (nitrogen, carbon dioxide, steam) and activated using steam. It was found that only slight differences were observed in physiochemical properties which translated into similar mechanical properties in rubber. Of the studied biochar samples, biochar synthesized from canola protein under nitrogen and subsequently steam cooled (activated) had physiochemical properties that most closely resembled carbon black. Of interest, it had a low ash content (5%), high fixed carbon

content (81%), and reduced polar surface functional groups. This translated into improved mechanical properties. However, it still underperformed compared to carbon black.

5.2 Recommendations for future research

The biochar yields were relatively low with less than 20% yield, in most cases. Low yields may be a limiting factor if biochar is to be considered a commercially viable substitute for carbon black in the future. The industry may be reluctant to using a material with low production efficiencies. In this research, fast pyrolysis was used which is known to favor bio-oil yields however, the biochar produced tends to have improved physicochemical properties for application in composite materials. Conversely, slow pyrolysis is characterized by slow heating rates and results in greater biochar yields. However, the highest pyrolysis treatment temperature is achieved after a longer period. It has been shown that high temperature pyrolysis improves the physicochemical properties. Therefore, future efforts should focus on the optimization of the biochar synthesis, to improve the biochar yield without compromising on the resulting properties.

The main drawback of the biochars produced from non-lignocellulosic feedstocks were their poor compatibility with the rubber (low interfacial adhesion). This is a result of the physicochemical properties of the biochar. To achieve better interfacial adhesion, and thus better dispersion of the bio-sourced filler into the rubber matrix, the surface properties of biochar could be modified to improve the compatibility. Specifically, the biochars in this study were found to have hydrophilic properties whereas the rubber matrix is hydrophobic. Combining materials with opposing properties, reduces the bond between the materials. Therefore, modifying the biochar surface to make them more hydrophobic could be the focus of future research.

Although biochar visually resembles carbon black, it lacks fundamental properties that make carbon black an effective reinforcing filler in rubber composites. The feedstocks available for biochar production are nearly endless, and trying to find a feedstock with adequate properties may be extremely time consuming. Rather than blindly attempting to find renewable feedstocks that have similar properties to carbon black, it may be advantageous to shift the focus on finding cost-effective engineering solutions that would adequately modify the physicochemical properties of any given biochar. Future research could focus on modifying biochar properties to resemble those of carbon black.

References

1. Young, J. *What the tire industry will look like in 2021 and beyond*. 2020; Available from: https://www.tirereview.com/tire-industry-2021-beyond/.
2. Smithers, *The future of global tires to 2024*. 2019.
3. Mordor Intelligence, *Natural rubber market - growth, trends, covid-19 impact, and forecasts (2021-2026)*. 2021.
4. U.S. Tire Manufacturers Association. *Environment - examples of sustainable materials - visions in action*. 2021; Available from: https://sustainability.ustires.org/environment/.
5. Michelin. *100% sustainable - Disruptive innovation in biosourced and recycled materials*. 2021; Available from: https://www.michelin.com/en/innovation/vision-concept/sustainable/.
6. OEC. *What is carbon black?* 2015; Available from: https://www.thecarycompany.com/media/pdf/specs/orion-what-is-carbon-black.pdf.
7. IPCC, *CO2 emission factor for carbon black production*, in *IPCC guidelines for national greenhouse gas inventories* 2006.
8. Tomczyk, A., Z. Sokolowska, and P. Boguta, *Biochar physicochemical properties: pyrolysis temperature and feedstock kind effects.* Reviews in Environmental Science and Biotechnology, 2020. **19**(1): p. 191-215.
9. Lay, M., A. Rusli, M.K. Abdullah, Z.A. Abdul Hamid, and R.K. Shuib, *Converting dead leaf biomass into activated carbon as a potential replacement for carbon black filler in rubber composites.* Composites Part B, 2020. **201**.
10. Peterson, S.C., S.R. Chandrasekaran, and B.K. Sharma, *Birchwood biochar as partial carbon black replacement in styrene-butadiene rubber composites.* Journal of Elastomers and Plastics, 2016. **48**(4): p. 305-316.
11. Jiang, C., J. Bo, X. Xiao, S. Zhang, Z. Wang, G. Yan, Y. Wu, C. Wong, and H. He, *Converting waste lignin into nano-biochar as a renewable substitute of carbon black for reinforcing styrene-butadiene rubber.* Waste Management, 2020. **102**: p. 732-742.
12. Peterson, S., *Evaluating corn starch and corn stover biochar as renewable filler in carboxylated styrene-butadiene rubber composites.* Journal of Elastomers and Plastics, 2012. **44**(1): p. 43-54.
13. Peterson, S.C., *Utilization of low-ash biochar to partially replace carbon black in styrene-butadiene rubber composites.* Journal of Elastomers and Plastics, 2013. **45**(5): p. 487-497.
14. Jong, L., S.C. Peterson, and M.A. Jackson, *Utilization of porous carbons derived from coconut shell and wood in natural rubber.* Journal of Polymers and the Environment : formerly: `Journal of Environmental Polymer Degradation', 2014. **22**(3): p. 289-297.
15. Li, M.-C., Y. Zhang, and U.R. Cho, *Mechanical, thermal and friction properties of rice bran carbon/nitrile rubber composites: Influence of particle size and loading.* Materials and Design, 2014. **63**: p. 565-574.
16. Peterson, S.C., *Silica-milled paulownia biochar as partial replacement of carbon black filler in natural rubber.* Journal of Composites Science, 2019. **3**(4): p. 107.
17. Peterson, S.C. and N. Joshee, *Co-milled silica and coppiced wood biochars improve elongation and toughness in styrene-butadiene elastomeric composites while replacing carbon black.* Journal of Elastomers and Plastics, 2018. **50**(8): p. 667-676.

18. Xue, B., X. Wang, J. Sui, D. Xu, Y. Zhu, and X. Liu, *A facile ball milling method to produce sustainable pyrolytic rice husk bio-filler for reinforcement of rubber mechanical property.* Industrial Crops & Products, 2019. **141**.
19. Lindenmuth, B.E., *Chapter 1. An overview of tire technology*, in *The pneumatic tire*. 2006, U.S. Department of Transportation, National Highay Traffic Safety Administration. p. 1-27.
20. Michelin. *Materials*. 2020; Available from: https://thetiredigest.michelin.com/an-unknown-object-the-tire-materials.
21. Datta, R.N. and F.A.A. Ingham, *Chapter 6. Rubber additives - compounding ingredients*, in *Rubber technologist's handbook*, S.K.D.a.J.R. White, Editor. 2002, Rapra Technology Limited: United Kingdom. p. 167-208.
22. Gent, A.N., *Chapter 2. Mechanical properties of rubber*, in *The pneumatic tire*. 2006, U.S. Department of Transportation, National Highway Traffic Safety Administration. p. 29-79.
23. Rodgers, B. and W. Waddell, *Chapter 9. The science of rubber compounding*, in *The science and technology of rubber* 2013, Elsevier Academic Press. p. 417-471.
24. Coran, A.Y., *Chapter 7. Vulcanization*, in *The science and technology of rubber*. 2013, Elsevier Academic Press. p. 337-381.
25. Bridgestone. *Long-term vision: towards 100% sustainable materials*. n.d.; Available from: https://www.bridgestone.com/responsibilities/environment/resources/.
26. Das, A., K.W. Stöckelhuber, R. Jurk, M. Saphiannikova, J. Fritzsche, H. Lorenz, M. Klüppel, and G. Heinrich, *Modified and unmodified multiwalled carbon nanotubes in high performance solution-styrene-butadiene and butadiene rubber blends.* Polymer, 2008. **49**(24): p. 5276-5283.
27. Xing, W., M. Tang, J. Wu, G. Huang, H. Li, Z. Lei, X. Fu, and H. Li, *Multifunctional properties of graphene/rubber nanocomposites fabricated by a modified latex compounding method.* Composites Science and Technology, 2014. **99**: p. 67-74.
28. Ismail, H., M.R. Edyham, and B. Wirjosentono, *Bamboo fibre filled natural rubber composites: the effects of filler loading and bonding agent.* Polymer Testing, 2002. **21**(2): p. 139-144.
29. Lopattananon, N., K. Panawarangkul, K. Sahakaro, and B. Ellis, *Performance of pineapple leaf fiber-natural rubber composites: The effect of fiber surface treatments.* Journal of Applied Polymer Science, 2006. **102**(2): p. 1974-1984.
30. Tang, H., Q. Qi, Y. Wu, G. Liang, L. Zhang, and J. Ma, *Reinforcement of elastomer by starch.* Macromolecular Materials and Engineering, 2006. **291**(6): p. 629-637.
31. Peterson, S.C. and L. Jong, *Effect of wheat flour pre-cooking on the composite modulus of wheat flour and carboxylated styrene-butadiene latex.* Composites Part A, 2008. **39**(12): p. 1909-1914.
32. Wang, Z.-F., Z. Peng, S.-D. Li, H. Lin, K.-X. Zhang, X.-D. She, and X. Fu, *The impact of esterification on the properties of starch/natural rubber composite.* Composites Science and Technology, 2009. **69**(11-12): p. 1797-1803.
33. Jong, L., *Reinforcement effect of soy protein/carbohydrate ratio in styrene—butadiene polymer.* Journal of Elastomers and Plastics, 2011. **43**(2): p. 99-117.
34. Moonlek, B. and K. Saenboonruang, *Mechanical and electrical properties of radiation-vulcanized natural rubber latex with waste eggshell powder as bio-fillers.* Radiation Effects and Defects in Solids, 2019. **174**(5-6): p. 452-466.

35. Mohamad Aini, N.A., N. Othman, M.H. Hussin, K. Sahakaro, and N. Hayeemasae, *Lignin as alternative reinforcing filler in the rubber industry: A review.* Frontiers in Materials, 2020. **6**.
36. Maslowski, M., J. Miedzianowska, and K. Strzelec, *The potential application of cereal straw as a bio-filler for elastomer composites.* Polymer Bulletin, 2019.
37. Mohanty, A., M. Misra, A. Bali, and A. Rodriguez-uribe, *Renewable replacements for carbon black in composites and methods of making and using thereof*. 2015, University of Guelph: Canada.
38. Mohanty, A., M. Misra, E. Olusegun Ogunsona, J. Anstey, S.E. Torres Galvez, A.M.F.M.-S. Codou, and D.F. Jubinville, *Biocarbon and nylon based hybrid carbonaceous biocomposites and methods of making those and using thereof*. 2017, University of Guelph.
39. Mohanty, A., M. Misra, A. Rodriguez-uribe, and S. Vivekanandhan, *Hybrid sustainable composites and methods of making and using thereof*. 2014.
40. Kan, T., V. Strezov, and T.J. Evans, *Lignocellulosic biomass pyrolysis: A review of product properties and effects of pyrolysis parameters.* Renewable & sustainable energy reviews, 2016. **57**: p. 1126-1140.
41. Li, D.C. and H. Jiang, *The thermochemical conversion of non-lignocellulosic biomass to form biochar: A review on characterizations and mechanism elucidation.* Bioresource Technology, 2017. **246**: p. 57-68.
42. Gent, S., M. Twedt, C. Gerometta, and E. Almberg, *Chapter two - Introduction to feedstocks*, in *Theoretical and applied aspects of biomass torrefaction : for biofuels and value-added products*. 2017, Elsevier: Oxford, United Kingdom. p. 17-39.
43. Nanda, S., P. Mohanty, K.K. Pant, S. Naik, J.A. Kozinski, and A.K. Dalai, *Characterization of North American lignocellulosic biomass and biochars in terms of their candidacy for alternate renewable fuels.* BioEnergy Research, 2013. **6**(2): p. 663-677.
44. Essandoh, M., B. Kunwar, C.U. Pittman, D. Mohan, and T. Mlsna, *Sorptive removal of salicylic acid and ibuprofen from aqueous solutions using pine wood fast pyrolysis biochar.* Chemical Engineering Journal, 2015. **265**: p. 219-227.
45. Kim, K.H., T.-S. Kim, S.-M. Lee, D. Choi, H. Yeo, I.-G. Choi, and J.W. Choi, *Comparison of physicochemical features of biooils and biochars produced from various woody biomasses by fast pyrolysis.* Renewable Energy, 2013. **50**: p. 188-195.
46. Domingues, R., R. , P. Trugilho, F. , C. Silva, A. , I.C. N.A. de Melo, L.n. C.A. Melo, Z. Magriotis, M. , and M. Sánchez-Monedero, A. *Properties of biochar derived from wood and high-nutrient biomasses with the aim of agronomic and environmental benefits*. PLoS ONE, 2017. **12**, DOI: 10.1371/journal.pone.0176884.
47. Yang, H. and K. Sheng, *Characterization of biochar properties affected by different pyrolysis temperatures using visible-near-infrared spectroscopy.* ISRN Spectroscopy, 2012: p. 1-7.
48. Suliman, W., J.B. Harsh, N.I. Abu-Lail, A.-M. Fortuna, I. Dallmeyer, and M. Garcia-Perez, *Influence of feedstock source and pyrolysis temperature on biochar bulk and surface properties.* Biomass and Bioenergy, 2016. **84**: p. 37-48.
49. Kloss, S., F. Zehetner, A. Dellantonio, R. Hamid, F. Ottner, V. Liedtke, M. Schwanninger, M.H. Gerzabek, and G. Soja, *Characterization of slow pyrolysis biochars:*

effects of feedstocks and pyrolysis temperature on biochar properties. Journal of environmental quality, 2012. **41**(4): p. 990-1000.
50. Mayakaduwa, S.S., I. Herath, Y.S. Ok, D. Mohan, and M. Vithanage, *Insights into aqueous carbofuran removal by modified and non-modified rice husk biochars.* Environmental science and pollution research international, 2017. **24**(29): p. 22755-22763.
51. Shen, Z., D. Hou, F. Jin, J. Shi, X. Fan, D.C.W. Tsang, and D.S. Alessi, *Effect of production temperature on lead removal mechanisms by rice straw biochars.* Science of the Total Environment, 2019. **655**: p. 751-758.
52. Peterson, S.C., M. Appell, M.A. Jackson, and A.A. Boateng, *Comparing corn stover and switchgrass biochar: Characterization and sorption properties.* Journal of Agricultural Science, 2013. **5**(1): p. 1-8.
53. Yang, F., S. Zhang, Y. Sun, K. Cheng, J. Li, and D.C.W. Tsang, *Fabrication and characterization of hydrophilic corn stalk biochar-supported nanoscale zero-valent iron composites for efficient metal removal.* Bioresource technology : biomass, bioenergy, biowastes, conversion technologies, biotransformations, production technologies., 2018. **265**: p. 490-497.
54. Feng, Y., Y. Xu, Y. Yu, Z. Xie, and X. Lin, *Mechanisms of biochar decreasing methane emission from Chinese paddy soils.* Soil Biology and Biochemistry, 2012. **46**: p. 80-88.
55. Chen, X., G. Chen, L. Chen, Y. Chen, J. Lehmann, M.B. McBride, and A.G. Hay, *Adsorption of copper and zinc by biochars produced from pyrolysis of hardwood and corn straw in aqueous solution.* Bioresource Technology, 2011. **102**(19): p. 8877-8884.
56. Nie, C., X. Yang, N.K. Niazi, X. Xu, Y. Wen, J. Rinklebe, Y.S. Ok, S. Xu, and H. Wang, *Impact of sugarcane bagasse-derived biochar on heavy metal availability and microbial activity: A field study.* Chemosphere, 2018. **200**: p. 274-282.
57. Sellin, N., D.R. Krohl, C. Marangoni, and O. Souza, *Oxidative fast pyrolysis of banana leaves in fluidized bed reactor.* Renewable Energy: Part A, 2016. **96**(Part A): p. 56-64.
58. Hale, S.E., V. Alling, V. Martinsen, J. Mulder, G.D. Breedveld, and G. Cornelissen, *The sorption and desorption of phosphate-P, ammonium-N and nitrate-N in cacao shell and corn cob biochars.* Chemosphere, 2013. **91**(11): p. 1612-1619.
59. Caban, M., A. Folentarska, H. Lis, P. Kobylis, A. Bielicka-Giełdoń, J. Kumirska, W. Ciesielski, and P. Stepnowski, *Critical study of crop-derived biochars for soil amendment and pharmaceutical ecotoxicity reduction.* Chemosphere, 2020. **248**.
60. Dhyani, V. and T. Bhaskar, *Chapter 9. Pyrolysis of biomass*, in *Biofuels : alternative feedstocks and conversion processes for the production of liquid and gaseous biofuels*. 2019, Academic Press: London, United Kingdom ;. p. 217-244.
61. Antal, M.J. and M. Grønli, *The art, science, and technology of charcoal production.* Industrial & Engineering Chemistry Research, 2003. **42**(8): p. 1619-1640.
62. Kataki, R., R. S. Chutia, M. Mishra, N. Bordoloi, R. Saikia, and T. Bhaskar, *Chapter 2 - Feedstock suitability for thermochemical processes*, in *Recent advnaces in thermochemical conversion of biomass*, Elsevier, Editor. 2015.
63. Jafri, N., W.Y. Wong, V. Doshi, L.W. Yoon, and K.H. Cheah, *A review on production and characterization of biochars for application in direct carbon fuel cells.* Process Safety and Environmental Protection, 2018. **118**: p. 152-166.

64. Gao, L.-Y., J.-H. Deng, G.-F. Huang, K. Li, K.-Z. Cai, Y. Liu, and F. Huang, *Relative distribution of Cd2+ adsorption mechanisms on biochars derived from rice straw and sewage sludge.* Bioresource Technology, 2019. **272**: p. 114-122.
65. Bolognesi, S., G. Bernardi, A. Callegari, A.G. Capodaglio, and D. Dondi, *Biochar production from sewage sludge and microalgae mixtures: properties, sustainability and possible role in circular economy.* Biomass Conversion and Biorefinery, 2019.
66. Jin, J., Y. Li, J. Zhang, S. Wu, Y. Cao, P. Liang, M.H. Wong, M. Wang, S. Shan, and P. Christie, *Influence of pyrolysis temperature on properties and environmental safety of heavy metals in biochars derived from municipal sewage sludge.* Journal of hazardous materials, 2016. **320**: p. 417-426.
67. Cantrell, K.B., P.G. Hunt, M. Uchimiya, J.M. Novak, and K.S. Ro, *Impact of pyrolysis temperature and manure source on physicochemical characteristics of biochar.* Bioresource technology, 2012. **107**: p. 419-28.
68. Cao, X. and W. Harris, *Properties of dairy-manure-derived biochar pertinent to its potential use in remediation.* Bioresource technology, 2010. **101**(14): p. 5222-8.
69. Cao, X., Y. Li, J. Mao, K.S. Ro, and M. Chappell, *Chemical structures of swine-manure chars produced under different carbonization conditions investigated by advanced solid-state ¹³C nuclear magnetic resonance (NMR) spectroscopy.* Energy and Fuels, 2011. **25**(1): p. 388-397.
70. Grycová, B., I. Koutník, and A. Pryszcz, *Pyrolysis process for the treatment of food waste.* Bioresource technology, 2016. **218**: p. 1203-7.
71. Li, L., J.S. Rowbotham, H.C. Greenwall, and P.W. Dyer, *Chapter 8. An introduction to pyrolysis and catalytic pyrolysis: versatile techniques for biomass conversion*, in *New and future developments in catalysis : catalytic biomass conversion*. 2013, Elsevier Ltd.: Amsterdam. p. 173-208.
72. Peterson, S.C., M.A. Jackson, and M. Appell, *Chapter 11. Biochar: sustainable and versatile*, in *Advances in applied nanotechnology for agriculture*. 2013, American Chemical Society: Washington DC. p. 193-205.
73. Brownsort, P.A., *Biomass pyrolysis processes: review of scope, control and variability*. 2009, UK biochar research center (UKBRC): United Kingdom.
74. Williams, P.T. and N. Nugranad, *Comparison of products from the pyrolysis and catalytic pyrolysis of rice husks.* Energy, 2000. **25**(6): p. 493-513.
75. Bridgwater, A.V., *Production of high grade fuels and chemicals from catalytic pyrolysis of biomass.* Catalysis Today, 1996. **29**(1): p. 285-295.
76. Jindo, K., H. Mizumoto, Y. Sawada, M.A. Sanchez-Monedero, and T. Sonoki, *Physical and chemical characterization of biochars derived from different agricultural residues.* Biogeosciences, 2014. **11**(23): p. 6613-6621.
77. Peterson, S.C. and S. Kim, *Using heat-treated starch to modify the surface of biochar and improve the tensile properties of biochar-filled styrene–butadiene rubber composites.* Journal of Elastomers & Plastics, 2019. **51**(1): p. 26-35.
78. Li, Q., C. Wu, S. Qian, and Y. Ma, *Effect of carbon black nature on vulcanization and mechanical properties of rubber.* Journal of Macromolecular Science, Part B: Physics, 2008. **47**(5): p. 837-846.
79. Balasooriya, W., B. Schrittesser, G. Pinter, T. Schwarz, and L. Conzatti, *The effect of the surface area of carbon black grades on HNBR in harsh environments.* Polymers, 2019. **11**(1).

80. Boguta, P., Z. Sokołowska, K. Skic, and A. Tomczyk, *Chemically engineered biochar - Effect of concentration and type of modifier on sorption and structural properties of biochar from wood waste.* Fuel, 2019. **256**.
81. Naghdi, M., M. Taheran, S.K. Brar, T. Rouissi, M. Verma, R.Y. Surampalli, and J.R. Valero, *A green method for production of nanobiochar by ball milling- optimization and characterization.* Journal of Cleaner Production, 2017. **164**: p. 1394-1405.
82. Lyu, H., B. Gao, F. He, A.R. Zimmerman, C. Ding, H. Huang, and J. Tang, *Effects of ball milling on the physicochemical and sorptive properties of biochar: Experimental observations and governing mechanisms.* Environmental pollution (Barking, Essex : 1987), 2018. **233**: p. 54-63.
83. Kumar, M., X. Xiong, Z. Wan, Y. Sun, D.C.W. Tsang, J. Gupta, B. Gao, X. Cao, J. Tang, and Y.S. Ok, *Ball milling as a mechanochemical technology for fabrication of novel biochar nanomaterials.* Bioresource Technology, 2020.
84. Enders, A., K. Hanley, T. Whitman, S. Joseph, and J. Lehmann, *Characterization of biochars to evaluate recalcitrance and agronomic performance.* Bioresource technology : biomass, bioenergy, biowastes, conversion technologies, biotransformations, production technologies., 2012. **114**: p. 644-653.
85. Chen, B., D. Zhou, and L. Zhu, *Transitional adsorption and partition of nonpolar and polar aromatic contaminants by biochars of pine needles with different pyrolytic temperatures.* Environmental science & technology, 2008. **42**(14): p. 5137-43.
86. Keiluweit, M., P.S. Nico, M.G. Johnson, and M. Kleber, *Dynamic molecular structure of plant biomass-derived black carbon (biochar).* Environmental science & technology, 2010. **44**(4): p. 1247-53.
87. ASTM, I., *ASTM D121-15, Standard Terminology of Coal and Coke*. 2015: West Conshohocken, PA.
88. Donnet, J.-B. and T.K. Wang, *Surface microstructure of carbon black: Advances in characterization by scanning tunneling microscopy.* Macromolecular Symposia, 1996. **108**(1): p. 97-109.
89. Ma, Z., Y. Yang, Q. Ma, H. Zhou, X. Luo, X. Liu, and S. Wang, *Evolution of the chemical composition, functional group, pore structure and crystallographic structure of bio-char from palm kernel shell pyrolysis under different temperatures.* Journal of Analytical and Applied Pyrolysis, 2017. **127**: p. 350-359.
90. Singh, B. and M.D. Raven, *Chapter 21. X-ray diffraction analysis of biochar*, in *Biochar : a guide to analytical methods*. 2017, CSIRO Publishing: Clayton, Vic. p. 245-252.
91. Liu, Y., Z. He, and M. Uchimiya, *Comparison of biochar formation from various agricultural by-products using FTIR spectroscopy.* Modern Applied Science, 2015. **9**(4).
92. Boehm, H.P., *Some aspects of the surface chemistry of carbon blacks and other carbons.* Carbon, 1994. **32**(5): p. 759-769.
93. Lewis, C., R. Buanpa, and S. Kiatkamjornwong, *Effect of rubber ratio, carbon black level, and accelerator level on natural rubber/bromobutyl rubber blend properties.* Journal of Applied Polymer Science, 2003. **90**(11): p. 3059-3068.
94. Johnston, C.T., *Chapter 18 - Biochar analysis by Fourier-transform infra-red spectroscopy*, in *Biochar : a guide to analytical methods*. 2017, CSIRO Publishing: Clayton, Vic. . p. 199-213.
95. O'Reilly, J.M. and R.A. Mosher, *Functional groups in carbon black by FTIR spectroscopy.* Carbon, 1983. **21**(1): p. 47-51.

96. Rositani, F., P.L. Antonucci, M. Minutoli, N. Giordano, and A. Villari, *Infrared analysis of carbon blacks.* Carbon, 1987. **25**(3): p. 325-332.
97. Sahakaro, K., *Chapter 3 - Mechanism of reinforcement using nanofillers in rubber nanocomposites*, in *Progress in rubber nanocomposites*, S. Thomas and H.J. Maria, Editors. 2017, Ser. Woodhead publishing series. p. 81-113.
98. Mukherjee, A., A.R. Zimmerman, and W. Harris, *Surface chemistry variations among a series of laboratory-produced biochars.* Geoderma, 2011. **163**(3): p. 247-255.
99. Singh, B., M. Mei Dolk, Q. Shen, and M. Camps-Arbestain, *Chapter 3. Biochar pH, electrical conductivity and liming potential*, in *Biochar : a guide to analytical methods*. 2017, CSIRO Publishing: Clayton, Vic. p. 23-38.
100. Hale, S.E., J. Lehmann, D. Rutherford, A.R. Zimmerman, R.T. Bachmann, V. Shitumbanuma, A. O'Toole, K.L. Sundqvist, H.P. Arp, and G. Cornelissen, *Quantifying the total and bioavailable polycyclic aromatic hydrocarbons and dioxins in biochars.* Environmental science & technology, 2012. **46**(5): p. 2830-8.
101. Hilber, I., F. Blum, J. Leifeld, H.P. Schmidt, and T.D. Bucheli, *Quantitative determination of PAHs in biochar: a prerequisite to ensure its quality and safe application.* Journal of agricultural and food chemistry, 2012. **60**(12): p. 3042-50.
102. Cornelissen, G. and S.E. Hale, *Polycyclic aromatic hydrocarbons in biochar*, in *Biochar: A guide to analytical methods*, CSIRO, Editor. 2017, CSIRO Publishing. p. 126-131.
103. Tang, Y., S. Sun, L. Zhang, Z. Du, J. Zhuang, and J. Pan, *Determination of 16 polycyclic aromatic hydrocarbons in tire rubber by ultra-high performance supercritical fluid chromatography combined with atmospheric pressure photoionization-tandem mass spectrometry.* Analytical Methods, 2018. **10**(40): p. 4902-4908.
104. Keiluweit, M., M. Kleber, M.A. Sparrow, B.R. Simoneit, and F.G. Prahl, *Solvent-extractable polycyclic aromatic hydrocarbons in biochar: influence of pyrolysis temperature and feedstock.* Environmental science & technology, 2012. **46**(17): p. 9333-41.
105. Wang, C., Y. Wang, and H.M.S.K. Herath, *Polycyclic aromatic hydrocarbons (PAHs) in biochar - Their formation, occurrence and analysis: A review.* Organic geochemistry., 2017. **114**: p. 1-11.
106. Wang, J., O. Emmanuel Stephen, Z. Wei, Z. Xian, Y. Bing, W. Michael Gatheru, and G. Yanzheng *Polyaromatic hydrocarbons in biochars and human health risks of food crops grown in biochar-amended soils: A synthesis study*. Environment International, 2019. **130**, DOI: 10.1016/j.envint.2019.06.009.
107. EBC, *European biochar certificate - guidelines for a sustainable production of biochar*. 2012, European biochar foundation: Arbaz, Switzerland.
108. IBI, *Standardized product definition and product testing guidelines for biochar that is used in soil*. 2015, International Biochar Initiative.
109. McGrath, T., R. Sharma, and M. Hajaligol, *An experimental investigation into the formation of polycyclic-aromatic hydrocarbons (PAH) from pyrolysis of biomass materials.* Fuel, 2001. **80**(12): p. 1787-1797.
110. Devi, P. and A.K. Saroha, *Effect of pyrolysis temperature on polycyclic aromatic hydrocarbons toxicity and sorption behaviour of biochars prepared by pyrolysis of paper mill effluent treatment plant sludge.* Bioresource Technology, 2015. **192**: p. 312-320.
111. Leblanc, J.L., *Rubber-filler interactions and rheological properties in filled compounds.* Progress in Polymer Science, 2002. **27**(4): p. 627-687.

112. Robertson, C., G. and N. Hardman, J. *Nature of carbon black reinforcement of rubber: Perspective on the original polymer nanocomposite*. Polymers, 2021. **13**, DOI: 10.3390/polym13040538.
113. ASTM standard D1765, *ASTM D 1765 Standard classification system for carbon blacks used in rubber products*. n.a.: 100 Barr Harbor Drive, West Conshohocken, PA 19428-2959, United States.
114. Yargicoglu, E.N., B.Y. Sadasivam, K.R. Reddy, and K. Spokas, *Physical and chemical characterization of waste wood derived biochars.* Waste Management, 2015. **36**: p. 256-268.
115. Chia, C.H., A. Downie, and P. Munroe, *Chapter 5. Characteristics of biochar: physical and structural properties*, in *Biochar for environmental management : science, technology and implementation*. 2015, Taylor and Francis Ltd: London ;. p. 89-110.
116. Kim, K.H., J.Y. Kim, J.W. Choi, and T.S. Cho, *Influence of pyrolysis temperature on physicochemical properties of biochar obtained from the fast pyrolysis of pitch pine (Pinus rigida).* Bioresource Technology, 2012. **118**: p. 158-162.
117. Pituello, C., O. Francioso, G. Simonetti, A. Pisi, A. Torreggiani, A. Berti, and F. Morari, *Characterization of chemical-physical, structural and morphological properties of biochars from biowastes produced at different temperatures.* Journal of Soils and Sediments, 2015. **15**(4): p. 792-804.
118. Liao, W. and S. Thomas, C. *Biochar particle size and post-pyrolysis mechanical processing affect soil pH, water retention capacity, and plant performance*. Soil Systems, 2019. **3**, DOI: 10.3390/soilsystems3010014.
119. Brown, R.A., A.K. Kercher, T.H. Nguyen, D.C. Nagle, and W.P. Ball, *Production and characterization of synthetic wood chars for use as surrogates for natural sorbents.* Organic Geochemistry, 2006. **37**(3): p. 321-333.
120. Pariyar, P., K. Kumari, M.K. Jain, and P.S. Jadhao, *Evaluation of change in biochar properties derived from different feedstock and pyrolysis temperature for environmental and agricultural application.* Science of the Total Environment, 2020. **713**.
121. Khimi, S.R. and K.L. Pickering, *A new method to predict optimum cure time of rubber compound using dynamic mechanical analysis.* Journal of Applied Polymer Science, 2014. **131**(6).
122. Ahmed, K., S.S. Nizami, and N.Z. Raza, *Characteristics of natural rubber hybrid composites based on marble sludge/carbon black and marble sludge/rice husk derived silica.* Journal of Industrial and Engineering Chemistry, 2013. **19**(4): p. 1169-1176.
123. Farid, A.S. and K.D. Arunashanthi, *Analysis of marching-modulus rubber rheograms.* Polymers and Polymer Composites, 2013. **21**(6): p. 377-386.
124. Jin, J., J.W.M. Noordermeer, W.K. Dierkes, and A. Blume, *The effect of silanization temperature and time on the marching modulus of silica-filled tire tread compounds.* Polymers, 2020. **12**(1).
125. Barana, D., *Lignin-based elastomeric composites for sustainable tyre technology*, in *Material science and nanotechnology*. 2017, University of Milano-Bicocca. p. 203.
126. Warasitthinon, N. and C.G. Robertson, *Interpretation of the tanδ peak height for particle-filled rubber and polymer nanocomposites with relevance to tire tread performance balance.* Rubber Chemistry and Technology, 2018. **91**(3): p. 577-594.

127. Peterson, S.C. and S. Kim, *Reducing biochar particle size with nanosilica and its effect on rubber composite reinforcement.* Journal of Polymers and the Environment, 2020. **28**(1): p. 317-322.
128. Li, Z., C. Reimer, M. Picard, A.K. Mohanty, and M. Misra, *Characterization of chicken feather biocarbon for use in sustainable biocomposites.* Frontiers in Materials, 2020. **7**.
129. Venkatesan, A.K., H.Y. Done, and R.U. Halden, *United States national sewage sludge repository at Arizona State University--a new resource and research tool for environmental scientists, engineers, and epidemiologists.* Environmental science and pollution research international, 2015. **22**(3): p. 1577-86.
130. Wattie, B., M.-J.e. Dumont, and M. Lefsrud, *Synthesis and properties of feather keratin-based superabsorbent hydrogels.* Waste and Biomass Valorization, 2018. **9**(3): p. 391-400.
131. Sharma, S., A. Gupta, A. Kumar, C.G. Kee, H. Kamyab, and S.M. Saufi, *An efficient conversion of waste feather keratin into ecofriendly bioplastic film.* Clean Technologies and Environmental Policy : Focusing on Technology Research, Innovation, Demonstration, Insights and Policy Issues for Sustainable Technologies, 2018. **20**(10): p. 2157-2167.
132. Srivatsav, V., C. Ravishankar, M. Ramakarishna, Y. Jyothi, T.N. Bhanuparakash, R. International Conference on Renewable Energy, and R. Education, *Mechanical and thermal properties of chicken feather reinforced epoxy composite.* AIP Conference Proceedings, 2018. **1992**.
133. Farhad Ali, M., M. Sahadat Hossain, T. Siddike Moin, S. Ahmed, and A.M. Sarwaruddin Chowdhury, *Utilization of waste chicken feather for the preparation of eco-friendly and sustainable composite.* Cleaner Engineering and Technology, 2021. **4**.
134. Martínez-Hernández, A.L., C. Velasco-Santos, M. de-Icaza, and V.M. Castaño, *Dynamical-mechanical and thermal analysis of polymeric composites reinforced with keratin biofibers from chicken feathers.* Composites Part B, 2007. **38**(3): p. 405-410.
135. Reddy, N. and Y. Yang, *Light-weight polypropylene composites reinforced with whole chicken feathers.* Journal of Applied Polymer Science, 2010. **116**(6): p. 3668-3675.
136. Mendez-Hernandez, M.L., B.A.R.-A. Salazar-Cruz, Jose Luis, I.A. Estrada-Moreno, and M.Y. Chavez-Cinco *Preparation and characterization of composites from copolymer styrene-butadiene and chicken feathers*. Polímeros, 2018. **28**, 368-372 DOI: 10.1590/0104-1428.08217.
137. Senoz, E., J.F. Stanzione, K.H. Reno, R.P. Wool, and M.E.N. Miller, *Pyrolyzed chicken feather fibers for biobased composite reinforcement.* Journal of Applied Polymer Science, 2013. **128**(2): p. 983-989.
138. Paz-Ferreiro, J., A. Nieto, A. Méndez, M.P.J. Askeland, and G. Gascó, *Biochar from biosolids pyrolysis: A review.* International Journal of Environmental Research and Public Health, 2018. **15**(5).
139. Pudełko, A., P. Postawa, T. Stachowiak, K. Malińska, and D. Dróżdż, *Waste derived biochar as an alternative filler in biocomposites - Mechanical, thermal and morphological properties of biochar added biocomposites.* Journal of Cleaner Production, 2021. **278**.
140. Enders, A. and J. Lehmann, *Chapter 2. Proximate analyses for characterising biochars*, in *Biochar : a guide to analytical methods*. 2017, CSIRO Publishing: Clayton, Vic. p. 9-22.

141. Anurita, S. and O. Dooshyantsingh *Effect of pyrolysis temperature on product yields of palm fibre and its biochar characteristics*. Materials Science for Energy Technologies. **3**, 575-583.
142. Kluska, J., D. Kardaś, Ł. Heda, M. Szumowski, and J. Szuszkiewicz, *Thermal and chemical effects of turkey feathers pyrolysis.* Waste Management, 2016. **49**: p. 411-419.
143. Swati, S., G. Arun, C. Syed Mohd Saufi Tuan, K. Chua Yeo Gek, P. Praddep Kumar, S. Malini, and T. Jayshree *Study of different treatment methods on chicken feather biomass* International Islamic University Malaysia Engineering Journal, 2017. **18**, DOI: 10.31436/iiumej.v18i2.806.
144. Tesfaye, T., B. Sithole, D. Ramjugernath, and V. Chunilall, *Valorisation of chicken feathers: Characterisation of chemical properties.* Waste Management, 2017. **68**: p. 626-635.
145. Mothé, M.G., L.M. Viana, and C.G. Mothé, *Thermal property study of keratin from industrial residue by extraction, processing and application.* Journal of Thermal Analysis and Calorimetry : An International Forum for Thermal Studies, 2018. **131**(1): p. 417-426.
146. Chaplin, M. *Infrared spectroscopy*. 2013; Available from: https://www.ifsc.usp.br/~lavfis2/BancoApostilasImagens/ApLuminescencia/Infrared Spectroscop1.pdf.
147. Nandiyanto, A.B.D., R. Oktiani, and R. Ragadhita, *How to read and interpret FTIR spectroscope of organic material.* Indonesian Journal of Science and Technology, 2019. **4**(1): p. 97-118.
148. Snowdon, M.R., A.K. Mohanty, and M. Misra, *A study of carbonized lignin as an alternative to carbon black.* ACS Sustainable Chemistry & Engineering, 2014. **2**(5): p. 1257-1263.
149. Zhang, J., F. Lü, H. Zhang, L. Shao, D. Chen, and P. He, *Multiscale visualization of the structural and characteristic changes of sewage sludge biochar oriented towards potential agronomic and environmental implication.* Scientific Reports, 2015. **5**(1).
150. Grube, M., J.G. Lin, P.H. Lee, and S. Kokorevicha, *Evaluation of sewage sludge-based compost by FT-IR spectroscopy.* Geoderma, 2006. **130**(3-4): p. 324-333.
151. Marculescu, C. and C. Stan, *Pyrolysis treatment of poultry processing industry waste for energy potential recovery as quality derived fuels.* Fuel, 2014. **116**: p. 588-594.
152. Chen, T., Y. Zhang, H. Wang, W. Lu, Z. Zhou, and L. Ren, *Influence of pyrolysis temperature on characteristics and heavy metal adsorptive performance of biochar derived from municipal sewage sludge.* Bioresource technology, 2014. **164**: p. 47-54.
153. Yuan, H., T. Lu, D. Zhao, H. Huang, K. Noriyuki, and Y. Chen, *Influence of temperature on product distribution and biochar properties by municipal sludge pyrolysis.* Journal of Material Cycles and Waste Management : Official Journal of the Japan Society of Material Cycles and Waste Management (JSMCWM) and the Korea Society of Waste Management (KSWM), 2013. **15**(3): p. 357-361.
154. Singh, M. and R. Vander Wal, *Nanostructure quantification of carbon blacks.* C, 2018. **5**(1): p. 2.
155. Ghosh, P., S. Katare, P. Patkar, J.M. Caruthers, V. Venkatasubramanian, and K.A. Walker, *Sulfur vulcanization of natural rubber for benzothiazole accelerated formulations: From reaction mechanisms to a rational kinetic model.* Rubber Chemistry and Technology, 2003. **76**(3): p. 592-693.

156. Fröhlich, J., W. Niedermeier, and H.D. Luginsland, *The effect of filler-filler and filler-elastomer interaction on rubber reinforcement.* Composites Part A, 2005. **36**(4): p. 449-460.
157. Tatiana, L.A.C.R., M.J. Marly, S. Dimitrios, and H.S. Robert *Evaluation of the influence of the polymer-filler interaction on compounds based on epoxidized elastomeric matrix and precipitated silica*. Polímeros, 2006. **16**, 111-115 DOI: 10.1590/S0104-14282006000200010.
158. Jong, L., *Dynamic mechanical properties of soy protein filled elastomers.* Journal of Polymers and the Environment, 2005. **13**(4): p. 329-338.
159. Ge, X., Z. Zhang, H. Yu, B. Zhang, and U.R. Cho, *Study on viscoelastic behaviors of bentonite/nitrile butadiene rubber nanocomposites compatibilized by different silane coupling agents.* Applied Clay Science, 2018. **157**: p. 274-282.
160. Bridgestone. *Long-term environmental vision (2050 and beyond): Towards 100% sustainable materials*. 2021; Available from: https://www.bridgestone.com/responsibilities/environment/resources/.
161. Goodyear. *Sustainable material usage*. 2021; Available from: https://corporate.goodyear.com/us/en/responsibility/sustainable-sourcing/sustainable-materials.html.
162. Continental. *Tires for the future*. 2021; Available from: https://www.continental-tires.com/car/tires/tires-for-the-future.
163. Sumitomo. *Sumitomo rubber establishes long-term sustainability policy: "Driving our future challenge 2050"*. 2021; Available from: https://www.srigroup.co.jp/english/newsrelease/2021/sri/2021_060.html.
164. Tire Manufacturers Association, U.S., *Sustainability: driving the U.S. tire manufacturing industry*. 2018.
165. Edwards, D.C., *Polymer-filler interactions in rubber reinforcement.* Journal of Materials Science, 1990. **25**(10): p. 4175-4185.
166. Li, Z.H., J. Zhang, and S.J. Chen *Effects of carbon blacks with various structures on vulcanization and reinforcement of filled ethylene-propylene-diene rubber*. eXPRESS Polymer Letters. **2**, 695-704 DOI: 10.3144/expresspolymlett.2008.83.
167. Sajjadi, B., W.-Y. Chen, and N.O. Egiebor, *A comprehensive review on physical activation of biochar for energy and environmental applications.* Reviews in Chemical Engineering, 2019. **vol. 35, no. 6**: p. p. 735-776.
168. Wang, L., Y.S. Ok, D.C.W. Tsang, D.S. Alessi, J.r. Rinklebe, H. Wang, O.e. Mašek, R. Hou, D. O'Connor, and D. Hou, *New trends in biochar pyrolysis and modification strategies: feedstock, pyrolysis conditions, sustainability concerns and implications for soil amendment.* Soil Use and Management, 2020. **36**(3): p. 358-386.
169. Colvin, H.A. and J.M. Opperman, *Method and formulation for reinforcing elastomers*. 2007, Cooper Tire and Rubber CO.
170. Jong, L., *Effect of soy protein concentrate in elastomer composites.* Composites Part A, 2006. **37**(3): p. 438-446.
171. Prochoń, M., A. Przepiórkowska, and H.H. Ngo *Innovative application of biopolymer keratin as a filler of synthetic acrylonitrile-butadiene rubber NBR*. Journal of Chemistry., 2013.

172. Jung, S.-H. and J.-S. Kim, *Production of biochars by intermediate pyrolysis and activated carbons from oak by three activation methods using CO2.* Journal of Analytical and Applied Pyrolysis, 2014. **107**: p. 116-122.
173. Senoz, E., R.P. Wool, C.W.J. McChalicher, and C.K. Hong, *Physical and chemical changes in feather keratin during pyrolysis.* Polymer Degradation and Stability, 2012. **97**(3): p. 297-307.
174. Zhao, Z., Y. Wang, M. Li, and R. Yang, *High performance N-doped porous activated carbon based on chicken feather for supercapacitors and CO2 capture.* RSC ADVANCES, 2015. **5**(44): p. 34803-34811.
175. Brebu, M. and I. Spiridon, *Thermal degradation of keratin waste.* Journal of Analytical and Applied Pyrolysis, 2011. **91**(2): p. 288-295.
176. Shi, W. and M.-J.e. Dumont, *Processing and physical properties of canola protein isolate-based films.* Industrial Crops & Products, 2014. **52**: p. 269-277.
177. Erdem, A. and M. Dogru, *Process intensification: activated carbon production from biochar produced by gasification.* Johnson Matthey Technology Review, 2020.
178. Demiral, H., İ. Demiral, B. Karabacakoğlu, and F. Tümsek, *Production of activated carbon from olive bagasse by physical activation.* Chemical Engineering Research and Design, 2011. **89**(2): p. 206-213.
179. Heideman, G., R.N. Datta, J.W.M. Noordermeer, and B. van Baarle, *Activators in accelerated sulfur vulcanization.* Rubber Chemistry and Technology, 2004. **77**(3): p. 512-541.
180. Mathew, N.M., *Chapter 2. Natural rubber*, in *Rubber technologist's handbook*, W. J.R. and D. S.K., Editors. 2001, Rapra Technology Ltd. p. 11-46.
181. Wang, H., W. Liu, J. Huang, D. Yang, and X. Qiu, *Bioinspired engineering towards tailoring advanced lignin/rubber elastomers.* Polymers, 2018. **10**(9).
182. Li, Y., B. Han, S. Wen, Y. Lu, H. Yang, L. Zhang, and L. Liu, *Effect of the temperature on surface modification of silica and properties of modified silica filled rubber composites.* Composites Part A, 2014. **62**: p. 52-59.
183. Chang, B.P., A. Gupta, R. Muthuraj, and T.H. Mekonnen, *Bioresourced fillers for rubber composite sustainability: current development and future opportunities.* Green Chemistry, 2021. **23**(15): p. 5337-5378.